Title
Primitive Model Simulations and Mean-Field Studies of Electric Double Layers

Author
Giera, Brian

Publication Date
2014

Peer reviewed|Thesis/dissertation

UNIVERSITY of CALIFORNIA
Santa Barbara

Primitive Model Simulations and Mean-Field Studies of Electric Double Layers

A dissertation submitted in partial satisfaction of the
requirements for the degree of

Doctor of Philosophy

in

Chemical Engineering

by

Brian Giera

Committee in charge:

Professor Todd M. Squires, Co-Chair
Professor M. Scott Shell, Co-Chair
Doctor Edward M. Kober
Professor Bradley F. Chmelka
Professor Frédéric Gibou

June 2014

The dissertation of Brian Giera is approved:

Edward M. Kober

Bradley F. Chmelka

Frédéric Gibou

M. Scott Shell, Co-Chair

Todd M. Squires, Co-Chair

June 2014

Primitive Model Simulations and

Mean-Field Studies of

Electric Double Layers

by

Brian Giera

Acknowledgements

Your PhD is part of your life;

enjoy your life.

Dr. Yu Jing

Life is an amazing journey! Throughout my PhD, I learned how to process my perceptions of the universe in order to help others learn how to process their perceptions of the universe. To make it through, I chose to evolve my worldview by relying on the knowledge base, insights, and advice from a community of individuals who, for the most part, similarly are evolving their own worldview. I also skateboarded quite a bit and listened to a *ton* of music. I had no idea what I was getting myself into and, at times, had no clue how I would get through it. Fortunately, I had the guidance, support, and patience from my family, friends, and colleagues—many of whom fit into several of these categories.

To my advisors Professors Todd M. Squires and M. Scott Shell: I have done a seemingly insurmountable amount of learning, which would not have been possible without both of you. I am ever grateful for your persistence, encouragement, understanding, and wisdom. Thank you for giving me all sorts of things to think about. You have done far more than train me as a scientist; you have helped me to develop my professionalism, character, and consciousness. You have taught me to focus my ideas and efforts in a way I could not have dreamt was possible. I look forward to future discussions!

I would like to thank the other members of my dissertation committee—Professors Bradley F. Chmelka and Frédéric Gibou, and Doctor Edward M. Kober and also (unof-

ficial member) Doctor Neil Henson. Your feedback and perspective greatly has helped shape my research and how I present my work.

I thank all current and former members of the Squires and Shell groups, my classmates, faculty and staff of the Chemical Engineering department, scientists and staff at Los Alamos National Laboratory's Institute for Multiscale Materials Studies, and California NanoSystems Institute's Summer Institute in Mathematics and Science program, and, of course, my Santa Barbarian friends. I enjoyed the time we spent conversing and commiserating and will always appreciate our experiences at conferences and concerts.

To my parents, siblings, and family (including soon-to-be in-laws): thank you so much for always listening, your love and words of comfort, and keeping me grounded. The conversations, vacations, and quick visits were invaluable, rejuvenating, and unforgettable. I would not have accomplished this were it not for your unwavering support!

Saving the best for last, I would like to dedicate this thesis to my bride-to-be, Serra: Not only are you the love of my life, but you are also my favorite co-worker, study buddy, lunch partner, and permanent roommate. All the life, learning, and love we have ahead of us is exhilarating. Please hurry up with your PhD so that you can join me wherever we end up next!

Curriculum Vitæ

Brian Giera

Education

2014	Doctor of Philosophy in Chemical Engineering, University of California, Santa Barbara.
2008	Honors Bachelor of Science in Chemical Engineering, Purdue University, West Lafayette.

Professional Experience

2008-2014	Graduate Researcher, University of California, Santa Barbara. Santa Barbara, CA
2009 & 2010	Guest Scientist, Los Alamos National Laboratory. Los Alamos, NM
2006-2007	Co-Founder, Small Business Start-Up. Fischer, IN
2005-2007	Chemical Engineering Co-Op, Givaudan. Itasca, IL & Querétaro, MX

Refereed Publications

- Brian Giera, Neil Henson, Edward M. Kober, Todd M. Squires, and M. Scott Shell. "Model-free test of local density mean-field behavior in electric double layers." *Physical Review E* **88** 011301 (2013)
- Brian Giera, Todd M. Squires, and M. Scott Shell. "Characterizing diffuse and correlated regions within electric double layers with finite-sized ions." *In preparation.*
- Brian Giera, Todd M. Squires, and M. Scott Shell. "Mean-field local-density approximation of electric double layers with differently-sized ions." *In preparation.*

Conference Presentations

- Brian Giera, Neil Henson, Edward M. Kober, Todd M. Squires, and M. Scott Shell. "Model-Free Test for Mean-Field Behavior within Electric Double Layers." American Institute of Chemical Engineers (AIChE) Annual Meeting. San Francisco, CA. 2013.
- Brian Giera, Neil Henson, Edward M. Kober, Todd M. Squires, and M. Scott Shell. "Model-Free Test of Local-Density Mean-Field Behavior in Electric Double Layers." Sandia National Laboratories LAMMPS Workshop. Albuquerque, NM. 2013.
- Brian Giera, M. Scott Shell, and Todd M. Squires. "Molecular Dynamic Simulations and Mean-field Models of the Electric Double Layers." Clorox-Amgen Graduate Student Symposium. Santa Barbara, CA. 2012.
- Brian Giera, M. Scott Shell, and Todd M. Squires. "Molecular Dynamic Studies of Charged Electric Double Layers Exhibiting Excluded Volume Effects." American Institute of Chemical Engineers (AIChE) Annual Meeting. Salt Lake City, UT. 2010.
- Brian Giera, M. Scott Shell, and Todd M. Squires. "Molecular Dynamics Studies of the Electric Double Layer." Sandia National Laboratories LAMMPS Workshop. Albuquerque, NM. 2010.
- Brian Giera, M. Scott Shell, and Todd M. Squires. "Molecular Dynamic Studies of the Electric Double Layers." Los Alamos National Laboratory Student Symposium. Los Alamos, NM. 2009.

Awards

2012	Best Oral Presentation, Clorox-Amgen Graduate Student Symposium
2010	Education Award, University of California, Santa Barbara Materials Research Laboratory
2009	Graduate Research Fellowship Program Honorable Mention, National Science Foundation
2008	Doctoral Scholars Fellowship, University of California, Santa Barbara
2003-2008	Chick Evans Caddie Scholarship, Western Golf Association

Abstract

Primitive Model Simulations and

Mean-Field Studies of

Electric Double Layers

by

Brian Giera

When a charged surface, such as an electrode, colloid, or protein, is submerged into an ionic fluid, ions within the electrolyte rearrange into electric double layers (EDLs) that electrostatically screen the interfacial charge. The temperature, absolute permittivity, bulk electrolyte concentration, and ion valence dictate the EDL thickness $\mathcal{O}(1-100\text{nm})$ over which the applied potential, due to the surface charge, drops. The electrostatic potential and ion distributions within EDLs have long been described by mean-field local-density approximations (LDAs) that assume flat electrodes, uncorrelated ions, and bulk forms for the chemical potential. LDAs model many-body interactions within electrolytes using effective fields, and, in the case of Gouy-Chapman theory, assume point-sized ions in a continuum solvent. Despite its restrictive assumptions, the LDA approach continues to remain in heavy use for over a century because it is simple, yet qualitatively captures important aspects of EDLs. Nevertheless, a conclusive framework for understanding the behavior and limitations of these widely used class of models remains to be drawn.

The objective of this work is to elucidate LDA failure mechanisms and supplement or

supplant mean-field treatments of electrochemical systems that fail to capture correlated behavior. In particular, we develop an exceedingly general method, which requires no *a priori* model and identifies whether EDLs in a given electrolyte can obey a LDA, or whether more advanced approaches (e.g. integro-differential equations, atomistic simulations, etc.) are required, irrespective of the source of LDA breakdown. This "model-free" approach uses empirical or simulated data to directly determine whether *any* LDA can possibly describe measured EDL profiles.

We demonstrate this model-free test with the Primitive Model using extensive molecular dynamics simulations of EDLs with explicitly treated ion interactions in which LDAs are by no means guaranteed to work. We combine continuum-level theoretical studies with complementary simulations in order to bridge the molecular and continuum descriptions of excluded volume effects within EDLs. We critically assess the accuracy of LDA models of implicit solvent electrolytes with equal and differently sized ions. We also pose a novel LDA model that seeks to address solvation, polarizability, and finite-size interactions present in actual and simulated EDLs with explicit solvent.

Contents

List of Figures

List of Tables

List of Abbreviations

Bik	Bikerman
Bik-LDA	Bikerman Local-Density Approximation
BMCSL	Boublík-Mansoori-Carnahan-Starling-Leland
BMCSL-LDA	Boublík-Mansoori-Carnahan-Starling-Leland Local-Density Approximation
CPU	Central Processing Unit
CS	Carnahan-Starling
CS-LDA	Carnahan-Starling Local-Density Approximation
DFT	Density Functional Theory
DH	Debye-Hückel
DH-LDA	Debye-Hückel Local-Density Approximation
DPBE	Dipolar Poisson-Boltzmann Equation
EDL	Electric Double Layer
EDLC	Electric Double Layer Capacitor (or supercapacitor)
EOS	Equation Of State
GC	Gouy-Chapman
GC-LDA	Gouy-Chapman Local-Density Approximation
IET	Integral Equation Theory
IL	Ionic liquid
LAMMPS	Large-scale Atomic/Molecular Massively Parallel Simulator
LDA	Local-Density Approximation
MC	Monte Carlo
MD	Molecular Dynamics
ODE	Ordinary Differential Equation
SPC	Simple Point Charge
PB	Poisson-Boltzmann
PBE	Poisson-Boltzmann Equation
PDE	Partial Differential Equation
PM	Primitive Model
WDA	Weighted-Density Approximation
WCA	Weeks-Chandler-Anderson

List of Symbols

$\Delta\phi$	Electrostatic potential dropped across the electric double layer	3
C	Capacitance	3
U_{stored}	Energy stored within a capacitor	3
$\mathbf{r}$	Position in space	7
$n^{\pm}$	Density of cations or anions	7
ϕ	Electrostatic potential	7
μ^i_{LDA}	Local-density approximation for the total chemical potential of an ion of type i	7
$\mu^i_*(T)$	Standard chemical potential of an ion of type i at temperature T	7
k_{B}	Boltzmann constant, 1.381×10^{-23} $\text{m}^2\text{kg/Ks}^2$	7
T	Temperature	7
n^i	Density of an ion of type i	7
$k_{\text{B}}T\ln n^i$	Ideal chemical potential of an ion of type i	7
q^i	Valence of an ion of type i	7
e	Elementary charge, 1.602×10^{-19} coulombs	7
μ^i_{ex}	Excess chemical potential of an ion of type i	7
$\mathbf{r}_{\text{B}}$	Position in the bulk	7
μ^i_{B}	Total bulk chemical potential of an ion of type i	7
n^i_{B}	Bulk density of an ion of type i	7
$k_{\text{B}}T\ln n^i_{\text{B}}$	Bulk ideal chemical potential of an ion of type i	7
ϕ_{B}	Bulk electrostatic potential	7
μ^i_{ex}	Bulk excess chemical potential of an ion of type i	7
$\tilde{\mu}^i_{\text{LDA}}$	Dimensionless local-density approximation for the total chemical potential of an ion of type i	7
$\ln\tilde{n}^i$	Dimensionless ideal chemical potential of an ion of type i	7
$\tilde{\phi}$	Dimensionless electrostatic potential	7
$\tilde{\mu}^i_{\text{ex}}$	Dimensionless excess chemical potential of an ion of type i	7
$\tilde{n}^i$	Dimensionless density of an ion of type i	7
ϕ_{T}	Thermal voltage, $\sim$26 mV at $\sim$300 K	7
$\tilde{n}^{\pm}$	Dimensionless density of cations or anions	7
ρ	Free charge density of ions	7
q^+	Cation valence	7
n^+	Cation density	7

Chapter I

Introduction

I.1 Organization of the Dissertation

Chapter I introduces electric double layers (EDLs) and the range of disciplines and technologies involving EDLs that underscore their broad importance. We motivate our pursuit of a better understanding of two prevalent modeling approaches used to describe EDLs: mean-field local-density approximations (LDAs) and Primitive Model simulations. In Chapter II, we present a model-free test that specifically identifies whether an EDL in a given electrolyte obeys a LDA, or whether a more advanced approach (e.g. integro-differential equations, atomistic simulations, etc.) is required, irrespective of the source of LDA breakdown. In Chapter III, we explore LDA breakdown mechanisms with complementary Primitive Model simulations by focusing on the simplest, non-trivial class of electrolytes: equi-sized ions of equal and opposite valence in a homogeneous, implicit solvent. In Chapter IV, we investigate electrolytes comprised of differently-sized and discuss the limitations of implicit solvent electrolyte models. Finally, Chapter V summarizes the

main results of the dissertation an provides future research directions to investigate EDL models that explicitly account for the solvent.

I.2 Motivation and Applications

Nanoscale electric double layers (EDLs) form at all interfaces between charged surfaces (including electrodes [Israelachvili, 1992], colloids [Quesada-Pérez et al., 2003], proteins [Grochowski and Trylska, 2007], and cell membranes [Andelman, 1995]) and electrolytes [Luo et al., 2006] or ionic liquids [Kornyshev, 2007]. The EDL is the excess concentration of ions that forms due to the competition between electrostatic attraction of oppositely-charged counter-ions towards the interface, and osmotic repulsion down resulting concentration gradients. Detailed ion density profiles are experimentally accessible for a variety of EDL systems [Fedorov and Kornyshev, 2014], *e.g.* from x-ray reflectivity measurements of liquid-liquid interfaces [Luo et al., 2006] and Langmuir monolayers [Shapovalov and Brezesinski, 2006, Shapovalov et al., 2007], or neutron scattering of colloidal clay systems [Williams et al., 1998]. EDLs play a central role in colloidal suspensions [Russel et al., 1989, Hansen and Lowen, 2000], polyelectrolytes [Vlachy, 1999], micro- and nanofluidics [Schoch et al., 2008, Van Der Heyden et al., 2006], and in electric double layer capacitors (EDLCs, or supercapacitors) [Conway, 1999, Simon and Gogotsi, 2008] that store energy electrochemically across the EDL. The EDL structure governs differential capacitance [Fedorov and Kornyshev, 2008], electrokinetic flow [Squires and Bazant, 2004, Netz, 2003, Van Der Heyden et al., 2005], surface conductivity [Messinger and Squires, 2010, Deryagin and Dukhin, 1969], capacitive desalination [Biesheuvel and

Bazant, 2010, Rica et al., 2012, Zhao et al., 2012], and rational design of EDLCs [Largeot et al., 2008a, Simon and Gogotsi, 2010].

Electric double layer capacitors are environmentally friendly energy storage devices that are used to regulate power supply to unbalanced electrical grids, recapture the braking energy of light rail cars, busses, and elevators, and store intermittent energy from solar, wind, or tidal energy sources [DOE, 2007]. An EDLC functions similarly to a parallel plate capacitor in which an applied voltage drives charge separation to electrochemically store energy. In a conventional capacitor, high surface area plates separated by a thin dielectric result in large capacitances. EDLCs, therefore, offer tremendous capacitances as charge separation occurs at the interface of high surface area electrodes across $\mathcal{O}(1-100)$ nm EDLs. An EDLC is comprised of two conducting electrodes that enclose an ionic fluid as shown in Figure I.1. EDLC electrodes are predominately made of porous carbon because of its controllable surface-area range of 1000 - 2000 m^2/g, high electrical conductivity, good corrosion resistance, wide temperature stability window, as well as low cost [Pandolfo and Hollenkamp, 2006, Simon and Gogotsi, 2008].

The potential dropped across the double layer $\Delta\phi$ and capacitance C of an EDLC determines the amount of stored energy

$$U_{\text{stored}} = \frac{1}{2}C(\Delta\phi)^2. \tag{I.2.1}$$

The electrical stability window of the ionic fluid determines the maximum voltage an EDLC can withstand. The breakdown voltage of aqueous and organic electrolytes typically is 0.9 and 2.5-2.7 volts, respectively [Simon and Gogotsi, 2008]. Ionic liquids (ILs) are solvent-free mixtures of ions that act as molten salts below 100 °C [Welton, 1999].

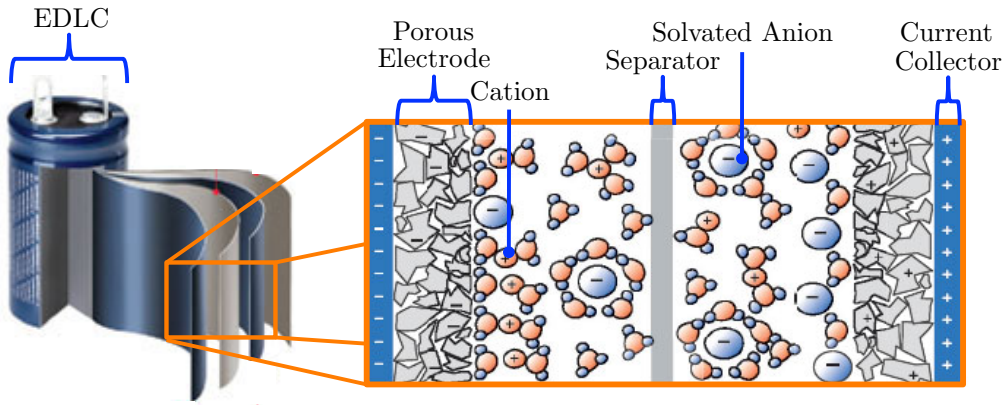

Figure I.1: Schematic of a charged electric double layer capacitor (EDLC) adapted from [Ed-China, 2010, Ultracapacitor, 2010]. EDLCs are comprised of high surface area porous electrodes immersed in an ionic fluid made up of cations, anions, and possibly solvent. An external potential difference and/or net charge density on the electrode causes ions to rearrange into nanoscale charge-screening EDLs that balance the interfacial charge. The ion-permeable separator prevents electrical contact between electrodes.

Certain ILs are electrochemically stable beyond 4 volts [Simon and Gogotsi, 2008] and are used in commercially available EDLCs [Lewandowski and Galiski, 2004, Sato et al., 2004, Tsuda and Hussey, 2007, Balducci et al., 2007]. However, ILs generally have low conductivity (<5 mS/cm) at room temperature [Hapiot and Lagrost, 2008], which limits their use to high temperature (>60 °C) applications such as breaking energy recovery in hybrid electric vehicles [Balducci et al., 2007]. To increase energy storage, the pores of modern EDLCs electrodes are engineered to be roughly the same size as the solvated and/or bare ions by using various carbon precursors and different synthesis techniques [Simon and Gogotsi, 2008]. Though it is not fully understood, large increases in capacitance arise as ions partially or fully desolvate [Chmiola et al., 2006, Lin et al., 2009] or as bare IL ions become confined [Largeot et al., 2008b] as they enter a charged pore of similar size. It is suspected that a distorted solvation shell allows for closer approach of the bare ion to the electrode, which may lead to improved capacitance [Chmiola et al., 2006].

Models and simulations have been developed to interpret and predict EDL structure and capacitance. Many simple approaches remain popular because they are relatively easy to use while still capturing many features of EDLs. The most widely-used approach to modeling EDLs are local-density approximations (LDAs) [Bazant et al., 2009, Gouy, 1910] that assume bulk-like mean-field ion interactions and neglect ion ordering. As such, LDA predictions inherently neglect non-local correlations and often fail when describing EDLs in experimentally relevant regimes [Israelachvili, 1992, Russel et al., 1989], *e.g.* highly packed regions near strongly charged electrodes. Despite their well-known failure mechanisms, LDA models have been proposed to treat short-ranged enthalpic [Caprio et al., 2004, Grochowski and Trylska, 2007] and steric interactions between equisized [Bikerman, 1942, Kilic et al., 2007b] and asymmetric [Biesheuvel and Soestbergen, 2007] ions, for the capacitance of ionic liquid systems [Kornyshev, 2007, Fedorov and Kornyshev, 2008, Fedorov et al., 2010], electrochemical cells [Rica et al., 2012, Conway, 1999], and ion distributions near liquid-liquid interfaces [Luo et al., 2006, Shapovalov and Brezesinski, 2006].

All mean-field electric double layers derived within the local-density framework obey universal self-similar scaling that yield strictly monotonic density profiles [Giera et al., 2013]. Consequently, planar LDA EDL profiles for a given electrolyte collapse onto a single, master curve when plotted against "similarity coordinates" that are a combination of system variables. Without assumptions or considering any specific LDA model, it is straightforward to analyze empirically or computationally-derived EDL profiles and determine similarity coordinates directly from free charge density contact value expressions [Giera et al., 2013]. If the LDA approach can possibly succeed, measured or com-

puted free charge density profiles will collapse onto a universal curve as a function of an intrinsic, derivable similarity coordinate. On the other hand, if measured EDL profiles do not collapse, similarity coordinates reveal the boundaries of LDA feasibility space, beyond which more sophisticated treatments capable of addressing correlation effects are needed. Models that can capture noncollapsing profiles require more involved integral equation theories [Quesada-Pérez et al., 2003], computationally expensive atomistic simulations [Jonsson et al., 1980, Torrie and Valleau, 1980, Moreira and Netz, 2002], or perhaps different approaches altogether. It would therefore be advantageous to know beforehand if LDAs, which give rapidly solvable partial differential equations, are feasible before deriving advanced EDL models.

I.3 Overview of Electric Double Layer Models

To be instructive, we give a review of two prominent implicit solvent models of fully charged electric double layer systems. Mean-field Local-density approximations (LDAs) assume homogenous ion interactions and adopt physically-motivated chemical potential models that neglect spatially dependent ion-ion and ion-wall correlations [Bazant et al., 2009]. The Primitive Model (PM) is the simplest possible electrolyte model that, unlike LDAs, explicitly accounts for size-induced and/or electrostatic correlations amongst ions with pairwise interaction potentials [Henderson, 1983]. We provide codes in Appendices A and B that we use to solve the LDA models and PM simulations discussed in Sections I.3.1 and I.3.2, respectively.

I.3.1 Mean-field Local-density Approximations

Local-density approximations require the chemical potential at every point in space $\mathbf{r}$ to depend *only* on local quantities such as the density of ions $n^{\pm}$ or electrostatic potential ϕ

$$\mu^i_{\mathrm{LDA}}\left(\mathbf{r}\right) = \mu^i_*(T) + k_{\mathrm{B}}T\ln n^i + q^i e\phi + \mu^i_{\mathrm{ex}}\,, \tag{I.3.1}$$

where k_{B} is the Boltzmann constant, T is temperature, q^i is ion valence, and e is the elementary charge. Equation (I.3.1) is expressed as the sum of the standard chemical potential, ideal chemical potential, mean electrostatic field, and excess chemical potential, respectively. Far from the electrode, the chemical potential approaches a constant bulk value

$$\mu^i_{\mathrm{LDA}}\left(\mathbf{r}\to\mathbf{r}_{\mathrm{B}}\right)\to\mu^i_{\mathrm{B}} = \mu^i_*(T) + k_{\mathrm{B}}T\ln n^i_{\mathrm{B}} + q^i e\phi_{\mathrm{B}} + \mu^i_{\mathrm{ex,B}}. \tag{I.3.2}$$

We express Eq. (I.3.1) relative to Eq. (I.3.2)

$$\tilde{\mu}^i_{\mathrm{LDA}}\left(\mathbf{r}\right) = \frac{\mu^i_{\mathrm{LDA}} - \mu^i_{\mathrm{B}}}{k_{\mathrm{B}}T} = \ln\tilde{n}^i + q^i\tilde{\phi} + \tilde{\mu}^i_{\mathrm{ex}} \equiv 0\,, \tag{I.3.3}$$

and define non-dimensional variables $\tilde{n}^i = n^i/n^i_{\mathrm{B}}$ and $\tilde{\phi} = (\phi-\phi_{\mathrm{B}})/\phi_{\mathrm{T}}$, where $\phi_{\mathrm{T}} = k_{\mathrm{B}}T/e$ is the thermal potential. We rearrange Eq. (I.3.3) for $\tilde{n}^{\pm}$, solve for the free charge density $\rho = e(q^+\ n^+ + q^-n^-)$,

$$\tilde{\rho}_{\mathrm{LDA}} \equiv \frac{\rho_{\mathrm{LDA}}}{2eI} = \frac{1}{2I}\sum_i^{\pm} n^i q^i \exp\left(-q^i\tilde{\phi}\right)\exp\left(-\tilde{\mu}^i_{\mathrm{ex}}\right)\,, \tag{I.3.4}$$

that we non-dimensionalize by the ionic strength

$$I = \frac{1}{2}\sum_i^{\pm} n^i_{\mathrm{B}}\left(q^i\right)^2. \tag{I.3.5}$$

We limit our discussion to symmetric electrolytes comprised of ions with equal and opposite valence $q^{\pm} = \pm q$, $I = n_{\mathrm{B}}q^2$, and that have equivalent bulk values for the density

$n_{\mathrm{B}}^{\pm}$=n_{B}, electrostatic potential ϕ_{B}, and because of stoichiometry $\mu_{\mathrm{B}}^{\pm}$=μ_{B}, Mean-field models for electric double layers relate the electrostatic potential and free charge density of ions using Poisson's equation

$$\lambda_{\mathrm{D}}^2 \nabla^2 \tilde{\phi} = -\tilde{\rho}\,, \tag{I.3.6}$$

where the Debye length

$$\lambda_{\mathrm{D}} = \frac{1}{\sqrt{8\pi\lambda_{\mathrm{B}} I}}. \tag{I.3.7}$$

naturally arises to define the characteristic distance over which ions electrostatically screen the net charge on the electrode. The pairwise Bjerrum length

$$\lambda_{\mathrm{B}} = \frac{e^2}{4\pi\varepsilon k_{\mathrm{B}} T} \tag{I.3.8}$$

characterizes the distance between elementary charges in a uniform continuum with permittivity ε. For charges separated farther than λ_{B}, the pairwise electrostatic energy is less than the thermal energy $k_{\mathrm{B}}T$.

For any given LDA, we can evaluate the capacitance via electrode charge density versus electrostatic voltage curves using $\tilde{\mu}_{\mathrm{LDA}}^{\pm}$ and the general definition for the reduced electrode charge density

$$\frac{\Sigma}{\Sigma_{\mathrm{ref}}} \equiv -\tilde{\nabla}\tilde{\phi}(0)\,, \tag{I.3.9}$$

where we nondimensionalize by

$$\Sigma_{\mathrm{ref}} = \frac{e}{4\pi\lambda_{\mathrm{B}}\lambda_{\mathrm{D}}}\,, \tag{I.3.10}$$

and the characteristic length is λ_{D}. To do this, we determine the roots of $\tilde{\mu}_{\mathrm{LDA}}^{\pm} = 0$ in Eq. (I.3.3) to obtain the free charge density's dependence on the voltage, i.e., find $\tilde{\rho}$ =

$\tilde{\rho}(\tilde{\phi},\tilde{\mu}^{+}_{\rm ex},\tilde{\mu}^{-}_{\rm ex},...)$ from Eq. (I.3.4). Since $(1/2)[(\tilde{\phi}')^2]' \equiv \tilde{\phi}''$ and $\tilde{\phi}'' = -\tilde{\rho}$ from Eq. (I.3.6), we rearrange Eq. (I.3.9) for the surface charge-voltage relationship

$$\tilde{\Sigma}_{\rm LDA} = {\rm sign}(\tilde{\phi}_0)\sqrt{-2\int_0^{\tilde{\phi}_0} \tilde{\rho}_{\rm LDA}\left(\hat{\phi},\tilde{\mu}^{+}_{\rm ex},\tilde{\mu}^{-}_{\rm ex},...\right){\rm d}\hat{\phi}}. \tag{I.3.11}$$

The ratio of $\tilde{\Sigma}_{\rm LDA}/\tilde{\phi}_0$ in Equation (I.3.11) gives the integral or total capacitance and ${\rm d}\tilde{\Sigma}_{\rm LDA}/{\rm d}\tilde{\phi}_0$ is the differential capacitance. Charge-voltage curves are relatively easy to measure [MacDonald and Jr, 1962] and provide a crucial metric for electric double layer capacitor design. However, Eq. (I.3.11) integrates out important features revealed by spatial EDL profiles that are obtained from the full solution of Eq. (I.3.6).

We complete the LDA model for planar EDLs by determining the potential that self-consistently solves Eqs. (I.3.4) and I.3.6) after specifying boundary conditions at the surface of the electrode

$$\tilde{\phi}\,(0) = \tilde{\phi}_0\,, \tag{I.3.12}$$

and in the bulk

$$\tilde{\phi}\,(\tilde{z}_{\rm B}) = \tilde{\phi}_{\rm B} \equiv 0. \tag{I.3.13}$$

Analytical LDA models define the bulk to be infinitely far from the surface, $\tilde{z}_{\rm B} \to \infty$. For LDAs that require numerical methods to solve, we specify the bulk to be $\tilde{z}_{\rm B} = 10$ and check our solutions against Eq. (I.3.3) to verify that the chemical potential is spatially invariant. Equation (I.3.4) is general and can be easily modified for electrolytes with additional species or even non-local excess terms like $\mu_{\rm w}(z)$ to arrive at non-LDA models that accounts for ion-wall interactions [Qiao and Aluru, 2003, Qiao and Aluru, 2004b, Joly et al., 2004].

The classic Poisson-Boltzmann approach represents the simplest mean-field planar LDA, which assumes ideal, point-like ions that establish and respond to a mean-electric-field in a structureless, continuum solvent. It is solved by the Gouy-Chapman [Gouy, 1910, Chapman, 1913] (GC) model of the EDL and is only appropriate for dilute electrolytes with weakly-charged ions and electrodes. In this idealized limit, the excess term in Eq. (I.3.1) vanishes to give the GC chemical potential

$$\tilde{\mu}^{\pm}_{\mathrm{GC}} = \ln \tilde{n}^{\pm} \pm q\tilde{\phi} \equiv 0\,, \tag{I.3.14}$$

which reveals GC ions to follow a direct Boltzmann distribution $\tilde{n}^{\pm} = \exp(\mp q\tilde{\phi})$. Rearranging for the free charge density and inserting into Eq. (I.3.6), we arrive at the Poisson-Boltzmann Equation

$$\tilde{\nabla}^2\tilde{\phi} = \sinh\left(q\tilde{\phi}\right). \tag{I.3.15}$$

The GC surface charge-voltage relationship for planar geometries from Eq. (I.3.11) gives

$$\tilde{\Sigma}_{\mathrm{GC}} = \sqrt{-2\cosh\left(q\tilde{\phi}_0\right)} = 2\sinh\left(\frac{q\tilde{\phi}_0}{2}\right). \tag{I.3.16}$$

In the Debye-Hückel (DH) limit characterized by dilute electrolytes, low surface voltages $\tilde{\phi}_0 \ll 1$, and infinitesimal applied charge densities $\tilde{\Sigma} \ll 1$, the linearized form of Eq. (I.3.15) is solved by $\tilde{\rho}_{\mathrm{DH}} = -\tilde{\phi}_{\mathrm{DH}}$, $\tilde{\phi}_{\mathrm{DH}} = \tilde{\phi}_0\exp(-\tilde{z})$, and $\tilde{\Sigma}_{\mathrm{DH}} = \tilde{\phi}_0$. All LDAs reduce to the DH form in the dilute regime far from weakly-charged EDLs. The exponential decay of the free charge density is also asymptotically exact in the limit of infinitely charged electrodes; differing only by constants [Attard, 1996].

Despite its near-ubiquitous use, the GC-LDA (and Eq. (I.3.15) more generally) has long been known to fail for various reasons. Boltzmann-distributed densities grow exponentially with $\tilde{\phi}$, predicting volume fractions that would exceed close packing of real

ions [Bikerman, 1942, Kilic et al., 2007b]. Here we discuss the widely-used Bikerman and Carnahan-Starling LDA models that move beyond GC by adopting chemical potential expressions from homogenous systems of equi-sized ions with bulk-volume fraction

$$\Phi_{\mathrm{B}} = \frac{\pi}{3} n_{\mathrm{B}} \sigma^3 \tag{I.3.17}$$

and diameter σ. Like the GC-LDA, these models assume an implicit solvent and neglect electrostatic correlation effects. However, they account for finite-sized effects with bulk-like forms for exclude volume contributions to the chemical potential that depend on the local volume fraction

$$\Phi\left(\mathbf{r}\right) = \frac{\Phi_{\mathrm{B}}}{2}(\tilde{n}^{+} + \tilde{n}^{-}). \tag{I.3.18}$$

The Bik-LDA adopts a mean-field lattice-gas model for the EDL with sites on a cubic lattice that contain at most one ion [Bikerman, 1942]. Empty sites represent the implicit solvent. Near sufficiently charged electrodes [Kilic et al., 2007b, Kilic et al., 2007a], lattice sites completely saturate with counter-ions such that $\Phi_{\mathrm{Bik}} = \sigma^3(n^{+} + n^{-}) \rightarrow 1$. The Bikerman excess chemical potential

$$\frac{\mu^{\pm}_{\mathrm{Bik,ex}}}{k_{\mathrm{B}}T} = -\ln\left(1 - \frac{\Phi_{\mathrm{B}}}{2}(\tilde{n}^{+} + \tilde{n}^{-})\right) \tag{I.3.19}$$

can be derived from the configurational degeneracies of non-overlapping ions amongst available lattice sites [Kornyshev, 2007]. Following Eqs. (I.3.2) and (I.3.3), the Bikerman chemical potential is expressed relative to its bulk value to give the dimensionless relation

$$\tilde{\mu}^{\pm}_{\mathrm{Bik}} = \ln\tilde{n}^{\pm} \pm q\tilde{\phi} + \ln\left(\frac{1 - \Phi_{\mathrm{B}}}{1 - \Phi_{\mathrm{B}}(\tilde{n}^{+} + \tilde{n}^{-})/2}\right) \equiv 0. \tag{I.3.20}$$

Equation (I.3.20) can be solved for $\tilde{n}^{\pm}$ to reveal a Fermi-Dirac (instead of a Boltzmann) distribution. The Bikerman free charge density is inserted into Eq. (I.3.6) to obtain

$$\tilde{\nabla}^2\tilde{\phi} = \frac{\sinh\left(q\tilde{\phi}\right)}{1 + 2\Phi_{\mathrm{B}}\sinh^2\left(q\tilde{\phi}/2\right)}. \tag{I.3.21}$$

The surface charge-voltage relationship for the Bik-LDA is given by

$$\tilde{\Sigma}_{\mathrm{Bik}} = \sqrt{\frac{2}{\Phi_{\mathrm{B}}}\ln\left[1 + 2\Phi_{\mathrm{B}}\sinh^2\left(q\tilde{\phi}_0/2\right)\right]}. \tag{I.3.22}$$

In the case of point-sized ions, $\Phi_{\mathrm{B}} \to 0$ and Eqs. (I.3.20-I.3.22) recover the GC-LDA and Poisson-Boltzmann Eq. (I.3.15).

More accurate models for excluded volume contributions to the bulk chemical potential frequently rely on the Percus-Yevik integral equation and virial and compressibility expansions of a homogeneous hard-sphere fluid [Hansen and McDonald, 1986, Barker and Henderson, 1976]. The Carnahan-Starling (CS) equation of state [Carnahan and Starling, 1969] is an accurate approximation [Song et al., 1989] that combines the hard-sphere equations of state from the virial and compressibility routes [McQuarrie, 1976] to obtain

$$\frac{\mu^{\pm}_{\mathrm{CS,ex}}}{k_{\mathrm{B}}T} = \frac{8\Phi - 9\Phi^2 + 3\Phi^3}{(1-\Phi)^3}. \tag{I.3.23}$$

The ideal and electrostatic chemical potentials and Equation (I.3.23) are expressed relative to the bulk to obtain the dimensionless total CS-LDA chemical potential [Bazant et al., 2009, Attard, 1993]

$$\tilde{\mu}^{\pm}_{\mathrm{CS}} = \ln\tilde{n}^{\pm} \pm q\tilde{\phi} + \frac{1}{(1-\Phi)^2} + \frac{2}{(1-\Phi)^3} + \frac{\Phi_{\mathrm{B}} - 3}{(1-\Phi_{\mathrm{B}})^3} \equiv 0. \tag{I.3.24}$$

The three terms that depend on the local and bulk volume fraction are analogous to the rightmost term in the Bik-LDA Eq. (I.3.20). As with all LDAs, the chemical potentials

for both ion types given by Eq. (I.3.24) are solved to determine the free charge density as a function of voltage that is then used in Eq. (I.3.6), i.e. find $\tilde{\rho}_{\mathrm{CS}}(\tilde{\phi})$ from $\{\tilde{\mu}^{+}_{\mathrm{CS}},\tilde{\mu}^{-}_{\mathrm{CS}}= 0, 0\}$. Although the CS-LDA requires numerical methods to solve, it recovers the GC limit as $\Phi_{\mathrm{B}} \to 0$, just like Bikerman theory.

I.3.2 Molecular Dynamics Simulations of Primitive Model Electrolytes

The Primitive Model of the electric double layer gives three physical length scales: the screening length λ_{D} that is calculated from equilibrated bulk ion concentrations; the Bjerrum length λ_{B} that is set by ion valence, thermal energy, and uniform permittivity ε; and the ion diameter σ that sets the total bulk volume fraction of ions $\Phi_{\mathrm{B}} = \sigma^3/(24\lambda_{\mathrm{B}}\lambda_{\mathrm{D}}^2)$. Nondimensionalizing lengths by λ_{D} reveals any PM EDL to be uniquely specified by three dimensionless parameters: Φ_{B}, $\lambda_{\mathrm{B}}/\lambda_{\mathrm{D}}$, and $\Sigma/\Sigma_{\mathrm{ref}}$. Exact solutions of the PM often are determined using correlation functions and integral equations, with simulation techniques like Density Functional Theory, Monte Carlo, or Molecular Dynamics (MD). In this thesis, we use MD simulations of the PM EDL that treat ions as charged particles in an implicit solvent between uniformly charged plates as shown in Figure I.2. We focus on PM EDLs in the canonical ensemble, in which the general expression for the chemical potential of an ion of type i is given by

$$\frac{\mu^i}{k_{\mathrm{B}}T} = -\left(\frac{\partial \ln Q}{\partial N^i}\right). \tag{I.3.25}$$

The total partition function is

$$Q = \left[\prod_{i}^{\pm} \frac{(k_{\mathrm{B}}T)^{N^i}}{N^i!} \exp\left(\frac{N^i \mu_*^i(T)}{k_{\mathrm{B}}T}\right)\right] \iint ... \int e^{-\tilde{U}(\mathbf{r}^N)} \mathrm{d}\mathbf{r}^N \,, \tag{I.3.26}$$

where the reduced potential energy

$$\tilde{U}(\mathbf{r}^N) \equiv \frac{U(\mathbf{r}^N)}{k_{\mathrm{B}}T} = \tilde{U}_{\mathrm{pair}}(\mathbf{r}^N) + \tilde{U}_{\mathrm{one}}(\tilde{z}^N) \tag{I.3.27}$$

is separated into pairwise ion-ion $\tilde{U}_{\mathrm{pair}}$ and one-body $\tilde{U}_{\mathrm{one}}$ ion-electrode interactions amongst $N = N^+ + N^-$ total ions [Hill, 1960]. We assume ions that have equal masses and thus identical standard chemical potentials $\mu_*^{\pm}(T) = -k_{\mathrm{B}}T \ln\left(k_{\mathrm{B}}T/\,\Lambda^3\right)$ and de Broglie wavelengths $\Lambda^{\pm} = \Lambda$.

For a given configuration of this PM, the ion-ion contribution to the potential energy depends on pairwise distances $r_{ij} = |\mathbf{r}^i - \mathbf{r}^j|$

$$\tilde{U}_{\mathrm{pair}}(\mathbf{r}^N) = \sum_{i<j}^{N} \tilde{U}_{\mathrm{Coulomb}}(r_{ij}) + \tilde{U}_{\mathrm{WCA}}(r_{ij} \leq \sigma). \tag{I.3.28}$$

The Coulomb potential is long-ranged

$$\tilde{U}_{\mathrm{Coulomb}}(r) = q^i q^j \frac{\lambda_{\mathrm{B}}}{r} \tag{I.3.29}$$

and captures electrostatic interactions between point-charges with λ_{B} given by Eq. (I.3.8). In this work, we use the repulsive Weeks-Chandler-Andersen [Weeks et al., 1971] (WCA) potential

$$\tilde{U}_{\mathrm{WCA}}(r \leq \sigma) = \frac{\epsilon_{\mathrm{WCA}}}{k_{\mathrm{B}}T}\left[\frac{(\sigma^6 - r^6)^2}{r^{12}}\right], \tag{I.3.30}$$

to account for finite-size effects between ions with characteristic energy ϵ_{WCA} that approach closer than their WCA diameter σ. Similar to hard-sphere systems, WCA particles separated farther than σ do not interact, i.e. $\tilde{U}_{\mathrm{WCA}}(r > \sigma) \equiv 0$. The very steep WCA

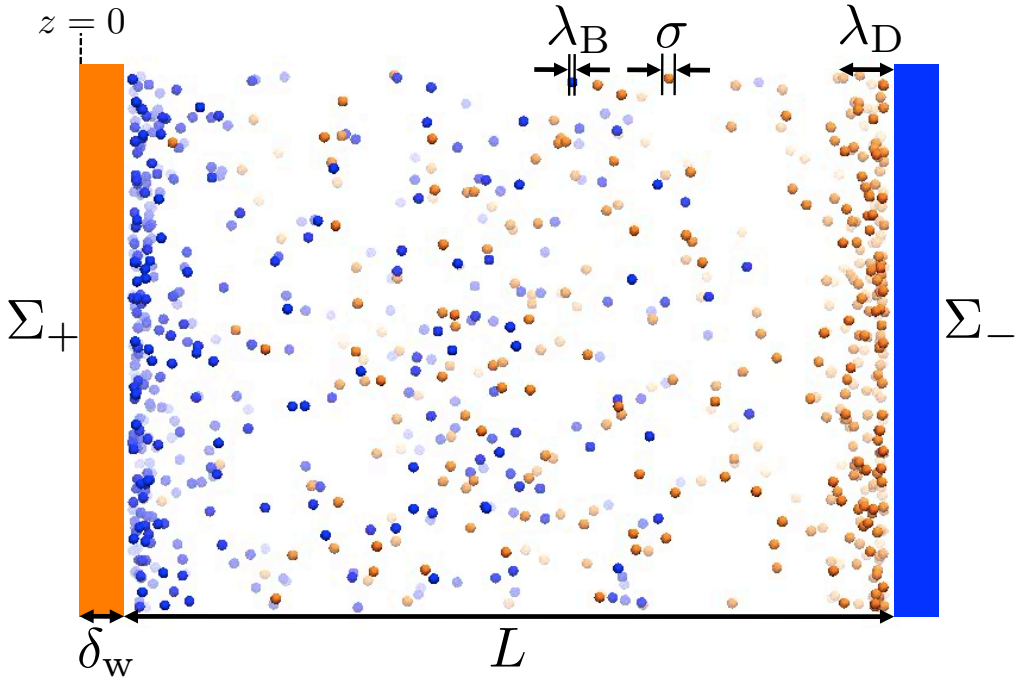

Figure I.2: Schematic of the Primitive Model of an implicit solvent electrolyte. Anions and cations (blue and orange spheres) concentrate near the cathode and anode (orange and blue rectangles) to screen the interfacial charge on the electrode and form electric double layers with characteristic thickness λ_D. Ion-ion interactions are treated explicitly using pairwise potentials [Eqs. (I.3.28)-(I.3.30)] that depend on the Bjerrum length λ_B and ion diameter σ. Wall-ion interactions are computed from one-body potentials [Eqs. (I.3.31)-(I.3.34)] that confine ions within a distance L between oppositely-charged electrodes with uniform charge density $\Sigma_\pm$ and wall thickness δ_w.

potential dictates the minimum inter-ion separation distance $r^{\min} \sim \mathcal{O}(\sigma)$. Therefore, the dominant contributions to the pairwise potential depend on the relative magnitudes of λ_{B} and σ. We assume any observable correlations are due only to finite-sized effects for electrolytes where $\lambda_{\mathrm{B}} \ll \sigma$.

The ion-electrode interactions include electrostatic and steric terms that only depend on the distance from electrodes separated by $\tilde{L} = L/\lambda_{\mathrm{D}}$

$$\tilde{U}_{\mathrm{one}}(\tilde{z}^{\mathrm{N}}) = \sum_{i=1}^{N} \tilde{U}_{\mathrm{field}}(\tilde{z}^i) + \tilde{U}_{\mathrm{w}}^{+}\left(\tilde{z}^i \leq \frac{\delta_{\mathrm{w}}}{\lambda_{\mathrm{D}}}\right) + \tilde{U}_{\mathrm{w}}^{-}(\tilde{z}^i \geq \tilde{L}). \tag{I.3.31}$$

The electrostatic field term in Equation (I.3.31),

$$\tilde{U}_{\mathrm{field}}(\tilde{z}) = -q^i \tilde{\Sigma} \tilde{z}\,, \tag{I.3.32}$$

accounts for the potential energy ions experience between two uniformly charged electrodes with equal and opposite surface charge density. The wall-ion interaction depends on the wall thickness parameter δ_{w} and the distance an ion penetrates either wall

$$\delta_{\mathrm{p}}(\tilde{z}) = \begin{cases} \delta_{\mathrm{w}} - \tilde{z}\lambda_{\mathrm{D}} & \text{if } \tilde{z} \leq \delta_{\mathrm{w}}/\lambda_{\mathrm{D}}, \\ 0 & \text{if } \delta_{\mathrm{w}}/\lambda_{\mathrm{D}} < \tilde{z} < L/\lambda_{\mathrm{D}}, \\ \tilde{z}\lambda_{\mathrm{D}} - L & \text{if } \tilde{z} \geq L/\lambda_{\mathrm{D}}. \end{cases} \tag{I.3.33}$$

The wall potential is the repulsive part of the 9-3 potential

$$\tilde{U}_{\mathrm{w}}^{\pm}(\delta_{\mathrm{p}}) = \frac{\epsilon_{\mathrm{w}}}{k_{\mathrm{B}}T}\sqrt{\frac{5}{18}}\left[\frac{1}{(1-\delta_{\mathrm{p}}/\delta_{\mathrm{w}})^9} - \frac{3}{(1-\delta_{\mathrm{p}}/\delta_{\mathrm{w}})^3} + 2\right] \tag{I.3.34}$$

with characteristic energy ϵ_{w} and $\tilde{U}_{\mathrm{w}}^{\pm}(\delta_{\mathrm{p}} = 0) = 0$.

A force balance between the electrostatic attraction and steric repulsion experienced by a counter-ion penetrating the wall,

$$-\frac{\mathrm{d}\tilde{U}_{\mathrm{field}}}{\mathrm{d}\tilde{z}} = -\frac{\mathrm{d}\tilde{U}_{\mathrm{w}}}{\mathrm{d}\delta_{\mathrm{p}}}\frac{\mathrm{d}\delta_{\mathrm{p}}}{\mathrm{d}\tilde{z}}\,, \tag{I.3.35}$$

gives

$$(1-\delta_{\mathrm{p}}/\delta_{\mathrm{w}})^{10}+\Delta\left((1-\delta_{\mathrm{p}}/\delta_{\mathrm{w}})^{6}-1\right)=0\,, \tag{I.3.36}$$

where

$$\Delta=\frac{3\sqrt{10}}{2}\left(\frac{\epsilon_{\mathrm{w}}\lambda_{\mathrm{D}}}{k_{\mathrm{B}}T\delta_{\mathrm{w}}\tilde{\Sigma}q^{\pm}}\right) \tag{I.3.37}$$

defines the relative strength of the parameters used in Eqs (I.3.32) and (I.3.34). For highly repulsive and strongly-charged electrodes, which is characterized by $\Delta\to 0$, the expected penetration distance,

$$1-\frac{\delta_{\mathrm{p}}}{\delta_{\mathrm{w}}}\sim\Delta^{\frac{1}{10}}\,, \tag{I.3.38}$$

is fairly insensitive to the applied field strength. Thus, the variance in δ_{p} is insignificant provided the wall potential is sufficiently steep.

I.4 Outlook

Local-density approximations and Primitive Model simulations have been used almost ubiquitously to describe electric double layers in many fields, ranging from implicit solvation models of biomolecular systems to thermodynamic solubility theories to electrokinetic flows, porous electrode dynamics, nanopore conductance, membrane potentials, to name a few. Throughout this thesis, we research LDA and PM descriptions of planar EDLs and investigate methods to systematically identify failure mechanisms to reveal LDA and PM feasibility space. We also seek to suitably adapt these approaches in the regimes they do fail in order to develop improved models that enhance understanding of electrochemical systems.

Chapter II

Model-free Test of Local-density Mean-field Behavior in Electric Double Layers

In this Chapter, we derive a self-similarity criterion that must hold if a planar electric double layer (EDL) can be captured by a local-density approximation (LDA), without specifying any specific LDA. Our procedure generates a similarity coordinate from EDL profiles (measured or computed), and all LDA-EDL profiles for a given electrolyte must collapse onto a master curve when plotted against this similarity coordinate. Non-collapsing profiles imply the inability of any LDA theory to capture EDLs in that electrolyte. We demonstrate our approach with molecular simulations, which reveal dilute electrolytes to collapse onto a single curve, and semi-dilute ions to collapse onto curves specific to each electrolyte, except where size-induced correlations arise.

II.1 Sustained Search for Improved Local-Density Approximations

For over a century, EDL structure has been almost universally modeled using the Poisson-Boltzmann equation (PBE), which takes the form

$$\lambda_{\mathrm{D}}^2 \nabla^2 \left(\frac{qe\phi}{k_{\mathrm{B}}T} \right) = \frac{n_- - n_+}{2n^{\mathrm{B}}} = \sinh \left(\frac{qe\phi}{k_{\mathrm{B}}T} \right), \tag{II.1.1}$$

for binary electrolytes, but can easily be generalized for multiple ion species and valences [Russel et al., 1989]. Here ϕ is the electrostatic excess chemical potential relative to the bulk, $\lambda_{\mathrm{D}} = (8\pi\lambda_{\mathrm{B}} n^{\mathrm{B}})^{-1/2}$ is the Debye 'screening' length, $n^{\mathrm{B}} = n_+^{\mathrm{B}} = n_-^{\mathrm{B}}$ is the bulk ion density, $\lambda_{\mathrm{B}} = (qe)^2/(4\pi\varepsilon k_{\mathrm{B}}T)$ is the Bjerrum length, beyond which thermal energy $k_{\mathrm{B}}T$ exceeds the electrostatic energy between charges $\pm qe$ in a uniform continuum with permittivity ε. The PBE (II.1.1), solved for planar EDLs by Gouy and Chapman (GC) [Gouy, 1910, Chapman, 1913], assumes ideal, point-like ions that establish (and respond to) a mean electric field in a structureless, continuum solvent.

Despite its near-ubiquitous use, the GC theory (and PBE more generally) has long been known to fail for various reasons. Boltzmann-distributed densities grow exponentially with ϕ, predicting ions of diameter σ that can exceed close-packing [Bikerman, 1942, Kilic et al., 2007b]. Experiments [Bazant et al., 2009, Israelachvili, 1992] and computations [Henderson and Boda, 2009, Qiao and Aluru, 2004a] suggest inherently non-PBE effects due to ion shape [Hansen and Lowen, 2000, Fedorov et al., 2010]; solvation [Wang and Wang, 2011, Kalcher et al., 2010]; size- [Kornyshev, 2007, Guerrero-García et al., 2010] and electrostatically-induced ordering [Lamperski and Henderson,

2011, Moreira and Netz, 2004, Gillespie et al., 2011, Grosberg et al., 2002, French et al., 2010, Levin, 2002]; dielectric inhomogeneities [López-García et al., 2011, Lauw et al., 2009, Pascall and Squires, 2010]; and physicochemical [Qiao and Aluru, 2003, Qiao and Aluru, 2004b, Joly et al., 2004] and discrete charge [Naji et al., 2005, Vangaveti and Travesset, 2012] wall-ion interactions.

Nonetheless, the PBE (II.1.1) remains appealing since it can be solved rapidly for systems and geometries that would be far larger than atomistic simulations would allow. A sustained search for modified PBEs has thus ensued [Bazant et al., 2009], seeking to preserve the local, mean-field assumptions that give simple PDEs like (II.1.1), while accounting for phenomena beyond PB/GC. Widely used local-density approximations (LDAs) assume ions to respond to additional interactions that depend *only* on local ion densities, with 'excess' chemical potential $\mu_{\pm}^{\mathrm{ex}}(n_i)$, as in bulk-like systems [Bazant et al., 2009, McQuarrie, 1976]. Wall-ion interactions $\mu_{\pm}^{\mathrm{wall}}(z)$ may also be included in the Boltzmann distribution,

$$n_{\pm} = n_{\pm}^{\mathrm{B}} \exp\left(\mp\frac{qe\phi}{k_{\mathrm{B}}T} - \frac{\mu_{\pm}^{\mathrm{ex}}(n_i)}{k_{\mathrm{B}}T} - \frac{\mu_{\pm}^{\mathrm{wall}}(z)}{k_{\mathrm{B}}T}\right), \tag{II.1.2}$$

or additional ion species, which are then used in (II.1.1) to yield a modified non-LDA PBE. LDAs have been used to treat short-ranged enthalpic [Caprio et al., 2004, Grochowski and Trylska, 2007] and steric interactions between equi-sized [Bikerman, 1942, Kilic et al., 2007b] and asymmetric [Biesheuvel and Soestbergen, 2007] ions, and to model ionic liquids [Kornyshev, 2007], electrochemical cells [Rica et al., 2012], and ion density profiles from x-ray reflectivity measurements of liquid-liquid interfaces [Luo et al., 2006] and Langmuir monolayers [Shapovalov and Brezesinski, 2006].

Despite their appealing simplicity, there is no reason to expect *a priori* that any LDA can accurately describe EDLs in a particular electrolyte [Levin, 2002]. For example, molecular simulations have revealed strong dielectric inhomogeneities [Bonthuis et al., 2011], which continuum EDL theories have treated using integro-differential equations [Bonthuis et al., 2011] or Ginzburg-Landau expansions [Bazant et al., 2011]; neither is compatible with a LDA theory. LDAs neglect structuring effects due to ion-surface, ion-ion, and ion-solvent correlations that may be significant in actual EDLs [Levin, 2002]. Increasingly powerful atomistic simulations can reveal EDL features for specific ion and solvent chemistries [Shim and Kim, 2010], but are typically impractically expensive for even moderate size or time scales. Ideally, a continuum theory could be developed for large-scale modeling that nonetheless respects the physico-chemical properties of a specific electrolyte, *e.g.* by incorporating $\mu_{\pm}^{\mathrm{ex}}$ obtained from molecular simulations or measurements into a LDA.

Current LDA searches assume some (physically-motived) form of $\mu_{\pm}^{\mathrm{ex}}$ and then assess the consequences. If a particular $\mu_{\pm}^{\mathrm{ex}}$ fails to capture measured or simulated EDL behavior, however, one does not know whether a different choice might succeed, or whether the LDA approach is itself bound to fail. It is thus crucial to know whether an EDL can possibly be captured by any LDA – and therefore whether a simple PDE can be derived for its description in more complex geometries and systems.

II.2 Solving Local-density Approximation Similarity Variables

Without assumptions or considering any specific LDA model, it is straightforward to analyze empirically or computationally-derived EDL profiles and determine "similarity variables" directly from free charge density contact value expressions. We can then use similarity variables to systematically determine whether it is possible for any LDA to describe EDLs in a particular electrolyte. This forms the basis of the "model-free" method we develop to identify EDL regimes that exhibit LDA behavior as described in Section II.3. If the LDA approach can possibly succeed, measured or computed free charge density profiles will collapse onto a universal curve as a function of an intrinsic, derivable similarity variable. Where measured EDL profiles do not collapse, similarity coordinates reveal the boundaries of LDA feasibility space, beyond which more sophisticated treatments capable of addressing correlation effects are needed.

We derive similarity variables by starting with a deceptively simple question: does an ion in an EDL 'know' the location of the surface (Fig. II.1)? In any LDA EDL, an ion located a distance z from a surface with charge density Σ would behave the same if a less-charged surface were Δz closer, provided that the effective charge density Σ_{eff} at Δz obeyed

$$\Sigma_{\text{eff}} = \Sigma - \Delta\Sigma = \Sigma + \int_0^{\Delta z} \rho(\hat{z}, \Sigma) \mathrm{d}\hat{z}. \tag{II.2.1}$$

More formally, any LDA description yields an EDL whose free charge density $\rho = qe(n_+ - n_-)$ falls onto a single, master curve $\rho(z, \Sigma)$. LDA-EDL density profiles, each with a

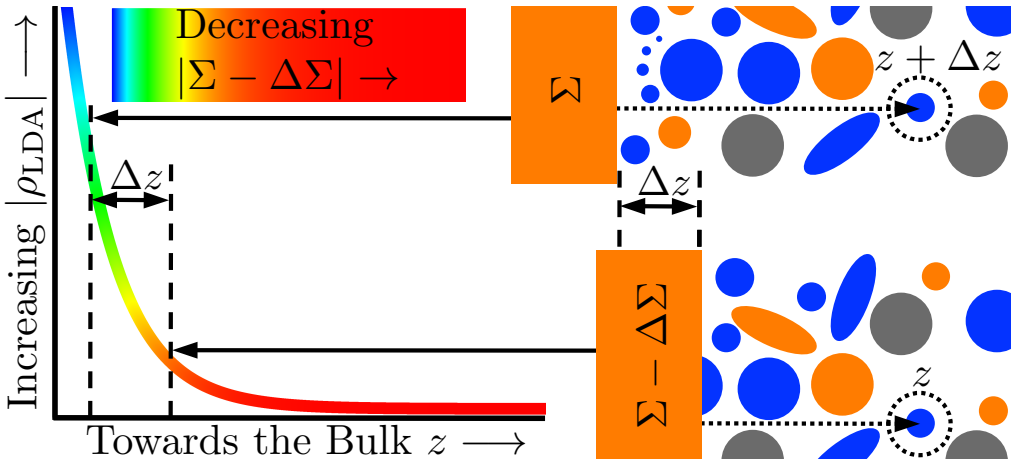

Figure II.1: Universality of local-density approximation electric double layers: any ion located a distance $z + \Delta z$ from an interface of surface charge density Σ (top right) would 'feel' no different than were the interface located a distance Δz closer (bottom right) with lower effective surface charge density $\Sigma - \Delta\Sigma$ given by Eq. (II.2.1). All LDA EDLs represent a portion of a single, universal charge density profile ρ_{LDA} (left).

different Σ, can thus be shifted by some $\Delta z(\Delta\Sigma)$ to fit onto the universal EDL profile.

This self-similarity enables an equation for the universal EDL curve for any local-density approximation to be derived explicitly, since charge densities in differently-charged EDLs obey the underlying self-similarity

$$\rho(z, \Sigma) = \rho(z + \Delta z, \Sigma + \Delta\Sigma), \tag{II.2.2}$$

where $\Delta\Sigma$ and Δz are related via Eq. (II.2.1). For small $\Delta\Sigma$ and Δz, the Taylor expansion of (II.2.2) and $\Delta\Sigma/\Delta z = -\rho(0, \Sigma)$ via (II.2.1) combine to give a self-consistency equation,

$$\left.\frac{\partial\rho}{\partial z}\right|_{\Sigma} = \left.\frac{\partial\rho}{\partial\Sigma}\right|_{z} \rho(0, \Sigma). \tag{II.2.3}$$

Any EDL that obeys a LDA — regardless of the specific $\mu_{\pm}^{\mathrm{ex}}(n_i)$ — must obey Eq. (II.2.3). Conversely, comparing simulated or measured EDL profiles against (II.2.3) directly reveals whether any simple LDA $\mu_{\pm}^{\mathrm{ex}}$ can possibly exist that successfully captures that EDL. Ion-wall interactions $\mu_{\pm}^{\mathrm{wall}}(z)$ do not obey this relation, but the arbitrariness of '$z = 0$' al-

lows Eq. (II.2.3) to be used once with an effective origin chosen to lie beyond the ion-wall interaction range.

The free charge density ρ can be derived explicitly from (II.2.3) using the method of characteristics, provided $\rho(0,\Sigma)$ is known, measured, or simulated. Furthermore, ρ depends only on a similarity variable $S(z,\Sigma;...)$, given by

$$S = \tilde{\Sigma}\exp\left(-\tilde{z} - \int_0^{\tilde{\Sigma}}\left[\frac{1}{\tilde{\rho}(0,\hat{\Sigma};...)} + \frac{1}{\hat{\Sigma}}\right]\mathrm{d}\hat{\Sigma}\right), \tag{II.2.4}$$

where we use non-dimensionalized variables $\tilde{z} = z/\lambda_\mathrm{D}$, $\tilde{\rho} = (\lambda_\mathrm{D}/\Sigma_\mathrm{ref})\rho$ and $\tilde{\Sigma} = \Sigma/\Sigma_\mathrm{ref}$, where $\Sigma_\mathrm{ref} = qe/(4\pi\lambda_\mathrm{B}\lambda_\mathrm{D})$. The charge density is then given by

$$\tilde{\rho}(S) = \tilde{\rho}(\tilde{z}=0, \tilde{\Sigma} = g^{-1}[S]), \tag{II.2.5}$$

where $g[\tilde{\Sigma}] = \tilde{\Sigma}\exp\left(-\int_0^{\tilde{\Sigma}}[1/\tilde{\rho}(0,\hat{\Sigma};...) + 1/\hat{\Sigma}]\mathrm{d}\hat{\Sigma}\right)$.

Given the free charge density at contact, S can be solved explicitly and embeds physical quantities like ion size σ, screening length λ_D, electrostatic strength λ_B, distance z, and surface charge density Σ. S then collapses LDA EDLs in a given electrolyte onto a single master curve. The Debye-Hückel (DH) limit, valid for low EDL potentials $\phi \ll k_\mathrm{B}T/qe$ and negligible excess contributions $\mu_\pm^\mathrm{ex} \to 0$, provides an instructive example. In this restrictive regime, the linearized Eq. (II.1.1) [Russel et al., 1989] gives

$$\tilde{\rho}_\mathrm{DH}(0,\tilde{\Sigma}) = -\tilde{\Sigma}, \tag{II.2.6}$$

and Eqns. (II.2.4-II.2.5) can be solved explicitly to give

$$S_\mathrm{DH} = \tilde{\Sigma}\exp(-\tilde{z}) \tag{II.2.7}$$

and

$$\tilde{\rho}_\mathrm{DH} = -S_\mathrm{DH}. \tag{II.2.8}$$

One may solve Eq. (II.2.3) by identifying a similarity-variable that yields solutions of the form $\tilde{\rho}(S[\tilde{z},\tilde{\Sigma}])$ where $S = f(b[\tilde{z}]\times g[\tilde{\Sigma}])$. Inspired by the Debye-Hückel (DH) solution given by Eq. (II.2.7), we posit $b = \exp(-\tilde{z})$ and substitute $\tilde{\rho} = f\left(g[\tilde{\Sigma};...]\times\exp(-\tilde{z})\right)$ in Eq. (II.2.3) to arrive at

$$-\left(\frac{\mathrm{d}f}{\mathrm{d}S}\right)ge^{-\tilde{z}} = \left(\frac{\mathrm{d}f}{\mathrm{d}S}\right)\left(\frac{\mathrm{d}g}{\mathrm{d}\tilde{\Sigma}}\tilde{\rho}(0,\tilde{\Sigma};...)\right)e^{-\tilde{z}}. \tag{II.2.9}$$

Noting $\mathrm{d}g/g = \mathrm{d}\ln g$, we first add and subtract the known form for $\tilde{\rho}_{\mathrm{DH}}(0,\tilde{\Sigma})$ described in Eq. (II.2.6) before evaluating

$$-\int \mathrm{d}\ln g = \int \frac{\mathrm{d}\hat{\Sigma}}{\tilde{\rho}_{\mathrm{DH}}(0,\hat{\Sigma})} + \int\left(\frac{1}{\tilde{\rho}(0,\hat{\Sigma})} - \frac{1}{\tilde{\rho}_{\mathrm{DH}}(0,\hat{\Sigma})}\right)\mathrm{d}\hat{\Sigma}\,, \tag{II.2.10}$$

which converges for all $\tilde{\Sigma}$.

Beyond the linear regime, the Gouy-Chapman theory yields an analytical similarity variable that measures the mean-field strength between an electrified plate and uncorrelated point-sized ions. Inserting the GC contact expression [Henderson, 1983],

$$\tilde{\rho}_{\mathrm{GC}}(0,\tilde{\Sigma}) = -\tilde{\Sigma}\sqrt{1+(\tilde{\Sigma}/2)^2}\,, \tag{II.2.11}$$

into Eq. (II.2.3) gives

$$S_{\mathrm{GC}} = 4e^{-\tilde{z}}\left[\sqrt{1-(2/\tilde{\Sigma})^2}-(2/\tilde{\Sigma})\right] = \left(\frac{2}{1+\sqrt{1+(\tilde{\Sigma}/2)^2}}\right)\tilde{\Sigma}e^{-\tilde{z}}\,, \tag{II.2.12}$$

that reduces to S_{DH} for $\tilde{\Sigma}\ll 1$. Notably, S_{GC} varies continuously between two limiting behaviors: (i) $S_{\mathrm{GC}}\to S_{\mathrm{DH}}\to 0$ far from weakly charged surfaces ($\tilde{z}\to\infty,\tilde{\Sigma}\to 0$), and (ii) $S_{\mathrm{GC}}\to 4$ near strongly charged surfaces ($\tilde{z}\to 0,\tilde{\Sigma}\to\infty$).

To determine the GC free charge density as a function of the GC similarity variable $\tilde{\rho}_{\mathrm{GC}}(S_{\mathrm{GC}}) = \rho_{\mathrm{GC}}/2qen^{\mathrm{B}}$, use $(1/2)[(\phi')^2]' = \phi'' = \sinh(\phi)\mathrm{d}\phi$ before integrating

Eq. (II.1.1), then solve for both the interfacial charge density $\tilde{\Sigma}$,

$$\tilde{\Sigma} = -\left.\frac{\mathrm{d}\tilde{\phi}}{\mathrm{d}\tilde{z}}\right|_{\tilde{z}=0} = 2\sinh\left(\frac{\tilde{\phi}^0}{2}\right)e^{-0}\,, \tag{II.2.13}$$

and the surface potential $\tilde{\phi}^0 = \phi^0 e/k_\mathrm{B}T = 2\sinh^{-1}(\tilde{\Sigma}/2)$. Integrate Eq. (II.1.1) a second time, substitute $\tilde{\phi}^0$, then rearrange to arrive at,

$$\tilde{\phi} = \tanh^{-1}\left(S_\mathrm{GC}/4\right). \tag{II.2.14}$$

Finally, insert Eq.(II.2.14) into Eq. (II.1.1) ,

$$\tilde{\rho}_\mathrm{GC} = -\frac{\mathrm{d}}{\mathrm{d}S_\mathrm{GC}}\left(\frac{\mathrm{d}\tilde{\phi}}{\mathrm{d}S_\mathrm{GC}}\frac{\mathrm{d}S_\mathrm{GC}}{\mathrm{d}\tilde{z}}\right)\frac{\mathrm{d}S_\mathrm{GC}}{\mathrm{d}\tilde{z}} = -\frac{16S_\mathrm{GC}(16+S_\mathrm{GC}^2)}{(16-S_\mathrm{GC}^2)^2}. \tag{II.2.15}$$

The GC free charge density thus diverges in the $S_\mathrm{GC} \to 4$ limit, $\tilde{\rho}_\mathrm{GC} \to \tilde{\rho}_\mathrm{DH}$ for $S_\mathrm{GC} \ll 1$, and approaches electroneutrality ($\tilde{\rho}_\mathrm{GC} \to 0$) as $S_\mathrm{GC} \to 0$.

Similarity variables from modified local-density approximations may require numerical methods to determine the often more complicated forms of $\tilde{\rho} = \tilde{\rho}(S(\tilde{z}, \tilde{\Sigma}; \Phi^\mathrm{B}, \sigma/\lambda_\mathrm{D}, ...)$. For instance, one can derive a modified mean-field theory that locally accounts for excluded volume effects between equisized ions using the Carnahan-Starling (CS) equation of state. The CS model describes a hard-sphere liquid with the following excess chemical potential

$$\frac{\mu_\mathrm{CS}^\mathrm{ex}}{k_\mathrm{B}T} = \frac{\Phi(8-9\Phi+3\Phi^2)}{(1-\Phi)^3}\,, \tag{II.2.16}$$

that depends on the local volume fraction of ions

$$\Phi(z) = \pi\sigma^3/6\sum n_i. \tag{II.2.17}$$

When used to describe repulsive, *e.g.* WCA particles, the value of Φ depends on an effective hard-sphere diameter assigned to the ions; we find that $\sigma \approx 0.90\sigma_\mathrm{WCA}$ does

an excellent job of reproducing actual chemical potentials calculated using the particle insertion technique. It is numerically easier and mathematically equivalent to solve for the case of a single electrode with the following chemical potential,

$$\tilde{\mu}_i[\tilde{\phi}, \tilde{n}_i] = \frac{\mu_i - \mu^{\mathrm{B}}}{k_{\mathrm{B}}T} = \ln(\tilde{n}_i) \pm q\tilde{\phi} + \tilde{\mu}^{\mathrm{ex}}_{\mathrm{CS}}[\Phi^{\mathrm{B}}(\tilde{n}_+ + \tilde{n}_-)/2] \equiv 0. \tag{II.2.18}$$

Now we express $\tilde{n}_-$ in terms of $\tilde{n}_+$ and $\tilde{\phi}$ by subtracting $\tilde{\mu}_+$ from $\tilde{\mu}_-$ and rearranging for $\tilde{n}_-$,

$$\tilde{n}_- = \tilde{n}_+ \exp(2q\tilde{\phi}). \tag{II.2.19}$$

Inserting Eq. (II.2.19) into Poisson's equation $\phi'' = -\tilde{\rho}$, we obtain,

$$\tilde{\phi}'' = \tilde{n}_+ \left(\exp(2q\tilde{\phi}) - 1\right)/2\,, \tag{II.2.20}$$

which is subject to boundary conditions at the electrode

$$\tilde{\phi}(\tilde{z} = 0) = \tilde{\phi}^0\,, \tag{II.2.21}$$

(or $\tilde{\phi}(L/\lambda_{\mathrm{D}}) = \tilde{\phi}^0_-$ for two electrodes) and in the bulk

$$\tilde{\phi}\,(\tilde{z} \to \infty) \to 0. \tag{II.2.22}$$

In practice for numerical reasons, we replace the second boundary condition in Eq. (II.2.22) at infinite distances with $\tilde{\phi}\,(L/2\lambda_{\mathrm{D}}) = 0$. We solve for $\tilde{n}_+(\Phi)$ by demanding that Eq. (II.2.19) be constant in space (a condition for equilbrium) and inserting into Eq. (II.2.18). Then, that is used with (II.2.20) and the boundary conditions to solve a single ODE, not coupled ones. In the case of $\Phi^{\mathrm{B}} = 0$, Eqns. (II.2.16) and (II.2.20) return their point-sized (Gouy-Chapman) expressions as expected. Numerically solving these equations, we then determine $\tilde{\rho}_{\mathrm{CS}}(0, \tilde{\Sigma})$ that is used to compute $S_{\mathrm{CS}}(\tilde{z}, \tilde{\Sigma}, \Phi^{\mathrm{B}})$.

II.3 Testing Electric Double Layers for a Suitable Local-density Approximation Without Making Assumptions

Having derived Eq. (II.2.3) — a general, model-free condition that must be satisfied for any planar EDL describable by LDAs — we now use molecular dynamics to explicitly simulate ions within fully formed EDLs for which LDA physics is by no means guaranteed. To focus on the general applicability of our results, we employ the simplest model for ions that captures many-body interactions, rather than using force fields and characteristics specific to a particular electrolyte system. Specifically, we use LAMMPS [Plimpton, 1995] to simulate Primitive Model (PM) electrolytes: charge-centered Weeks-Chandler-Andersen [Weeks et al., 1971] ions of diameter σ_{WCA} and charge $\pm qe$ in an implicit Langevin solvent [Schneider and Stoll, 1978] with constant permittivity ε, bound by uniformly charged repulsive 9/3 surfaces separated by a distance L in a xy-periodic system. Defining system parameters gives three physical length scales: the Bjerrum length λ_{B} that reflects ion valence, permittivity and thermal energy; the screening length λ_{D}, which is measured from equilibrated bulk ion concentrations; and the effective hard-core ion diameter $\sigma \approx 0.90\sigma_{\mathrm{WCA}}$ that sets the bulk volume fraction $\Phi^{\mathrm{B}} = \sigma^3/(24\lambda_{\mathrm{B}}\lambda_{\mathrm{D}}^2)$. We choose the system size L to be large enough by comparison to be irrelevant. Nondimensionalizing lengths by λ_{D} reveals any PM electrolyte/surface to be uniquely specified by three dimensionless parameters: Φ^{B}, $\lambda_{\mathrm{B}}/\lambda_{\mathrm{D}}$, and $\Sigma/\Sigma_{\mathrm{ref}}$. We list parameters from all PM simulations in Section II.5.

For each PM electrolyte $\{\Phi^{\mathrm{B}};\ \lambda_{\mathrm{B}}/\lambda_{\mathrm{D}}\}$ and surface charge $\tilde{\Sigma}$, we equilibrate $\mathcal{O}$(800-1400) ions for five million MD time steps, then evenly collect fifty thousand snapshots over fifty million steps, requiring 50-100 CPU hours per run. We then measure the time-averaged free charge density and effective local surface charge vs. distance $\tilde{z}$ from the wall, and regression fit $\tilde{\rho}_{\mathrm{PM}}(\tilde{z})$ versus $\tilde{\Sigma}_{\mathrm{eff}}(\tilde{z})$ to a second order polynomial. Having regression fit the Primitive Model profiles with $\tilde{\rho}_{\mathrm{PM}}(0,\tilde{\Sigma}) = a_1\tilde{\Sigma} + a_2\tilde{\Sigma}^2$, we then use (II.2.4) to obtain PM similarity variables of the form

$$S_{\mathrm{PM}}(\tilde{z},\tilde{\Sigma}) = e^{-\tilde{z}}\left(a_1 + a_2\tilde{\Sigma}\right)^{1/a_1}\tilde{\Sigma}^{-(1+a_1)/a_1}. \tag{II.3.1}$$

If any viable LDA theory exists for that electrolyte $\{\Phi^{\mathrm{B}};\ \tilde{\lambda}_{\mathrm{B}}\}$, then computed $\tilde{\rho}_{\mathrm{PM}}$ profiles, re-plotted against S_{PM}, must collapse onto a master curve.

Figure II.2 shows EDL profiles computed in seven distinct PM electrolytes with ions from low to moderate valence ($0.05 \lesssim \lambda_{\mathrm{B}}/\lambda_{\mathrm{D}} \lesssim 1$) and very low volume fractions $\Phi^{\mathrm{B}} \leq 8\times10^{-4}$, each for 100 distinct surface charge densities ($0 \leq \tilde{\Sigma} \lesssim 10$) and measured at 250 distinct positions. Under these dilute conditions, one would expect the PB/GC theory to hold, especially at small $\tilde{\sigma}$, $\tilde{\lambda}_{\mathrm{B}}$, and $\tilde{\Sigma}$. Indeed, $\tilde{\rho}_{\mathrm{PM}}$ collapses when plotted against S_{PM} (Fig. II.2a), and also against $\tilde{\Sigma}_{\mathrm{eff}}$ (Fig. II.2b). Furthermore, even *different* electrolytes collapse onto the *same* curve, irrespective of the specific electrolyte properties $\{\Phi^{\mathrm{B}};\ \tilde{\lambda}_{\mathrm{B}}\}$, as is true for GC theory. In fact, the GC similarity variable S_{GC} (II.2.12) captures the observed universal profile very well (Fig. II.2c), and closely matches the computed, model-free S_{PM} (Fig. II.2d).

Next, we simulate semi-dilute electrolytes with weakly-charged but moderately sized PM ions ($\lambda_{\mathrm{B}} \ll \sigma < \lambda_{\mathrm{D}}$), where we suspect GC will fail due to finite-sized effects. We

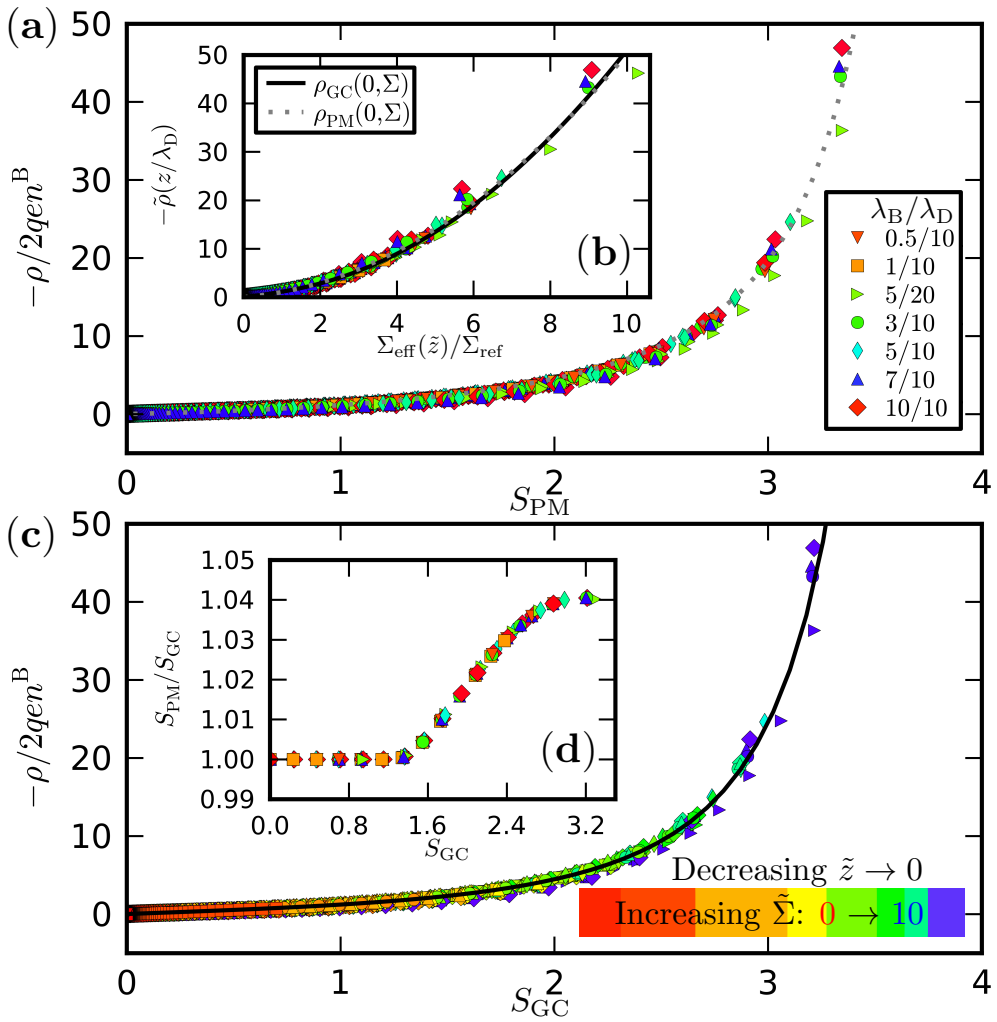

Figure II.2: MD simulations of dilute Primitive Model electrolytes ($\Phi^{\mathrm{B}} \leq 8 \times 10^{-4}$) show underlying LDA behavior. (a) For a wide range of conditions, free charge density profiles all collapse onto a universal curve, when plotted against a similarity coordinate S_{PM}, which is derived from (II.2.4) using $\rho_{\mathrm{PM}}(0, \Sigma)$ obtained from simulation data. (b) The charge density $\rho(z, \Sigma)$ collapses when plotted against $\Sigma_{\mathrm{eff}}(z)$, which is itself indicative of LDA behavior. (c) The Gouy-Chapman similarity variable (II.2.12) also collapses simulation data well. (d) The similarity variables S_{PM} and S_{GC}, independently-derived, are practically indistinguishable for $S_{\mathrm{GC}} \leq 0.4$, and differ by less than 4% for $1.6 < S_{\mathrm{GC}} \lesssim 3.2$.

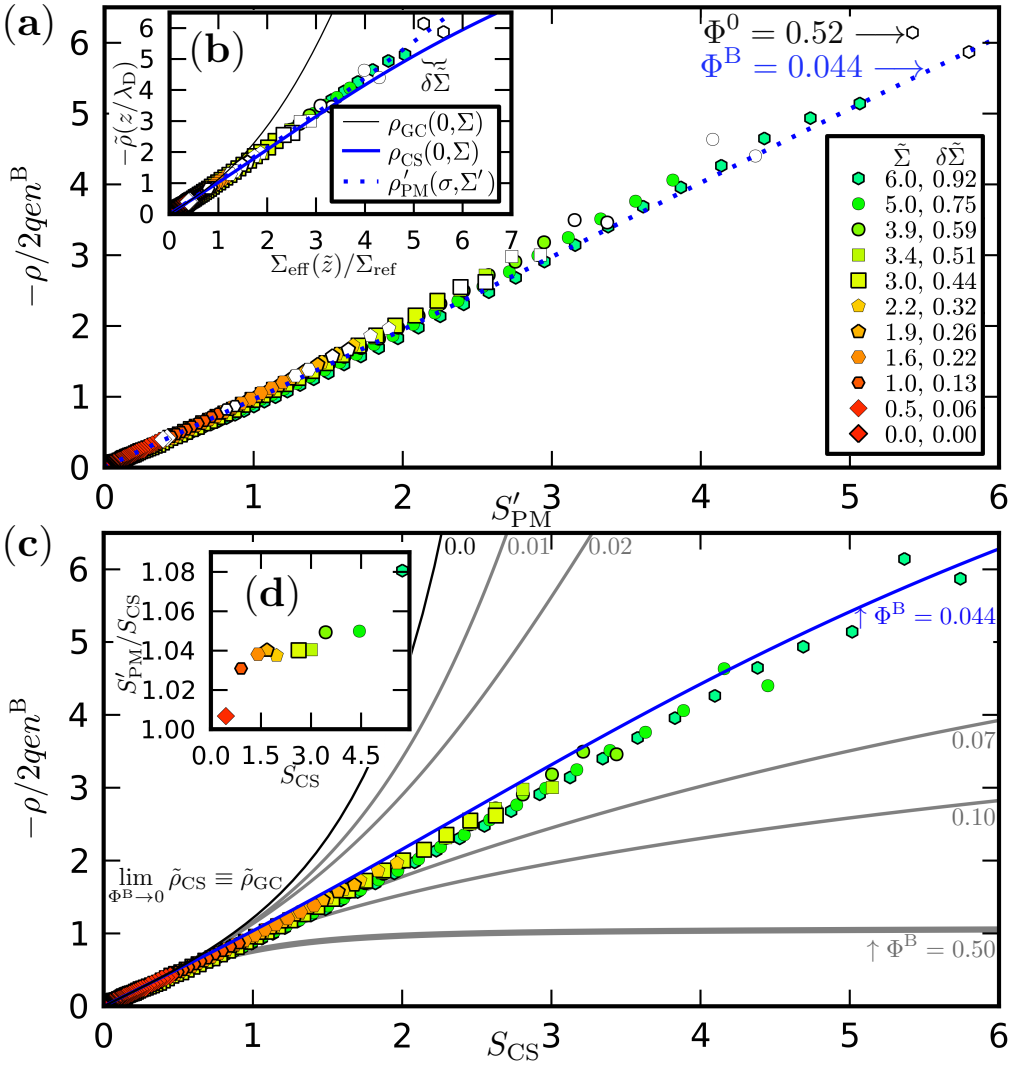

Figure II.3: MD simulations of PM electrolytes with large ($\sigma/\lambda_D \simeq 3/15$), weakly charged ($\lambda_B/\lambda_D \simeq 0.1/15$) ions at constant bulk volume fraction $\bar{\Phi}^B = 0.044 \pm 0.001$ show LDA behavior, beyond a surface monolayer (with packing fraction Φ^0). (a) Charge density profiles for various surface charge densities $\tilde{\Sigma}$ collapse onto a single curve when plotted against S'_{PM}, obtained by evaluating (II.2.4) using measured data. (b) EDL density profiles collapse when plotted against $\tilde{\Sigma}_{eff}$ that is reduced by the measured charge density of the monolayer $\delta\tilde{\Sigma}$. (c) The similarity coordinate S_{CS} generated using the Carnahan-Starling LDA approach also collapses simulated density profiles beyond the correlated region. A one-parameter (Φ^B) family of universal EDL curves is generated from (II.2.4)-(II.2.5) using the CS-LDA approach. (d) The theoretical S_{CS} matches the measured S'_{PM} to within 10% for these simulations.

then determine whether such non-GC EDLs can nonetheless be captured by LDAs using our model-free method (Fig. II.3). For these ions, specific wall-ion interactions drive surface ion monolayers to form at high $\tilde{\Sigma}$ and/or Φ^{B}. Since our model-free test holds outside the range of specific wall-ion interactions, we define '$\tilde{z} = 0$' in Eq. (II.2.4) to lie beyond the surface ion monolayer, $\tilde{z} > \sigma/\lambda_{\mathrm{D}}$, and adopt a reduced applied surface charge density

$$\tilde{\Sigma}' = \tilde{\Sigma} - \delta\tilde{\Sigma}\,, \tag{II.3.2}$$

where

$$\delta\tilde{\Sigma} = -\int_0^{\sigma/\lambda_{\mathrm{D}}} \tilde{\rho}_{\mathrm{PM}} \mathrm{d}\hat{z}\,, \tag{II.3.3}$$

corrects for the monolayer charge. Indeed, Fig. II.3b shows density profiles $\tilde{\rho}'_{\mathrm{PM}}(\tilde{z} = \tilde{\sigma}, \tilde{\Sigma}'; \bar{\Phi}^{\mathrm{B}} = 0.044)$ for eleven simulations that collapse onto a single curve when plotted against $\tilde{\Sigma}_{\mathrm{eff}}$ and the similarity variable S'_{PM}. Despite GC breakdown, our test reveals EDLs in these electrolytes to obey some underlying LDA model.

Motivated by the existence of a viable LDA theory, we consider the Carnahan-Starling [Carnahan and Starling, 1969] (CS) hard-sphere model that accounts for excess hard-sphere repulsions $\mu^{\mathrm{ex}}_{\mathrm{CS}}(\Phi)$ using the local volume fraction [Bazant et al., 2009, Russel et al., 1989] of same sized ions. Evaluating the computed contact expression $\tilde{\rho}_{\mathrm{CS}}(\tilde{z} = 0, \tilde{\Sigma}; \Phi^{\mathrm{B}})$, we calculate $S_{\mathrm{CS}}(\tilde{z}, \tilde{\Sigma}; \Phi^{\mathrm{B}})$ via Eq. (II.2.4), and generate a family of universal curves for different Φ^{B} in Fig. II.3c. The CS-LDA correctly produces the universal curve onto which the EDLs simulated with $\bar{\Phi}^{\mathrm{B}} \simeq 0.044$ collapse against $\tilde{\Sigma}_{\mathrm{eff}}$ (Fig. II.3b) — but only up to a point, beyond which collapse is lost due to non-local ordering adjacent to the surface. The CS-LDA approach misses the oscillatory portions of PM EDLs, as

any LDA would, but decently captures the mean-field strength of steric interactions in non-correlated EDL regimes.

II.4 Conclusion

In summary, we have presented a general and powerful formalism to identify and elucidate local-density approximation behavior in planar EDLs, following a simple observation: LDA ions do not know the interface location. Our model-free approach enables EDL profiles – whether simulated or measured – to be directly analyzed, and to determine whether any LDA can possibly succeed. In the regimes where the computed S does not collapse the EDL profiles, any search for a LDA will be fruitless.

In explicit MD simulations of GC-like electrolytes, our approach generated a similarity variable that successfully collapsed a wide range of simulated EDLs onto a universal curve that matched the GC prediction. In electrolytes where GC fails due to steric repulsion between ions, our approach collapses measured EDL profiles onto non-GC universal profiles — but only up to a point, beyond which collapse is lost due to non-local ordering adjacent to the electrode. A modified PBE that treats finite-size interactions using the Carnahan-Starling equation of state captured this data particularly well. More generally, our approach immediately reveals whether it is possible for any LDA theory to predict measured (or simulated) profiles, and plots like Figs. II.2b and II.3b inform when and whether one should pursue LDA treatments at all.

Lastly, the model-free test holds for planar EDLs, which are (fortunately) the easiest to compute and measure. Irrespective, the results of the approach presented here hold

for more general geometries. We expect that once a LDA is revealed to be possible for a given electrolyte, and the corresponding $\mu_{\pm}^{\rm ex}(n_i)$ determined, the modified PBE derived using the appropriate LDA (Eqs. II.1.1-II.1.2) should hold as a three-dimensional PDE, valid for more general geometries.

II.5 Appendix: Simulation Details

In the tables below, we list parameters from all Primitive Model simulations with total number of ions $N_{\rm tot}$ of diameter $\sigma_{\rm WCA}$ and Bjerrum length $\lambda_{\rm B}$; measured screening length $\lambda_{\rm D}$; and electrode charge density Σ as defined in the text. In the case of monovalent ions ($|q_{\pm}| = 1$) in an aqueous electrolyte at room temperature, the Bjerrum length is $\lambda_{\rm B} = 0.7$ nm. For instance, the square orange markers in Figure 2 represent simulations with $\sigma_{\rm WCA}/\lambda_{\rm B} = 1/1$ (meaning the diameter of the solvated ions is 0.7 nm) and $\lambda_{\rm B}/\lambda_{\rm D} = 1/10$. The solvated ion diameters would correspond to NaCl ions with screening length $\lambda_{\rm D} \approx 7$ nm, bulk ion concentrations $[{\rm Na}_+] = [{\rm Cl}_-] = \rho^{\rm B}$ where $\rho^{\rm B} \equiv (8\pi\lambda_{\rm B}\lambda_{\rm D}^2)^{-1}$ is

$$\rho^{\rm B} = \left(\frac{10^{30}}{8\pi \times 7{\rm m} \times 70^2{\rm m}^2}\right)\left(\frac{{\rm m}^3}{10^3{\rm L}}\right)\left(\frac{\rm mole}{6.022\times 10^{23}}\right) \approx 2\times 10^{-3}\ {\rm M}\,, \qquad \text{(II.5.1)}$$

and ionic strength to be $(q_{\rm Na}^2\rho_{\rm Na}^{\rm B} + q_{\rm Cl}^2\rho_{\rm Cl}^{\rm B})/2 \approx 2$ mM. The total bulk volume fraction of ions is

$$\Phi^{\rm B} = \frac{\pi\sigma^3}{6}2\rho^{\rm B} \equiv \frac{\sigma^3}{24\lambda_{\rm B}\lambda_{\rm D}^2} = \left(\frac{(0.90\times 7)^3{\rm m}^3\times 10^{-30}}{24(7{\rm m}\times 10^{-10})(70^2{\rm m}^2\times 10^{-20})}\right) \approx 3\times 10^{-4}. \qquad \text{(II.5.2)}$$

Table II.1: Figure II.2 PM Results: $\sigma_{\mathrm{WCA}}/\lambda_{\mathrm{B}} = 1/0.5$

Σ	λ_{D}	N_{tot}	$\phi^0 e/k_{\mathrm{B}}T$
0.0000	9.977	800	0.00
0.0040	9.970	802	0.27
0.0080	10.096	802	0.54
0.0122	10.010	806	0.80
0.0166	9.982	808	1.08
0.0212	10.012	816	1.36
0.0262	9.990	818	1.65
0.0315	9.989	824	1.88
0.0374	9.993	838	2.19
0.0510	10.016	858	2.76
0.0589	10.052	870	3.06
0.0678	10.053	884	3.32
0.0888	9.976	924	3.94
0.1154	9.953	980	4.59

Table II.2: Figure II.2 PM Results: $\sigma_{\mathrm{WCA}}/\lambda_{\mathrm{B}} = 1/1$

Σ	λ_{D}	N_{tot}	$\phi^0 e/k_{\mathrm{B}}T$
0.0000	9.986	800	0.01
0.0020	10.019	802	0.30
0.0040	9.994	802	0.51
0.0061	10.012	806	0.82
0.0083	10.027	808	1.10
0.0106	9.920	816	1.35
0.0131	9.900	820	1.65
0.0158	9.971	830	1.91
0.0187	9.923	840	2.16
0.0255	9.939	864	2.75
0.0295	9.940	882	2.98
0.0339	9.863	908	3.27

Table II.3: Figure II.2 PM Results: $\sigma_{\mathrm{WCA}}/\lambda_{\mathrm{B}} = 2/5$

Σ	λ_{D}	N_{tot}	$\phi^0 e/k_{\mathrm{B}}T$
0.0000	20.073	800	0.02
0.0004	20.084	806	0.53
0.0008	19.913	816	1.05
0.0013	19.854	838	1.57
0.0019	19.809	870	2.09
0.0026	19.949	914	2.59
0.0034	20.074	972	3.12
0.0044	20.055	1050	3.63
0.0096	20.184	1454	5.17

Table II.4: Figure II.2 PM Results: $\sigma_{\mathrm{WCA}}/\lambda_{\mathrm{B}} = 1/3$

Σ	λ_{D}	N_{tot}	$\phi^0 e/k_{\mathrm{B}}T$
0.0000	10.004	800	0.00
0.0007	10.002	802	0.28
0.0013	9.951	802	0.59
0.0020	9.953	806	0.86
0.0028	9.943	808	1.10
0.0035	9.999	816	1.38
0.0044	9.967	818	1.65
0.0053	10.005	824	1.94
0.0062	10.012	838	2.18
0.0073	10.024	848	2.46
0.0085	9.999	858	2.73
0.0098	10.045	870	3.00
0.0113	10.004	884	3.28
0.0129	10.036	902	3.55
0.0148	9.966	924	3.84
0.0192	9.865	980	4.41
0.0321	10.038	1128	5.63

Table II.5: Figure II.2 PM Results: $\sigma_{\mathrm{WCA}}/\lambda_{\mathrm{B}} = 1/5$

Σ	λ_{D}	N_{tot}	$\phi^0 e/k_{\mathrm{B}}T$
0.0000	10.239	800	0.00
0.0004	10.211	802	0.30
0.0008	10.248	802	0.56
0.0012	10.192	806	0.82
0.0016	10.261	810	1.12
0.0021	10.293	812	1.39
0.0026	10.348	812	1.68
0.0031	10.336	812	1.96
0.0037	10.481	812	2.20
0.0050	10.573	812	2.84
0.0058	10.690	812	3.10
0.0066	10.890	812	3.35
0.0087	11.147	812	3.97
0.0113	11.570	812	4.62

Table II.6: Figure II.2 PM Results: $\sigma_{\mathrm{WCA}}/\lambda_{\mathrm{B}} = 1/7$

Σ	λ_{D}	N_{tot}	$\phi^0 e/k_{\mathrm{B}}T$
0.0000	9.993	800	0.00
0.0003	10.000	802	0.31
0.0006	10.009	802	0.60
0.0009	9.977	806	0.89
0.0012	10.013	808	1.17
0.0015	10.018	816	1.47
0.0019	10.006	818	1.75
0.0022	10.031	824	2.01
0.0027	9.980	838	2.30
0.0031	9.997	848	2.53
0.0036	10.068	858	2.80
0.0042	10.046	870	3.04
0.0048	10.095	884	3.31
0.0056	10.112	902	3.58
0.0063	10.045	924	3.84
0.0083	9.980	980	4.32
0.0138	10.029	1128	5.37

Table II.7: Figure II.2 PM Results: $\sigma_{\mathrm{WCA}}/\lambda_{\mathrm{B}} = 1/10$

Σ	λ_{D}	N_{tot}	$\phi^0 e/k_{\mathrm{B}}T$
0.0000	9.938	800	0.03
0.0002	10.060	802	0.37
0.0004	9.951	802	0.75
0.0006	10.015	806	1.14
0.0008	10.042	808	1.47
0.0011	9.963	816	1.84
0.0013	10.033	818	2.10
0.0016	10.030	824	2.39
0.0019	9.993	838	2.68
0.0022	10.107	848	2.98
0.0026	10.081	858	3.29
0.0029	10.098	870	3.49
0.0034	10.111	884	3.78
0.0039	10.252	902	4.02
0.0044	10.137	924	4.26
0.0058	10.027	980	4.76
0.0096	10.241	1128	5.74

Table II.8: Figure II.3 PM Results: $\sigma_{\mathrm{WCA}}/\lambda_{\mathrm{B}} = 3/0.10$

Σ	λ_{D}	N_{tot}	$\phi^0 e/k_{\mathrm{B}}T$
0.3848	14.799	1312	4.55
0.2961	14.739	1232	3.57
0.2259	14.872	1162	2.90
0.1964	14.769	1136	2.56
0.1700	14.802	1104	2.25
0.1247	14.847	1066	1.73
0.1051	14.923	1048	1.53
0.0872	14.941	1034	1.27
0.0553	14.939	1016	0.83
0.0268	14.961	1004	0.39
0.0000	15.027	1000	0.00

Chapter III

Characterizing Diffuse and Correlated Electric Double Layers with Finite-sized Ions

In Chapter II, we show all mean-field electric double layers derived within the local-density framework obey universal self-similar scaling that yield strictly monotonic density profiles [Giera et al., 2013]. Consequently, planar LDA EDL profiles for a given electrolyte collapse onto a single, master curve when plotted against "similarity coordinates" that are a combination of system variables. Without assumptions or considering any specific LDA model, it is straightforward to analyze empirically or computationally-derived EDL profiles and derive similarity coordinates directly from free charge density contact value expressions. The model-free test for applicability of LDAs determines whether the LDA approach can possibly succeed, but not which LDA is appropriate. Here, we compare

predictions of several common LDAs against extensive Molecular Dynamics simulations that incorporate steric interactions.

III.1 Motivation

One of the most important physical interactions to capture is the excluded volume of ions that arise in ionic EDLs [Bazant et al., 2009]. We use a variant of the Primitive Model that treats the ions as charged Weeks-Chandler-Andersen [Weeks et al., 1971] spheres in an implicit solvent. We examine the Bikerman [Bikerman, 1942] (Bik) and Carnahan-Starling [Bazant et al., 2009] (CS) LDA models that incorporate excess terms in the chemical potential to account for the finite-size of ions in a continuum solvent. The Bik-LDA is a long-standing lattice-gas model with an analytical free charge density [Bazant et al., 2009, Kornyshev, 2007]. It assumes ions occupy a cubic lattice where the empty sites, which represent solvent, saturate with ions at large applied electrode charge densities. The CS-LDA adopts the Carnahan-Starling equation of state [Carnahan and Starling, 1969] that models ions as a structureless hard-sphere fluid. We compare extensive PM simulations against the Bik- and CS-LDA to illustrate where they work and explain their breakdown mechanisms.

We find the CS equation of state accurately predicts the measured chemical potential components from our PM simulations over a wide range of electrolytes and volume fractions in near-bulk regions far from the electrode, whereas the Bikerman model fails at all but infinitesimal volume fractions. Consequently, the resulting CS-LDA model outperforms the Bik-LDA when predicting the total capacitance, ideal chemical potential

of ions, voltage, and excluded volume chemical potential profiles. Since the LDA framework permits only monotonic density profiles [Paasch and Übensee, 1982, Attard, 1996], these LDAs fail to capture oscillatory portions of PM EDLs that arise from correlated ion packing, as could be expected of any LDA. Independent of any specific LDA, we define a correlation length, ℓ_{cor}, that gives a useful diagnostic of EDL behavior near the breakdown of LDAs. We examine the PM EDLs to identify the thickness of the correlated region, ℓ_{cor}, beyond which non-local effects are negligible where the general LDA approach should hold. We then demonstrate where and why these LDAs fail by evaluating how ℓ_{cor} depends on bulk volume fraction and applied charge density. At distances farther than ℓ_{cor} from the electrode, the CS-LDA accurately predicts PM EDL profiles from a wide range of electrode charge densities and bulk volume fractions.

III.2 Computing the Chemical Potential from Primitive Model Electrolytes

We perform 2D periodic MD simulations using LAMMPS [Plimpton, 1995] to compute Primitive Model electric double layers. The system is maintained at constant temperature with a Langevin thermostat [Schneider and Stoll, 1978], which approximates the dynamics due to an implicit solvent. Charge-centered WCA ions with characteristic energy $\epsilon_{\text{WCA}} = k_{\text{B}}T$ are confined within a distance L between two repulsive walls with uniform charge density $\pm\Sigma$, thickness δ_{w}, and characteristic energy $\epsilon_{\text{w}} = k_{\text{B}}T$ via Eqs. (I.3.28-I.3.34). We evaluate the Coulomb potential with a PPPM slab Ewald sum [Hockney and

Eastwood, 1989] with the default accuracy of 10^{-4}. We choose the periodic dimensions and spacing between the electrodes to exceed all other length scales to be irrelevant to predicted behaviors. For each PM electrolyte $\{\Phi_{\rm B};\ \lambda_{\rm B}/\lambda_{\rm D}\}$ and surface charge $\tilde{\Sigma}$, we equilibrate $\mathcal{O}$(800-1400) ions for 5 million time steps, then collect 50 thousand snapshots over 50 million steps, requiring 50-100 CPU hours per run. We then measure time-averaged ion densities, voltages, and spatial profiles of the excluded volume excess chemical potential using Widom insertion [Widom, 1978, Frenkel and Smit, 2001] using 250-500 million total test insertions per simulation.

Unlike local-density approximation EDLs described by Eqs. (I.3.4) and (I.3.6), we configure the PM to account explicitly for the pairwise interactions in Eq. (I.3.30) that can give rise to non-mean-field behavior. In molecular simulations, the chemical potential components can be computed directly and independently using particle coordinates from PM EDLs. By symmetry, profiles will be uniform in the periodic x- and y-dimensions. At equilibrium, the reduced ion density at each instant is given by

$$\tilde{n}^i(\tilde{z}) \equiv \frac{n^i(\tilde{z})}{n_{\rm B,PM}} = \frac{1}{n_{\rm B,PM}} \sum_i^{\pm} \frac{\delta_{\rm Dirac}[\tilde{z} - \tilde{z}^i]}{A}\,, \tag{III.2.1}$$

where A is electrode area, $\delta_{\rm Dirac}$ is the Dirac delta-function, and the bulk density is

$$n_{\rm PM,B} = \left\langle n^{\pm} \left(\frac{\tilde{L}-1}{2} \le \tilde{z}_{\rm B} \le \frac{\tilde{L}+1}{2} \right) \right\rangle. \tag{III.2.2}$$

is average value in the bulk for all 50 thousand snapshots. At each snapshot, the free charge density along the $\tilde{z}$-direction is

$$\tilde{\rho}(\tilde{z}) \equiv \frac{\rho}{2en_{\rm PM,B}} = \frac{1}{2} \sum_i^{N^i} q^i \tilde{n}^i(\tilde{z}). \tag{III.2.3}$$

The instantaneous voltage is calculated using Eqs. (I.3.6) and (III.2.3)

$$\tilde{\phi}(\tilde{z}) \equiv \frac{\phi - \phi_{\mathrm{B}}}{\phi_{\mathrm{T}}} = -\frac{1}{2}\int_{\tilde{z}}^{\tilde{z}^{\mathrm{B}}} \left(\int_{\tilde{z}}^{\tilde{z}^{\mathrm{B}}} \tilde{\rho}(\hat{s}) \mathrm{d}\hat{s} \right) \mathrm{d}\hat{z}. \tag{III.2.4}$$

Equation (III.2.4) is consistent with our convention in Section I.3.1, i.e. $\tilde{\phi}(\tilde{z}^{\mathrm{B}}) \equiv 0$. In these PM EDL simulations, ions have the same size and electrodes have opposite charges. Therefore, the average total voltage dropped across either EDL is equal and opposite, i.e. $\langle\tilde{\phi}\rangle(0) = -\langle\tilde{\phi}\rangle((L + 2\delta_{\mathrm{w}})/\lambda_{\mathrm{D}})$.

Finally, we can compute the excluded volume chemical potential using Widom insertion [Widom, 1978, Frenkel and Smit, 2001]. For sufficiently large $N^{\pm}$, Eq. (I.3.25) can be expressed as

$$\left\langle \tilde{\mu}^i \right\rangle = \frac{\mu_*^{\pm}(T) - \mu_{\mathrm{B}}}{k_{\mathrm{B}}T} + \ln\left\langle n^i \right\rangle - \ln\left\langle e^{-\Delta\tilde{U}^0} \right\rangle , \tag{III.2.5}$$

which requires ensemble-averaging Boltzmann factors of the change in energy $\Delta\tilde{U}^0 = \tilde{U}(N+1,V,T) - \tilde{U}(N,V,T)$ due to a randomly-inserted test ion with charge q^0. Comparing Eqs. (I.3.3) and (III.2.5), the rightmost term with $\Delta\tilde{U}^0$ equals the electrostatic potential and excess chemical potential. In the limit $q^0 \to 0$, Eq. (I.3.27) equals Eq. (I.3.30) and accounts *only* for excluded volume – and *not* electrostatic – contributions to the chemical potential [Svensson et al., 1991].

Widom insertion is inaccurate in regimes that approach close packing, which is $\Phi^{\mathrm{HS}} \gtrsim 0.64$ for hard spheres [Berryman, 1983]. In very dense regions, inserted WCA test particles will likely overlap multiple neighboring particles so that $\Delta\tilde{U}^0 \gg 1$. The numerical precision needed to ensemble-average exponentially small Boltzmann factors requires an impractical number of test insertions. Eq. (III.2.5) can thus be used to directly measure the excluded volume chemical potential $\mu^{\mathrm{EV},\pm} = \mu^{\mathrm{EV}}$ in non-close-packed

regions if the test particle is uncharged. We use these measurements in a variety of PM EDLs to compare against LDA models for the chemical potential with bulk-like expressions that only depend on local quantities, such as the packing fraction.

III.3 Results and Discussion

Here, we assess the Bikerman and Carnahan-Starling LDAs that seek to model steric effects within diffuse regions of the EDL. Thus, LDAs break down wherever ions exhibit correlations that often occur near highly charged electrodes and/or in very concentrated regions. Before comparing how effectively the CS-LDA and Bik-LDA capture simulated PM EDL profiles, we first determine an effective hard ion size as input to these models. For the Bik-LDA, the lattice spacing is often taken to be the solvation shell diameter for ions in aqueous EDLs [Kilic et al., 2007b], fit to experimental data [Bazant et al., 2009], or is assigned by enforcing voltage-dependent expressions to distinguish between differently-sized cations and anions in the case of ionic liquids [Kornyshev, 2007]. For the CS equation of state for hard-spheres, Barker, et. al. [Barker and Henderson, 1976] prescribes an effective hard-sphere diameter σ_{eff} from the WCA diameter σ that we set in simulation

$$\sigma_{\text{eff}} = \int_0^{\sigma} \left[1 - e^{-\tilde{U}_{\text{WCA}}(r)}\right] \mathrm{d}r. \tag{III.3.1}$$

We compute σ_{eff} from Eq. (I.3.23) to calculate the CS-LDA. The effective size of the WCA ions we use in our simulations nearly is constant, e.g. $\sigma_{\text{eff}}/\sigma = 0.9048 \pm 10^{-5}$ for $(0.5 \leq \sigma \leq 6.1)$.

III.3.1 Diffuse Electric Double Layer Descriptions

Figure III.1 shows CS-LDA and Bik-LDA predictions of excluded volume chemical potential measurements taken from 343 PM EDL simulations that span weakly and strongly charged ions. Fig. III.1 also includes values obtained using fully periodic Monte Carlo simulations of uncharged WCA particles, where electrostatic correlations and wall-ordering effects are explicitly omitted, in Fig. III.1(a). We evaluate various LDA models for μ^{EV} as a function of local packing fraction within three distinct spatial regimes: in the bulk [Fig. III.1(a)], in the semi-diffuse region located between three and six WCA ion diameters from the electrode [Fig. III.1(b)], and adjacent to the electrode within three ion diameters [Fig. III.1(c)]. In all cases, CS-LDA outperforms the Bik-LDA over all volume fractions, especially in bulk-like regions and at smaller packing fractions. CS predictions are practically indistinguishable from bulk chemical potential measurements, provided we use the effective hard sphere diameter given by Eq. (III.3.1). Bik-LDA, however, consistently under-predicts and disagrees qualitatively even if we use a best fit with the effective ion size as a free parameter.

Far from the electrode, PM ions interact as they would in a purely homogenous system [Fig. III.1(a)]. CS accurately describes bulk-like excluded volume interactions in both dilute and highly-packed regimes. Closer to the wall, steric contributions cannot be described solely from the local volume fraction. In the intermediate region between the bulk and wall, the PM chemical potential no longer collapses onto CS due to emergent size-induced correlations at $\Phi \gtrsim 0.40$ [Fig. III.1(b)]. Adjacent to the electrode, both LDAs fail dramatically beyond $\Phi \gtrsim 0.10$, where ion ordering is significant at [Fig. III.1(c)]. Con-

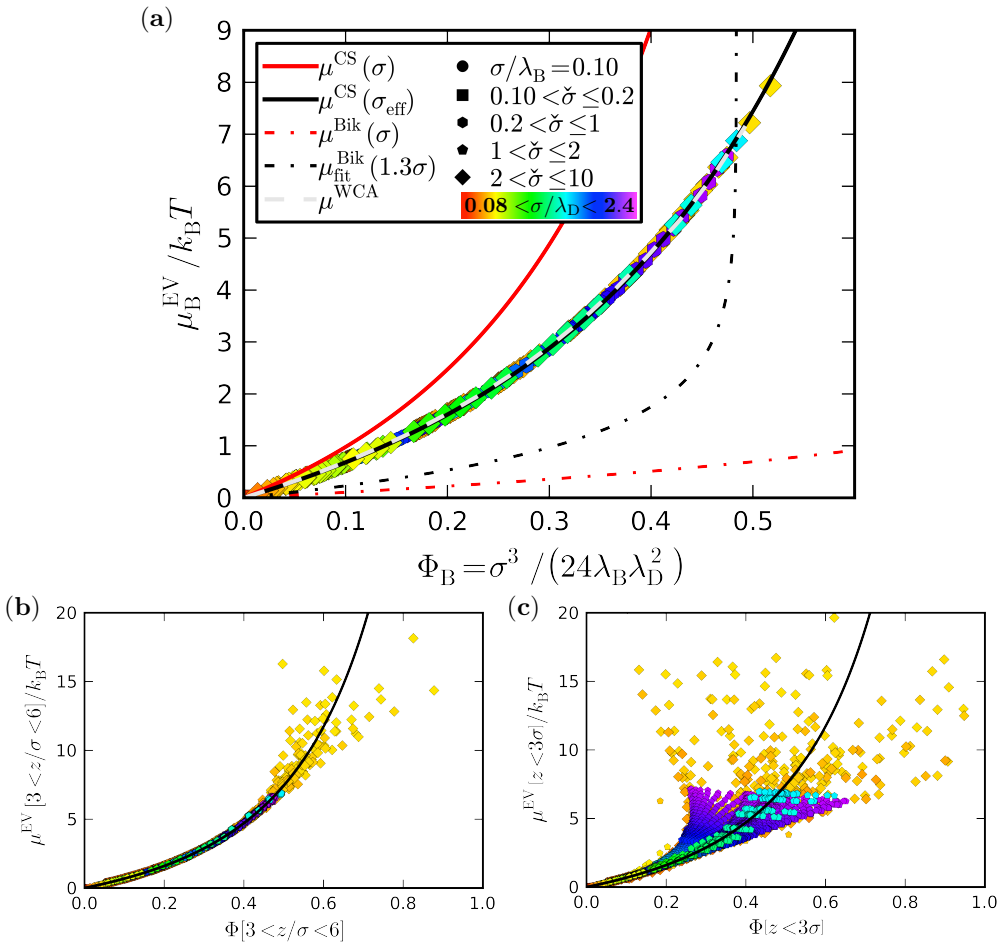

Figure III.1: Local-density approximations for the excluded volume excess chemical potential and Primitive Model measurements from weakly- and strongly-charged electric double layers $0 \leq \tilde{\Sigma} \leq 15$. (a) Bulk measurements from PM EDLs [markers] and uncharged WCA particles $\left[\mu^{\rm WCA}\right]$ collapse onto the Carnahan-Starling LDA $\left[\mu^{\rm CS}\right]$ when using the effective hard-sphere diameter from Eq. (III.3.1). The Bikerman LDA $\left[\mu^{\rm Bik}\right]$ fails at all but infinitesimal volume fractions, even when determining a best fit $\left[\mu^{\rm Bik}_{\rm fit}\right]$ with the effective lattice size as a free parameter. (b) Between 3-6 ion diameters from the electrode, CS fails to capture $\mu^{\rm EV}$ for $\Phi \gtrsim 0.40$ due to significant ion ordering. (c) Adjacent to the electrode, CS works only for semi-dilute volume fractions $\Phi \lesssim 0.10$.

sequently, we expect the CS-LDA to predict EDL profiles better in uncorrelated regimes with low to moderate volume fractions and within bulk-like regions.

Figure III.2 presents the same data as in Fig. III.1 in a heat map that shows how deviations of the excluded volume chemical potential from CS and measured bulk values vary with local volume fraction and distance from the electrode. Darker colors correspond to larger deviations from bulk chemical potential expressions. Grey regions could feasibly be described by a LDA model. Deviations beyond $\pm 3\ k_{\mathrm{B}}T$ are removed in order to give a clearer qualitative picture. Test particle insertions into the valleys (red regions) would require more energy than if inserted into a homogeneous system at the same local volume fraction. This physically corresponds to the reduced density between correlated consecutive layers of ions packed near the surface. Thus, CS cannot account for the reduced density between adjacent ion layers. Figure III.2(a) shows noticeable differences above $\Phi \gtrsim 0.15$ that exhibit oscillations at higher volume fractions that dampen with increasing distance. Figure III.2(b) is an analogous plot to Fig. III.2(a) that uses a cubic spline interpolant of bulk PM EDL measurements as a function of volume fraction instead of Eq. (I.3.23). The two heat maps are similar, which demonstrates the accuracy of the CS model. Each comparison exhibits alternating peaks and valleys, which is consistent with ion ordering in PM EDLs. The bulk chemical potential expressions in Figure III.2 fail to capture significant ion-ion correlations near the electrode.

Having compared Bik-LDA and CS-LDA models with measured excluded volume chemical potential from PM EDLs of different ion charges, sizes, and bulk concentrations, we more closely evaluate these LDAs using a smaller subset of simulations with weakly-charged ions over a range of applied electrode surface charge densities. We use these

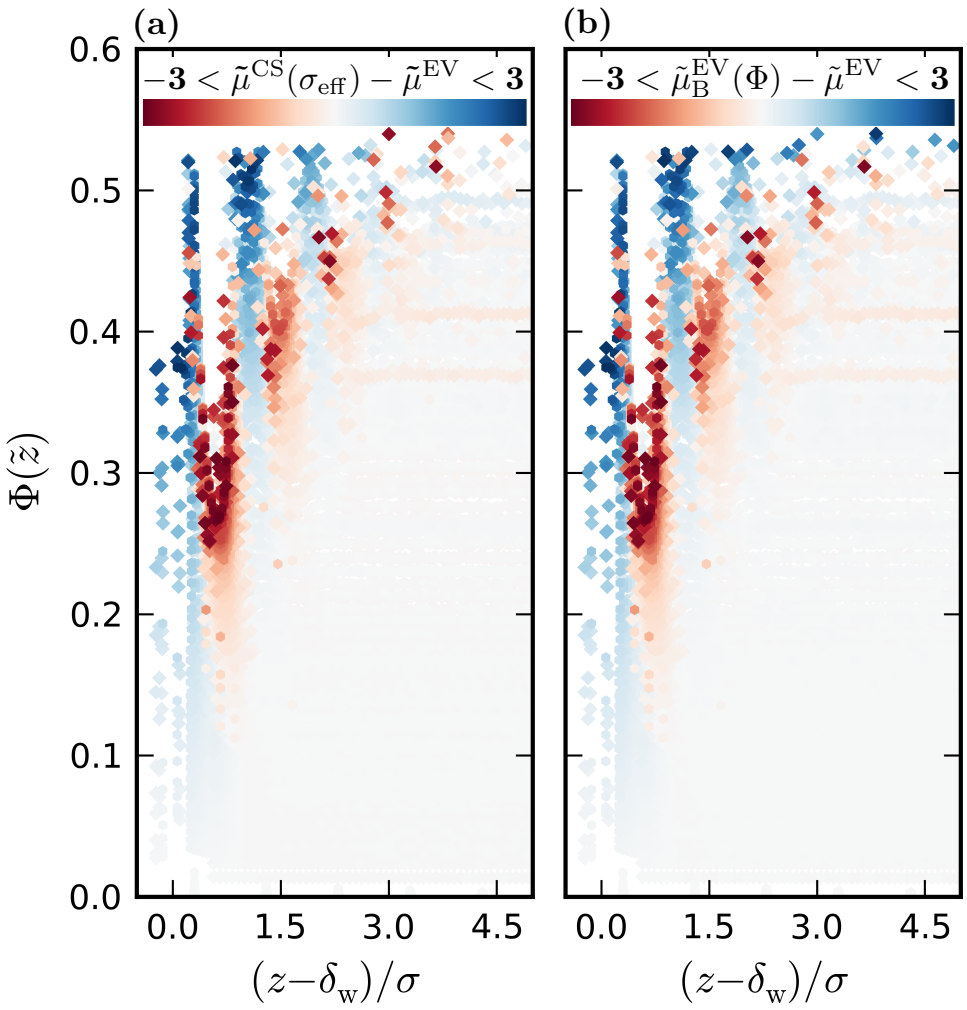

Figure III.2: Deviations of the measured local chemical potential from CS predictions (left) and measured bulk values (right) within $\pm 3\ k_{\mathrm{B}}T$ for the same data as in Figure III.1. Blue peaks correspond to the excluded volume of ion layers and red valleys signify the void space between layers. Excluded volume correlations are significant within oscillatory regions where LDA models fail.

simulations to elucidate LDA breakdown regimes as low valence PM EDLs respond to different volume fractions and applied field strengths. Since these specific LDAs neglect electrostatic correlations, we restrict PM EDLs whose ions cannot approach closer than the Bjerrum length, i.e. $\lambda_B/\sigma \ll 1$. Imposing this constraint, we simulate 8 sets of PM EDLs that differ by ion diameter: each with nearly the same bulk volume fraction within a set, but under 11 different applied surface charge densities ranging $0 \leq \tilde{\Sigma} < 7.1$. These 88 simulations have nearly identical Bjerrum lengths $\tilde{\lambda}_B = 0.0068 \pm 0.0002$ and roughly constant screening lengths $\bar{\lambda}_D = 14.6 \pm 3\%$.

Figure III.3 compares the surface charge density versus voltage predictions from the Debye-Hückel, Gouy-Chapman, Bikerman, and Carnahan-Starling local-density approximations against the Primitive Model simulation results. For EDLs with finite-sized ions, the voltage drop across PM EDLs is greater for larger bulk volume fractions at any given applied charge density. At small voltages and electrode charge densities, all of the LDAs and PM EDLs collapse onto the linear DH-LDA capacitance. However, the DH, GC, and Bik-LDAs fail to predict the capacitance for $\{\tilde{\phi}_0, \tilde{\Sigma}\} \gtrsim 1$. Only the CS-LDA accurately captures excluded volume interactions at increased voltages and bulk volume fractions. The DH and GC-LDAs, which neglect steric effects, always predict larger capacitances for PM EDLs with non-zero volume fractions.

The Bik-LDA is better than GC in that it does not predict divergent capacitances. Instead, it overpredicts the capacitance because the Bikerman excluded volume chemical potential, Eq. (I.3.19), grossly underestimates measured values for $\tilde{\mu}^{EV}$ [Fig. III.1(a-c)]. Over the studied range of $\Phi_B \leq 0.42$, the energy required to pack spherical WCA ions exceeds that of lattice ions. Bikerman counter-ions reach higher concentrations that PM

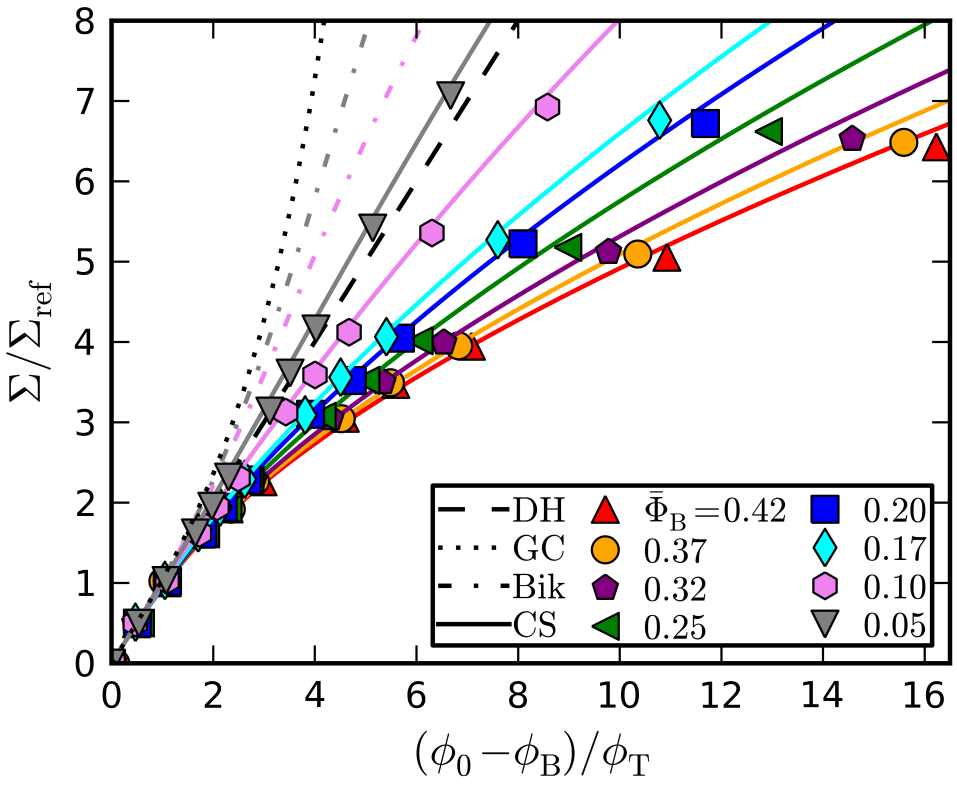

Figure III.3: Surface charge density versus total potential drop from 8 sets of PM EDLs that differ in bulk volume fraction. All simulations collapse onto LDA predictions in the low charge limit $\{\tilde{\Sigma}, \tilde{\phi}_0\} \to 0$. Beyond $\tilde{\phi}_0 \gtrsim 1$, Debye-Hückel and Gouy-Chapman diverges and Bikerman always overestimates the integrated capacitance $(\tilde{\Sigma}/\tilde{\phi}_0)$ so only semi-dilute curves are included for clarity. Carnahan-Starling qualitatively matches PM capacitance, but consistently gives higher values at increased charge densities and bulk volume fractions.

EDLs simulations allow, which in turn leads to greater capacitances at large voltages. The CS-LDA describes the PM over the range of measured surface potentials for these 8 sets of bulk volume fractions. CS accurately predicts $\tilde{\mu}^{\mathrm{EV}}$ except near the electrode where, like GC and Bikerman, it underestimates the majority of measured values [Fig. III.1c]. CS thus slightly overestimates the capacitance for strongly charged electrodes $\tilde{\Sigma} \gtrsim 5$ and appreciable bulk volume fractions $\Phi_{\mathrm{B}} \geq 0.10$, which implies that it will underestimate PM voltage profiles in this regime.

Considering the CS-LDA captures the total capacitance over a wide range of electrode surface charge densities and bulk volume fractions [Fig. III.3], how well does it describe spatial profiles for each of the chemical potential components? To address this, we solve the CS-LDA via Poisson's Eq. (I.3.6) using Eq. (I.3.24). Figure III.4 compares CS-LDA predictions with PM EDLs of moderate and large bulk volume fractions. We truncate the profiles at ten ion diameters from the wall, beyond which the simulated and CS-LDA chemical potential profiles converge to their bulk values. In accordance with Figs. III.1-III.3, CS-LDA predictions best-describe PM EDLs with smaller volume fractions in regions far from weakly-charged electrodes where profiles are observed to be monotonic. Ideal chemical potentials from simulation exhibit size-induced oscillations, which cannot be captured by CS or *any* LDA model. Co-ion densities are exceedingly small, $\tilde{n}^{+} \approx \exp(-10)$, near the surface where the CS-LDA is most prone to failure. The oscillatory region for counter-ions is more pronounced at higher charge densities and larger bulk volume fractions. As expected from capacitance measurements [Fig. III.3], the electrostatic potential from CS-LDA is slightly lower than PM profiles.

The CS-LDA qualitatively describes the PM excluded volume excess chemical poten-

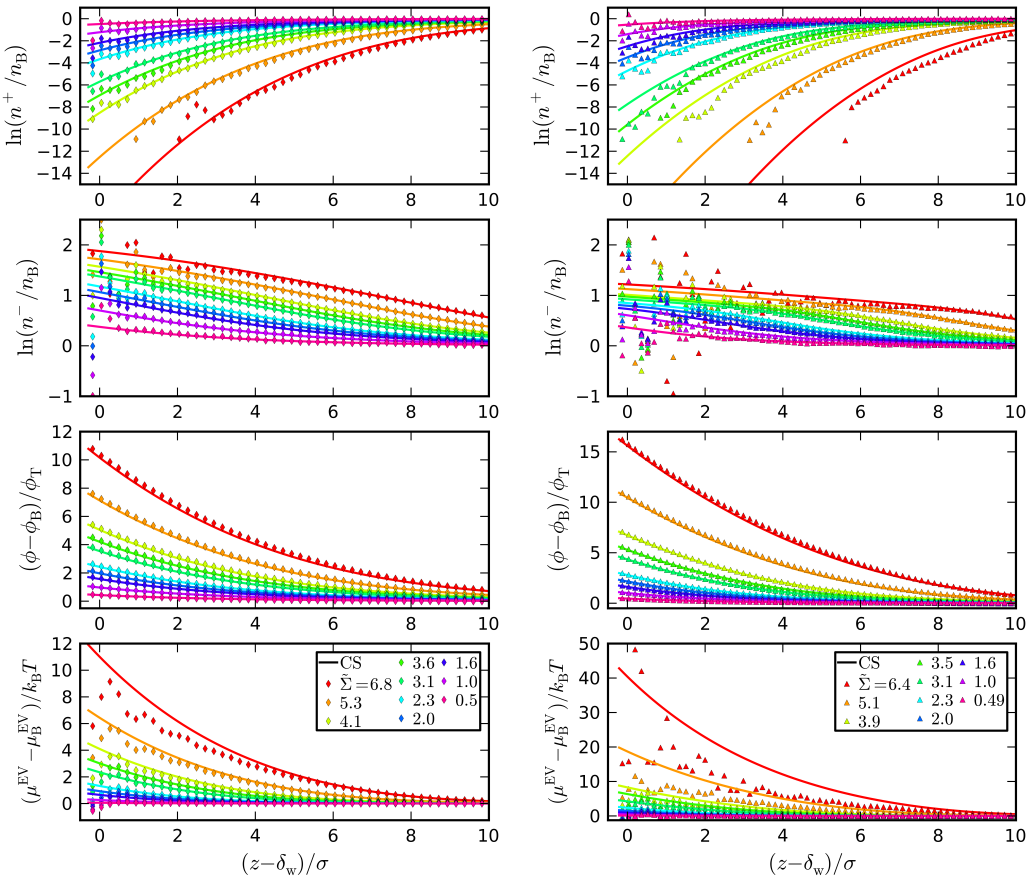

Figure III.4: Components of the chemical potential from CS-LDA and PM EDL simulations at $\bar{\Phi}_B = 0.20$ [left] and $\bar{\Phi}_B = 0.42$ [right]. Size-induced oscillations within PM EDLs are less pronounced in the chemical potential profiles of co-ions [first row] than counter-ions [second row], and are more pronounced at larger electrode charge densities and bulk volume fraction. The total voltage [third row] dropped across both CS and PM EDLs increases with bulk volume fraction and electrode charge density due to increasingly significant excluded volume interactions. Measured values for the excluded volume chemical potential [fourth row] become unreliable in densely correlated regimes owing to use of the Widom insertion method.

tial far from weakly-charged electrodes. Closer to the electrode, the CS-LDA overpredicts measured values as in Figs. III.1 and III.2. PM EDLs with $\bar{\Phi}_{\rm B} = 0.20$ exhibit oscillations in $\tilde{\mu}^{\rm EV}$ within two ion diameters at large electrode densities $\tilde{\Sigma} \gtrsim 2$. In PM EDLs with $\bar{\Phi}_{\rm B} = 0.42$, Widom insertions are not reliable in dense regions near highly charged $\tilde{\Sigma} \gtrsim 3.9$ electrodes. WCA ions overlap at the largest electrode surface charge density where the surface packing fraction is extremely large $\Phi_0 \approx \Phi_{\rm B} \exp(2.5)/2 > 1$. Figure III.5 gives snapshots from PM EDL simulations that demonstrate larger ions to overlap more readily as they approach the electrode. EDLs with large packing fractions are prone to ion layering, which is distinct from diffuse behavior farther from the electrode. The general LDA approach, which neglects pairwise ion interactions, would fail to describe these highly correlated PM EDL regimes.

III.3.2 Characterizing Correlations

There may be correlations that do not manifest oscillations along the spatial axis. For instance, Monte Carlo simulations of Primitive Model EDLs comprised of point-sized counter-ions ($\lambda_{\rm B} \gg \sigma$) exhibit significant 2-dimensional ordering at strongly-charged electrodes with discrete or uniform charge densities [Moreira and Netz, 2004]. These so-called 2D Wigner crystals exist in equilibrium with a diffuse electrolyte far from the electrode. Despite these highly correlated long-ranged Coulomb interactions, the counter-ion densities in the z-direction are well-described by monotonic non-LDA models derived from strong coupling theory [Netz, 2001].

We simulate a limited class of electrolytes with weakly-charged ions. We maintain

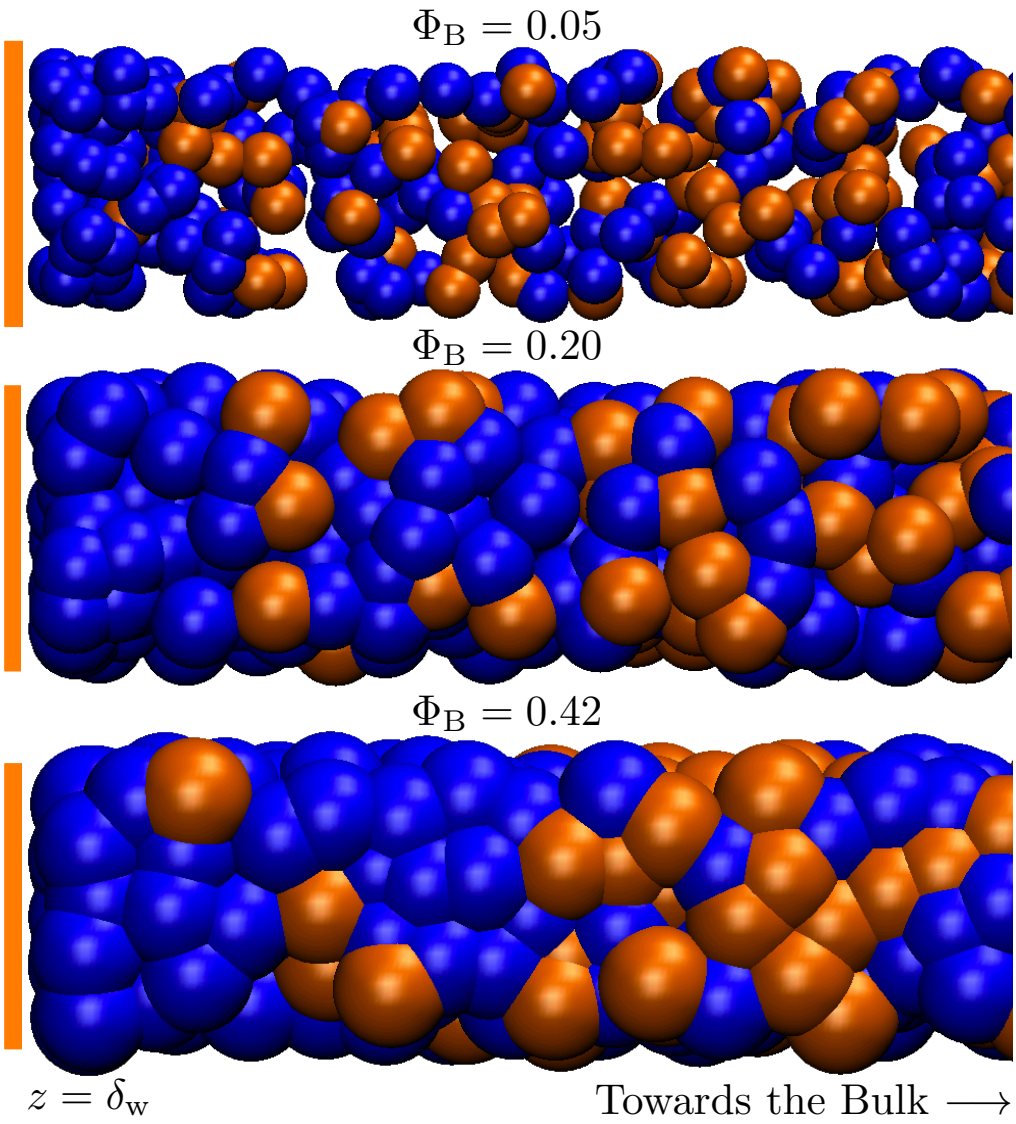

Figure III.5: Snapshots from PM EDL simulations with distinct bulk volume fractions and nearly equal surface charge densities $\tilde{\bar{\Sigma}} = 3.09 \pm 0.04$ give a qualitative picture of how the ion layering depends on bulk volume fraction $\Phi_B = \{0.05, 0.20, \text{and } 0.42\}$ and/or relative ion size $\tilde{\sigma} = \{0.21, 0.33, \text{and } 0.42\}$. The time-averaged profiles of the two largest PM EDLs [Fig. III.4] reveal oscillations in ion density to be more pronounced at larger ion sizes.

Coulomb correlations are negligible by comparison to size-induced correlations for PM EDLs characterized by $\lambda_B \ll \sigma$. In Fig. III.4, ideal and excluded chemical potential profiles exhibit oscillations and reveal that even weakly-charged PM ions form correlated layers at the electrode, which grow with increasing applied charge density and bulk volume fraction. We define correlated EDL regimes in terms of *oscillations* in free charge density profiles. Despite these steric correlations, CS-LDA predictions appears to describe the PM simulations outside of some correlation length ℓ_{cor}.

In principle, one could compare PM to LDA profiles and define ℓ_{cor} wherever deviations exceed some meaningful threshold. However, this estimate for ℓ_{cor} would then be influenced by whatever LDA and/or subjective criteria were chosen. To elucidate how ℓ_{cor} depends on the properties of the electrolyte and applied field strength, we determine ℓ_{cor} from the location where oscillations in $\tilde{\rho}$ can be attributable only to bulk fluctuations. Independent of any particular LDA model, we adopt (admittedly subjective) criterion to develop an algorithm to extract ℓ_{cor} solely from simulated PM free charge density profiles as described in the Section III.5.

Figure III.6 demonstrates this approach on PM EDLs with a large bulk volume fraction, $\bar{\Phi}_B = 0.42$, for a range of applied surface charge densities. We first generate a quintic spline interpolant $\tilde{\rho}_{spline}$ from discrete free charge density profiles, each measured at 250 distinct positions. We then compute the numerical derivative to locate all extrema, $z^{\blacktriangle}$, by solving $d\tilde{\rho}_{spline}(z^{\blacktriangle})/dz = 0$. To ascertain whether or not a given $z^{\blacktriangle}$ is ℓ_{cor}, we identify the extremum farthest from the electrode that is due to finite-size induced ordering. Ion layering is evident near the electrode where extrema alternate between peaks and valleys. In addition, adjacent maxima and minima have $\mathcal{O}(\sigma)$ spacing. Farther from the bulk, it

is less clear if extrema are the result of excluded volume interactions, bulk fluctuations, or from numerical anomalies in our interpolating function. To determine ℓ_{cor} independent from a specific LDA, each extremum is examined as a possible candidate boundary between diffuse and correlated regimes.

Although a specific LDA model is not used in Fig. III.6, the values for ℓ_{cor} obtained from the model-free approach appear to capture the spatial regimes where CS-LDA departs from the the free charge density profiles. Admittedly, the algorithm could be refined by applying additional and/or different criteria. For instance, $z^{\blacktriangle}$ also can be interrogated from the wall moving bulk-wards to determine ℓ_{cor} from the average result. It is possible to establish various thresholds that depend on $\tilde{\Sigma}$, Φ_{B}, or even incorporate additional information from simulations such as the voltage, excluded volume chemical potential, total density $\tilde{n}^{+} + \tilde{n}^{-}$, or higher derivatives of $\tilde{\rho}$. In principle, one may take a more opportunistic approach and assume a particular LDA model to prime the search; however, this defeats the original intent to determine ℓ_{cor} purely from the simulation data.

We apply this algorithm to 88 PM EDL simulations of weakly-charged ions with fixed Bjerrum and screening length [shown previously in Fig. III.3]. We normalize ℓ_{cor} by ion diameter, which is the only parameter besides $\tilde{\Sigma}$ that varies between simulations. Figure III.7 aggregates these results into a contour plot that succinctly shows PM EDLs with low $\tilde{\Sigma}$ and Φ_{B} to exhibit negligible correlations, while the thickest correlated regions correspond to large $\tilde{\Sigma}$ and Φ_{B}. This result corroborates Figs. III.4 and III.6 in that at any given Φ_{B}, the correlated layer(s) grow(s) with increasing field strength. PM EDLs with the largest Φ_{B} exhibit correlated layers up to seven ion diameters at the highest $\tilde{\Sigma}$. We hypothesize any PM EDL with weakly-charged ions ($\lambda_{\text{B}} \lesssim \sigma \lesssim \lambda_{\text{D}}$) should exhibit

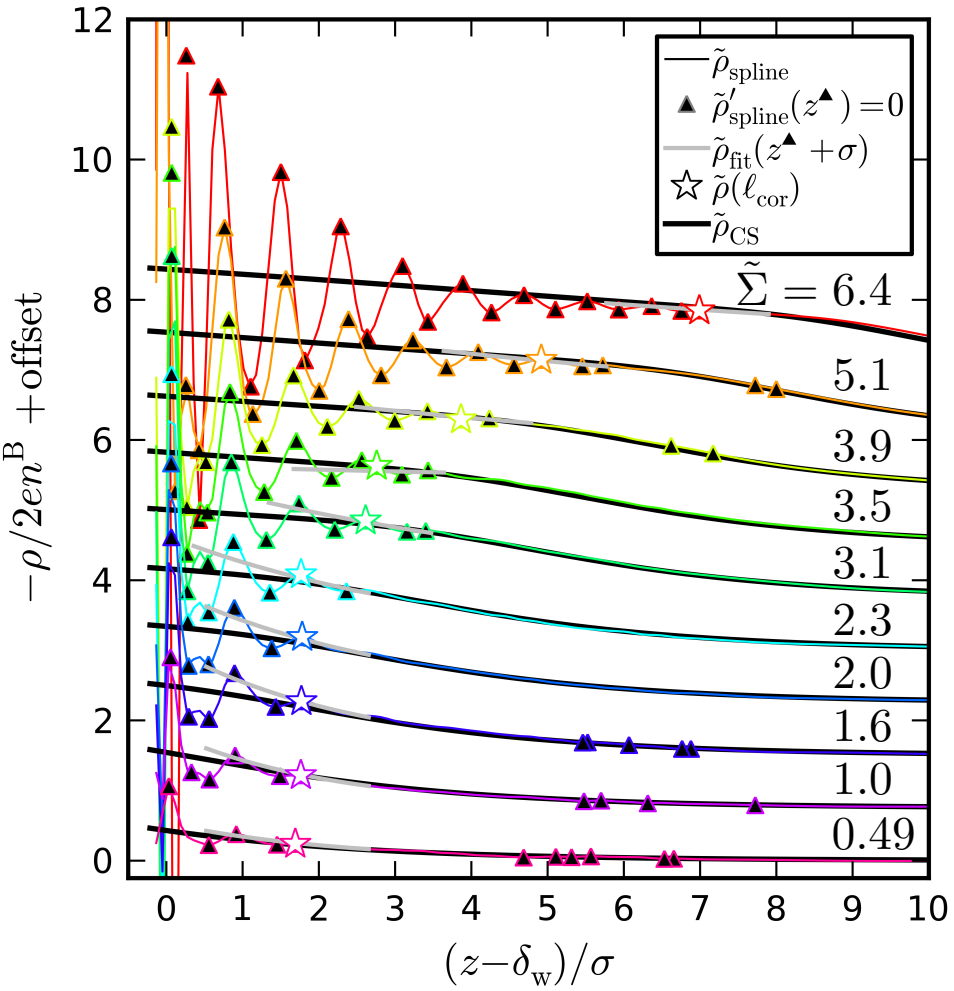

Figure III.6: A model-free method to determine $\ell_{\rm cor}$ from simulated PM free charge densities with $\bar{\Phi}_{\rm B} = 0.42$. We generate spline interpolants from discrete profiles, find extrema $z^{\blacktriangle}$, and identify $\ell_{\rm cor}$ by examining deviations of potentially correlated regions $\tilde{\rho}(z^{\blacktriangle}-\sigma)$ from exponential fits of bulk-like regions $\tilde{\rho}_{\rm fit}(z^{\blacktriangle}+\sigma)$. Although $\ell_{\rm cor}$ appears to coincide with onset of deviations from CS-LDA profiles, this approach is independent of CS or *any* specific LDA.

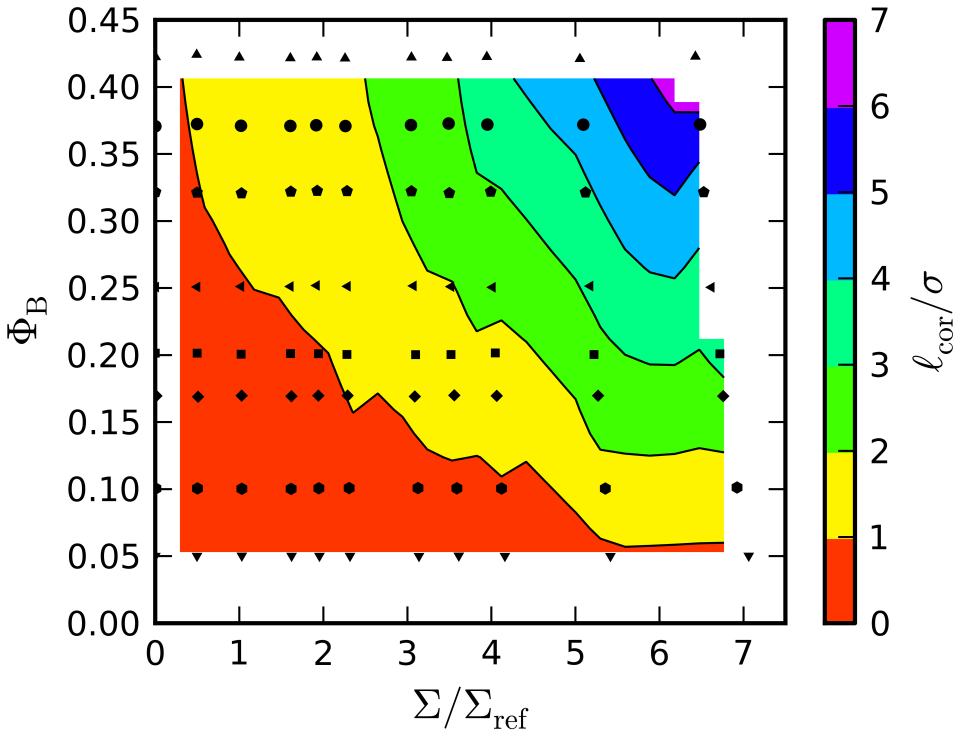

Figure III.7: Contour plot of the correlation length measured 88 PM EDLs of constant Bjerrum and screening length using the algorithm demonstrated in Fig. III.6. The correlated region is observed to grow with increasing electrode charge density and bulk volume fraction.

similar qualitative trends as in Fig. III.7 as long as electrostatic correlations are mitigated by ions that are larger than the Bjerrum length.

Having extracted ℓ_{cor} from PM EDLs, we now explore the properties of the correlated region. Since size-induced oscillations are the result of ion layering, the ion diameter is the appropriate characteristic length scale for the correlated region. We thus non-dimensionalize Poisson's Eq. (I.3.6) by the ion diameter and express the voltage relative to the surface (as opposed to the bulk) potential

$$2en_B\left(\frac{\lambda_D}{\sigma}\right)^2\tilde{\nabla}^2\left(\frac{\phi-\phi_0}{\phi_T}\right)=-\rho_{cor}. \tag{III.3.2}$$

From Equation (III.3.2), we define the reduced correlated free charge density

$$\tilde{\rho}_{\rm cor} \equiv \frac{\rho_{\rm cor}}{2en_{\rm B}} \left(\frac{\sigma}{\lambda_{\rm D}} \right)^2 = \rho_{\rm cor} \frac{\sigma^2}{\Sigma_{\rm ref} \lambda_{\rm D}}. \tag{III.3.3}$$

We integrate Eq. (III.3.2) once to obtain the correlated surface charge

$$\tilde{\Sigma}_{\rm cor} \equiv -\Sigma_{\rm cor} \frac{\sigma}{\Sigma_{\rm ref} \lambda_{\rm D}} = \int_0^{\tilde{\ell}_{\rm cor}} \tilde{\rho}_{\rm cor} {\rm d}\hat{z} \tag{III.3.4}$$

and again to obtain the voltage drop across the correlated region

$$\Delta\tilde{\phi}_{\rm cor} \equiv -\left(\frac{\phi_{\rm cor} - \phi_0}{\phi_{\rm T}} \right) = \int_0^{\tilde{\ell}_{\rm cor}} \left(\int_0^{\tilde{\ell}_{\rm cor}} \tilde{\rho}_{\rm cor}(\hat{s}) {\rm d}\hat{s} \right) {\rm d}\hat{z}. \tag{III.3.5}$$

The ratio of Eqs. (III.3.4) and (III.3.5) gives the integrated capacitance of the correlated EDL region.

Figure III.8 shows $\tilde{\Sigma}_{\rm cor}$ versus $\Delta\tilde{\phi}_{\rm cor}$ on a logarithmic scale to reveal the correlated EDL capacitance across nearly three decades of computed values. Correlated PM EDL capacitance is observed to obey a power law, which we determine by fitting data from all bulk volume fractions. Without fitting, the CS-LDA accurately predicts correlated regions of semi-dilute, moderate, and highly-concentrated PM electrolytes. Although the free charge density exhibits oscillations within $\tilde{\ell}_{\rm cor}$, integrating $\tilde{\rho}_{\rm cor}$ to obtain $\tilde{\Sigma}_{\rm cor}$ and $\Delta\tilde{\phi}_{\rm cor}$, which follow CS-LDA.

Since the CS-LDA captures the correlated PM EDL capacitance across a large range of charge densities, surface potential, and bulk volume fractions, we use it as a benchmark to quantify non-LDA contribution from the entire PM EDLs. We do not need to know the correlation length, but instead define the non-LDA free charge density by subtracting the CS-LDA predictions from the PM profiles

$$\tilde{\rho}_{\rm nonLDA} \equiv \frac{\rho_{\rm nonLDA}}{2en_{\rm B}} = \tilde{\rho} - \tilde{\rho}_{\rm CS}\,, \tag{III.3.6}$$

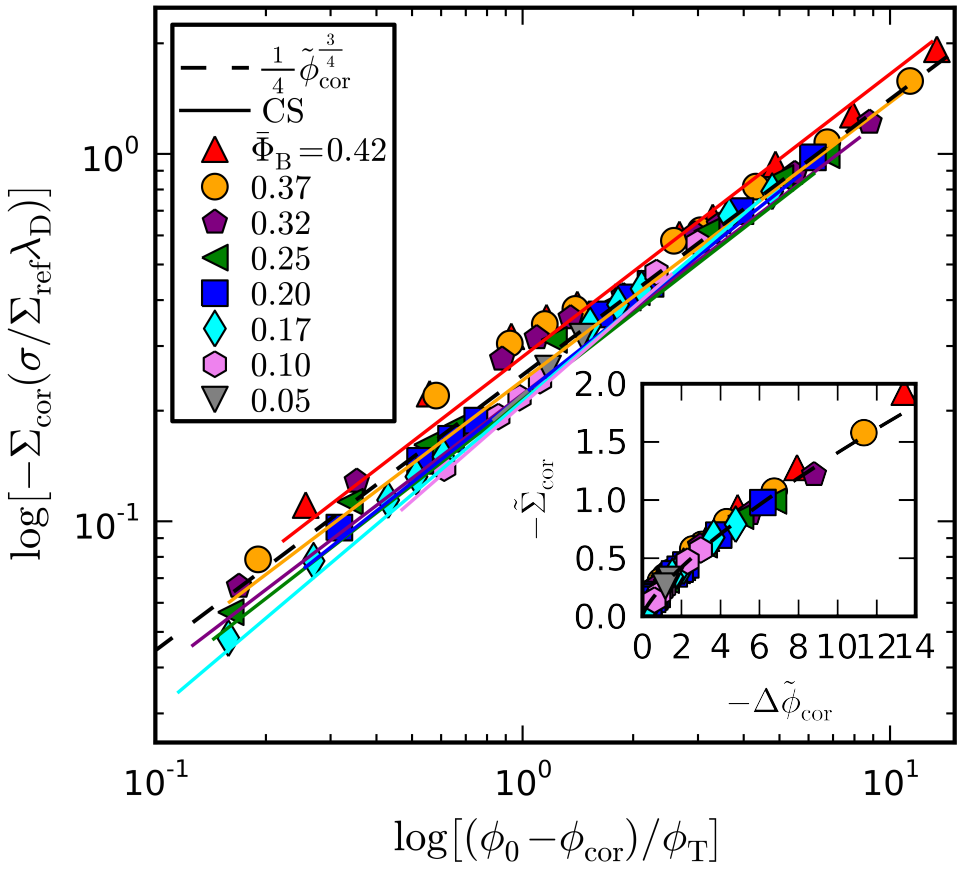

Figure III.8: Surface charge density versus electrostatic potential dropped across the correlated layer of dilute and concentrated CS-LDA and PM electrolytes. CS-LDA captures the correlated capacitances at each bulk volume fraction. A best fit of data for all bulk volume fractions reveals correlated PM EDLs to follow a 3/4 power law for nearly three decades of charge density and surface potential measurements.

where distance is non-dimensionalized by λ_D. We integrate $\tilde{\rho}_{\text{nonLDA}}$ to obtain the non-LDA contributions to the electric charge density

$$\tilde{\Sigma}_{\text{nonLDA}} \equiv \frac{\Sigma_{\text{nonLDA}}}{\Sigma_{\text{ref}}} = -\int_0^{z_B/\lambda_D} \tilde{\rho}_{\text{nonLDA}} \mathrm{d}\hat{z}\,, \tag{III.3.7}$$

and integrate Eq. III.3.7 to get the non-local electrostatic potential drop for the entire electrolyte

$$\tilde{\phi}_{\text{nonLDA}} \equiv \frac{\phi_{\text{nonLDA}}}{\phi_T} = \int_0^{z_B/\lambda_D} \tilde{\Sigma}_{\text{nonLDA}} \mathrm{d}\hat{z}. \tag{III.3.8}$$

Figure III.9 indicates that the minimal variance in the non-local surface charge density ($\tilde{\Sigma}_{\text{nonLDA}} \lesssim \pm 0.22$) and non-local surface potential ($\tilde{\phi}_{\text{nonLDA}} \lesssim \pm 0.60$) indicate the CS-LDA to accurately predict the overall capacitance of the PM EDLs.

III.4 Conclusion

In this chapter, we compare predictions from several mean-field local-density approximations of Primitive Model simulations of the electric double layer to elucidate LDA failure mechanisms. The PM treats ion-ion interactions with pairwise potentials to explicitly capture ion-ion correlations that LDAs do not. We explore the specific case of size-induced correlations in which non-LDA ion layering gives rise to oscillatory ion densities and chemical potentials. We investigate chemical potential profiles from these models across low and high bulk volume fractions and electrode charge densities. We also examine spatial free charge densities to determine the boundary, ℓ_{cor}, between correlated and diffuse EDL regimes. We find the Carnahan-Starling LDA to accurately describe the diffuse portion of PM chemical potential profiles [Figs. III.1-III.4] at distances beyond

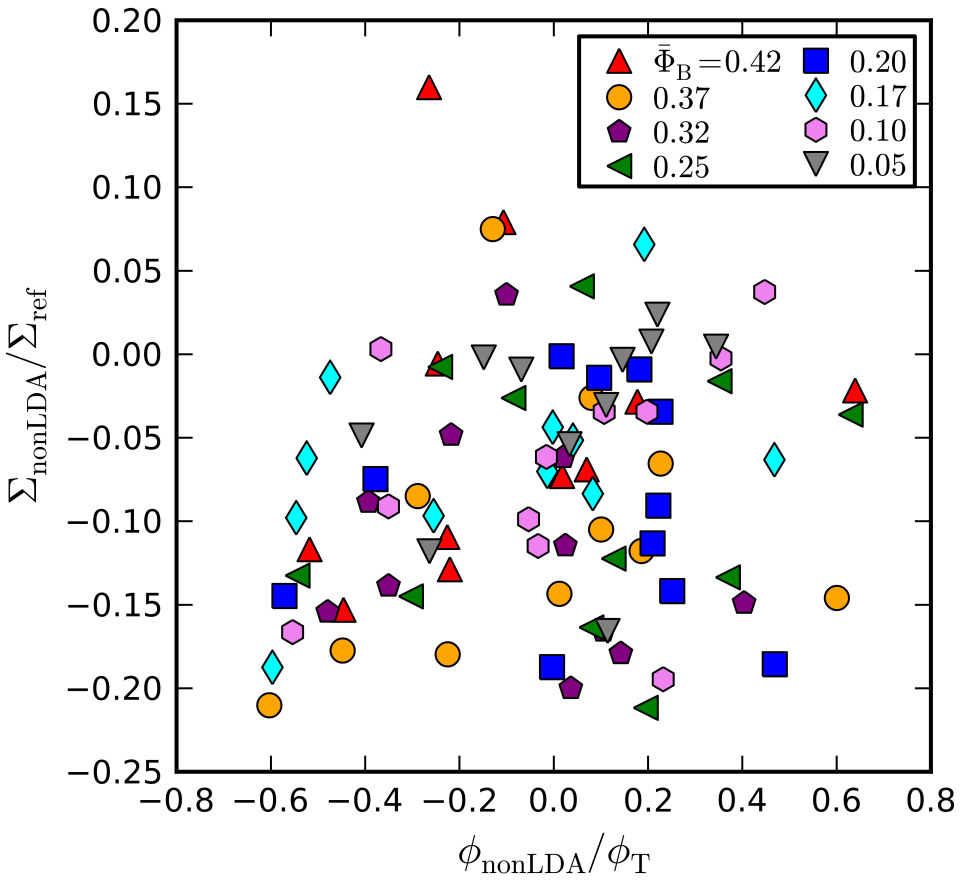

Figure III.9: Contributions from the non-local surface charge density and electrostatic potential beyond the Carnahan-Starling local-density approximation do not exhibit a clear trend. The small values for $\tilde{\Sigma}_{\mathrm{nonLDA}}$ and $\tilde{\phi}_{\mathrm{nonLDA}}$ indicate the accuracy of the CS-LDA predictions of these PM EDL simulations.

the correlation length from the electrode [Fig. III.6]. Within the correlated layer, the free charge density exhibits non-monotonicity that is impossible to describe by any LDA. Nevertheless, the CS-LDA accurately describes the total capacitance of the correlated region of PM electrolytes comprised of weakly-charged ions for a wide range of bulk volume fractions.

III.5 Appendix: Model-free Determination of the Correlation Length

We develop a model-free test to distinguish ℓ_{cor} from all $z^{\blacktriangle}$ that exploits the scaling of highly-charged bulk-like EDLs with equi-sized ions, i.e. $\tilde{\rho}_{\text{LDA}}(\tilde{\phi} \gg 1) \approx \exp\left(+\tilde{\phi} - \tilde{\mu}^{\text{EV}}\right)$. We postulate free charge density profiles within diffuse EDLs regimes to follow an exponential decay similar to Debye-Hückel

$$\tilde{\rho}(z \pm \Delta z) \approx b \exp\left(-z/g\right) \tag{III.5.1}$$

across small spatial windows $\Delta z \to 0$. Although Debye-Hückel is known to fail to describe free charge densities with finite charge densities, we postulate that Equation (III.5.1) *might* describe $\tilde{\rho}(z \pm \Delta z)$ over very short distances $\sigma \sim \mathcal{O}(\Delta z)$ provided that we determine constants b and g by fitting bulk-wards data. To clarify, we examine each candidate correlation boundary, $z^{\blacktriangle}$, fit an exponential to the portion of the PM profiles within one ion diameter towards bulk, and find $R^2 \geq 0.85$. We then use $\tilde{\rho}_{\text{fit}}$ to compare the free charge density towards the bulk $\tilde{\rho}(z^{\blacktriangle} + \sigma)$ to the potentially correlated free charge density portion nearer the electrode $\tilde{\rho}(z^{\blacktriangle} - \sigma)$. More specifically, we compute the root

mean square in order to quantify deviations between $\tilde{\rho}_{\text{fit}}$ and $\tilde{\rho}(z^{\blacktriangle} \pm \sigma)$. If we find *both* a maxima and minima that exceed five times the RMS, we declare $z^{\blacktriangle}$ to be ℓ_{cor} and do not interrogate the remaining $z^{\blacktriangle}$. If the difference is negligible, we investigate the nearest extremum that is closer to the electrode. Whenever $\tilde{\rho}(z^{\blacktriangle} + \sigma) \approx \tilde{\rho}(z^{\blacktriangle} - \sigma)$ is true for all $z^{\blacktriangle}$, the free charge density is entirely bulk-like and there is no correlation length, which is likely at low $\tilde{\Sigma}$ and Φ_{B}.

Chapter IV

Local-Density Approximations of Electrolytes with Size Asymmetric Ions

In this Chapter, we explore electric double layer systems comprised of equal-charged ions with dissimilar size. In Chapter III, we show that the Carnahan-Starling local-density approximation (CS-LDA) gives surprisingly accurate predictions of the total capacitance and chemical potential profiles. Motivated by these findings, we examine a local-density approximation (LDA) based on an extension of the CS equation of state to account for mixtures of particles that vary in size and concentration derived by Boublík, Mansoori, Carnahan, Starling, and Leland (BMCSL) [Boublík, 1970, Mansoori et al., 1971]. Here we compare the BMCSL-LDA to Primitive Model (PM) simulations of electrolytes that span a range of volume fractions and size ratios. We find the BMCSL-LDA

predicts PM capacitance profiles when counter-ions are larger than co-ions; however, it captures neither the capacitance nor the chemical potential profiles when co-ions are larger than counter-ions.

IV.1 Motivation

Ion size asymmetry is a well-established source of size-induced correlation that results in oscillatory free charge density profiles [Bazant et al., 2009]. Oscillatory profiles are often said to signal "overcharging" because ion correlations decrease entropy, causing the diffuse electric double layer to contract; this in turn attracts more counter-ions than required to neutralize the surface charge [Guldbrand et al., 1984, Israelachvili, 1992, Hansen and Lowen, 2000]. Monte Carlo (MC) simulations of electrolytes with asymmetrically sized hard-sphere ions between planar electrodes exhibit overcharging at small applied potentials when the counter-ions are smaller than co-ions [Guerrero-García et al., 2010]. Furthermore, Density Functional Theory and MC simulations of ionic liquids with unequal ion sizes show the capacitance of positively and negatively charged electrodes to exhibit asymmetric maxima. At a given bulk concentration, the capacitance of an electrode peaks at higher values as the size of the counter-ion decreases [Lamperski et al., 2014].

A variety of models have been proposed to capture the behavior of differently-sized ions [Bazant et al., 2009]. A contact-value theorem for mixtures of ions has been proposed that suggests size asymmetry can cause charge separation at the electrode that results in a non-zero potential at zero charge density [Henderson and Boda, 2009]. However, compar-

isons to MC simulations reveal the contact-value expression holds only at small electrode charge densities [Bhuiyan and Henderson, 2011] and also fails at low concentrations [Feng and Chapman, 2011]. Integral equation theories (IETs) qualitatively agree with the Gouy-Chapman model for dilute solutions of monovalent ions where short-ranged correlations are negligible [Attard, 1996]. IETs have been shown to capture correlations in more concentrated systems comprised of asymmetrically-sized ions [Quesada-Pérez et al., 2003]. IETs make approximations to the Ornstein-Zernike equation [McQuarrie, 1976] to relate the total and direct correlation functions for solvent (if desired) and ions to their densities and interaction potentials [Vlachy, 1999, Attard, 1996, Quesada-Pérez et al., 2003].

IETs demonstrate overcharging caused by ion correlation effects in systems with monovalent counter-ions smaller than co-ions in a variety of scenarios: with two planar electrodes [Greberg and Kjellander, 1998, Martin-Molina et al., 2006] or a spherical macro-ion electrode [Guerrero-García et al., 2010], multivalent ions with planar [Quesada-Perez et al., 2004, Greberg and Kjellander, 1998, Martin-Molina et al., 2006] and spherical [González-Tovar et al., 2004] electrodes, highly concentrated electrolytes [Quesada-Perez et al., 2004], and highly charged electrodes [Greberg and Kjellander, 1998, Guerrero-García et al., 2010]. IETs successfully capture ion density oscillations that results from correlation effects, which are not possible to describe with local-density approximations. However, *all* IETs fail for dilute solutions of multivalent ions [Jimenez-Angeles et al., 2003, Henderson et al., 1983, Rogde and Hafskjold, 1983] as the species' radial distribution functions in such systems indicate the formation of dimers, which is a subject of controversy and suspected to be an artifact of the simplified Ornstein-Zernike equation

[Henderson et al., 1983]. Additionally, these methods require significant effort to solve numerically [Attard, 1996, Bazant et al., 2009].

Although LDAs cannot capture oscillatory portions of density profiles, we explore their ability to describe electrolytes with weakly charged ions of different size for a range of concentration, size ratios, and bulk volume fractions. Specifically, we investigate the Boublík, Mansoori, Carnahan, Starling, and Leland (BMCSL) [Boublík, 1970, Mansoori et al., 1971, Hansen and McDonald, 1986] equation of state that accounts for systems of hard-sphere electrolytes comprised of ions with unequal size. It is a mathematically convenient expression that has been incorporated into local-density approximations to describe electric double layer systems with dissimilar ion sizes [Biesheuvel and Soestbergen, 2007, Lue et al., 1999]. The BMCSL-LDA predicts different capacitance profiles for anodes and cathodes for electrolytes with size asymmetric ions [Caprio et al., 2004]. In this Chapter, we use the BMCSL-LDA to analyze a variety of EDL systems with moderate volume fractions of asymmetrically sized ions that are weakly- and oppositely-charged.

IV.2 Overview of the BMCSL Local-Density Approximation

The BMCSL equation of state is determined using the virial and compressibility expansions of mixtures of hard-spheres [Hansen and McDonald, 1986], which are then combined according to the Carnahan-Starling (CS) EOS. The compressibility equation is derived from fluctuations in the grand canonical ensemble while the virial equation is

obtained by differentiating the logarithm of the configurational integral. These two routes are identical provided exact forms for the radial distributions of hard-sphere mixtures are used.

Although there are many ways to approximate the radial distribution function [McQuarrie, 1976], the BMCSL and CS theories use the Percus-Yevik integral equation [Mansoori et al., 1971] and Scaled Particle Theory [Boublík, 1970] to determine the compressibility factor $Z = PV/Nk_{\mathrm{B}}T$ from the virial and compressibility routes. The generalized forms for the compressibility factor Z^c and virial Z^v for a hard-sphere mixture of m components are given by [Lebowitz and Rowlinson, 1964],

$$\begin{aligned} Z^c &= \left[(1+\Phi+\Phi^2) - 3\Phi(y_1+y_2\Phi)\right](1-\Phi)^{-3}\,, \\ Z^v &= Z^c - 3\Phi^3 y_3 (1-\Phi)^{-3}\,, \end{aligned} \tag{IV.2.1}$$

where the total volume fraction

$$\Phi = \frac{\pi}{6} n^{\mathrm{B}} \sum_i^m \sigma_i^3 x_i = \sum_i^m \Phi_i \tag{IV.2.2}$$

is determined from the mole fraction of the i^{th} component. Here y_1, y_2, and y_3 are defined as follows

$$\begin{aligned} y_1 &= \sum_{j>i=1}^m \Upsilon_{ij}(\sigma_i+\sigma_j)/\sqrt{\sigma_i\sigma_j}\,, \\ y_2 &= \sum_{j>i=1}^m \Upsilon_{ij} \sum_{k=1}^m \left(\frac{\Phi_i}{\Phi}\right) \frac{\sqrt{\sigma_i\sigma_j}}{\sigma_k}\,, \\ y_3 &= \left[\sum_{i=1}^m \left(\frac{\Phi_i}{\Phi}\right)^{2/3} x_i^{1/3}\right]^3 \end{aligned} \tag{IV.2.3}$$

with

$$\Upsilon_{ij} = \left[\sqrt{\Phi_i\Phi_j}/\Phi\right]\left[(\sigma_i-\sigma_j)^2/(\sigma_i\sigma_j)\right]\sqrt{x_i x_j}. \tag{IV.2.4}$$

In the case of single component system $\sigma_i = \sigma_j$, the CS EOS for a pure hard-sphere

system is determined from Equation (IV.2.1) via [Mansoori et al., 1971]

$$Z^{\mathrm{CS}} = \frac{1}{3}\left(2Z^{\mathrm{c}} + Z^{v}\right). \tag{IV.2.5}$$

which agrees with hard-sphere simulations at volume fractions below close packing $\Phi^{\mathrm{HS}} \lesssim 0.64$ [Song et al., 1989]. Z^{BMCSL} is determined according to Eqs. (IV.2.1)-(IV.2.5) for the case of unequal ion sizes. The excess chemical potential is derived directly from the compressibility [Mulero et al., 1999, McQuarrie, 1976]

$$\mu_{\mathrm{ex}} = k_{\mathrm{B}}T\left[\int_0^{\Phi}\frac{Z-1}{\Phi}\mathrm{d}\hat{\Phi} + Z - 1\right]. \tag{IV.2.6}$$

We derive a mean-field theory that uses the excess chemical potential for an ion of size σ [Biesheuvel and Soestbergen, 2007] in a system of $m = 2$ components by solving Eqs. (IV.2.1)-(IV.2.6) and rearranging to obtain

$$\begin{aligned}\mu_{\mathrm{ex}}^{\mathrm{BMCSL}}(\sigma) = k_{\mathrm{B}}T\Bigg[&\sigma^3\xi_2^3\left(\frac{\xi_3^2 - 5\xi_3 + 2}{\xi_3^2(1-\xi_3^3)}\right) - \left(1 + \frac{2\sigma^3\xi_2^3}{\xi_3^3} - \frac{3\sigma^2\xi_2^2}{\xi_3^2}\right)\ln(1-\xi_3)\\ &+\frac{3\sigma\xi_2 + 3\sigma^2\xi_1 + \sigma^3\xi_0}{1-\xi_3} + \frac{3\sigma^2\xi_2}{(1-\xi_3)^2}\left(\frac{\xi_2}{\xi_3} + \sigma\xi_1\right)\Bigg],\end{aligned} \tag{IV.2.7}$$

where the diameters of big σ_{big} and small σ_{small} ions and the density of big $\tilde{n}_{\mathrm{big}}$ and small $\tilde{n}_{\mathrm{small}}$ ions is accounted for by

$$\xi_\alpha = \frac{\pi n^{\mathrm{B}}}{6}\left(\tilde{n}_{\mathrm{big}}\sigma_{\mathrm{big}}^{\alpha} + \tilde{n}_{\mathrm{small}}\sigma_{\mathrm{small}}^{\alpha}\right). \tag{IV.2.8}$$

Equation (IV.2.8) is a function of the subscript α and equals the total volume fraction of big Φ_{big} and small Φ_{small}, i.e $\xi_3 = \Phi \equiv \Phi_{\mathrm{big}} + \Phi_{\mathrm{small}}$.

The BMCSL excess chemical potential is used to express the total chemical potential of a mixture of ions

$$\tilde{\mu}_i^{\mathrm{BMCSL}} = \frac{\mu_i^{\mathrm{BMCSL}} - \mu_i^{\mathrm{B}}}{k_{\mathrm{B}}T} = \ln\tilde{n}_i + q^i\tilde{\phi} + \frac{\mu_{\mathrm{ex}}^{\mathrm{BMCSL}}(\sigma_i) - \mu_{\mathrm{ex,B}}^{\mathrm{BMCSL}}(\sigma_i)}{k_{\mathrm{B}}T}. \tag{IV.2.9}$$

In practice, Equation (IV.2.9) is solved numerically to determine the free charge density as a function of electrostatic potential $\tilde{\rho}_{\mathrm{BMCSL}}(\tilde{\phi})$. The free charge density is used in Eq. (I.3.11) to compute the surface charge density versus electrostatic potential to obtain the total capacitance. The spatial profiles for the electrostatic potential, ion densities, and excess chemical potentials are determined by solving Poisson's Eq. (I.3.6) with $\tilde{\rho}_{\mathrm{BMCSL}}(\tilde{\phi})$. We provide Mathematica code in Appendix A that follows the procedures outlines in Chapter I.3.1 to solve the BMCSL-LDA.

Although Eq. (IV.2.7) gives an expression notably more complicated than the CS model, the limiting cases of the BMCSL excess chemical potential help describe its behavior. Equation (IV.2.7) vanishes in the limits of point-sized ions

$$\mu_{\mathrm{ex}}^{\mathrm{BMCSL}}(\sigma_{\mathrm{big}} \to \sigma_{\mathrm{small}} \to 0) \to 0\,, \tag{IV.2.10}$$

and/or infinitely dilute concentrations

$$\begin{aligned} \mu_{\mathrm{ex}}^{\mathrm{BMCSL}}(n^{\mathrm{B}} \to 0) &\to 0\,, \\ \mu_{\mathrm{ex}}^{\mathrm{BMCSL}}(\tilde{n}_{\mathrm{big}} \to \tilde{n}_{\mathrm{small}} \to 0) &\to 0\,, \end{aligned} \tag{IV.2.11}$$

in which case Eq. (IV.2.9) recovers Gouy-Chapman theory. In the limit of point-sized ions amongst finite-sized ions, Eq. (IV.2.7) gives

$$\begin{aligned} \mu_{\mathrm{ex}}^{\mathrm{BMCSL}}(\sigma_{\mathrm{small}} \to 0) &\to -k_{\mathrm{B}}T \ln\left(1-\Phi_{\mathrm{big}}\right)\,, \\ \mu_{\mathrm{ex}}^{\mathrm{BMCSL}}(\sigma_{\mathrm{big}} \neq 0) &\to \mu_{\mathrm{ex}}^{\mathrm{CS}}(\sigma_{\mathrm{big}}) = k_{\mathrm{B}}T \frac{\Phi_{\mathrm{big}}(8-9\Phi_{\mathrm{big}}+3\Phi_{\mathrm{big}}^2)}{(1-\Phi_{\mathrm{big}})^3}. \end{aligned} \tag{IV.2.12}$$

In the limit of a nearly pure system where the density of one species is vanishingly small, Eq. (IV.2.7) gives a similar form to Eq. (IV.2.12)

$$\begin{aligned} \mu_{\mathrm{ex}}^{\mathrm{BMCSL}}(\tilde{n}_i \to 0) &\to -k_{\mathrm{B}}T \ln\left(1-\Phi_j\right)\,, \\ \mu_{\mathrm{ex}}^{\mathrm{BMCSL}}(\tilde{n}_j \neq 0) &\to \mu_{\mathrm{ex}}^{\mathrm{CS}}(\sigma_{\mathrm{j}}) = k_{\mathrm{B}}T \frac{\Phi_j(8-9\Phi_j+3\Phi_j^2)}{(1-\Phi_j)^3}. \end{aligned} \tag{IV.2.13}$$

In systems with $m = 1$ components where ions have the same size, BMCSL recovers the Carnahan-Starling excess chemical potential for

$$\mu_{\rm ex}^{\rm BMCSL}(\sigma_{\rm big} \to \sigma_{\rm small}) \to \mu_{\rm ex}^{\rm CS}(\Phi) = k_{\rm B}T\frac{\Phi(8 - 9\Phi + 3\Phi^2)}{(1-\Phi)^3}. \tag{IV.2.14}$$

Eq. (IV.2.14) applies to both ion types and is different than Eqs. (IV.2.12) and (IV.2.13) in which large and small ions have distinct forms for the excluded volume chemical potential.

IV.3 Methods

We perform 2D periodic MD simulations using LAMMPS [Plimpton, 1995] to model Primitive Model electrolytes of cations and anions with equal valence and unequal diameters. As discussed in Chapters I.3.2 and III.2, the system is maintained at constant temperature with a Langevin thermostat [Schneider and Stoll, 1978], which approximates the dynamics due to an implicit solvent. Charge-centered WCA ions with characteristic energy $\epsilon_{\rm WCA} = k_{\rm B}T$ and diameters σ_i are confined within a distance L. At the boundaries are two repulsive walls with uniform charge density $\pm\Sigma$, thickness $\delta_{\rm w}$, and characteristic energy $\epsilon_{\rm w} = k_{\rm B}T$ via Eqs. (I.3.28-I.3.34). Since the electrodes are oppositely charged, the counter-ions to the anode are co-ions to the cathode. Thus every PM simulation gives two distinct EDLs each with inverse ratios of the counter-ion to co-ion diameter $\sigma_{\rm c}/\sigma_{\rm co}$. We determine the ion size to be the effective hard-sphere radius given by Eq. (III.3.1) as input to Eq. (IV.2.9).

We ensure that any observable spatial correlations in the EDL are due only to excluded volume effects by enforcing $\lambda_{\rm B} < \sigma_{\rm small}$ in all simulations. We evaluate the Coulomb

potential with a PPPM slab Ewald sum [Hockney and Eastwood, 1989] with the default accuracy of 10^{-4}. We choose the periodic dimensions and spacing between the electrodes to exceed all other length scales so that they are irrelevant to predicted behaviors. For each PM electrolyte $\{\Phi^{\mathrm{B}}; \lambda_{\mathrm{B}}/\lambda_{\mathrm{D}}\}$ and surface charge $\tilde{\Sigma}$, we equilibrate $\mathcal{O}$(800-1400) ions for 5 million time steps, then collect 50 thousand snapshots over 50 million steps, requiring 50-100 CPU hours per run. We then measure time-averaged ion densities, voltages, and spatial profiles of the excluded volume excess chemical potentials using the Widom insertion method [Widom, 1978, Frenkel and Smit, 2001], with 250-500 million total test insertions per simulation per ion size.

IV.4 Results and Discussion

Figure IV.1 compares the surface charge density versus voltage predictions from the Gouy-Chapman and BMCSL local-density approximations against the Primitive Model simulations of electrolytes, across a wide range of ion size ratios and bulk volume fractions. The voltage drop across PM EDLs is greater for larger bulk volume fractions and increasingly large counter-ions at any given applied charge density. The capacitance, which is given by $\tilde{\Sigma}/\tilde{\phi}_0$, decreases with increasing counter-ion size. At small voltages and electrode charge densities, all of the LDAs and PM EDLs collapse onto the linear GC-LDA capacitance. Beyond $\{\tilde{\phi}_0, \tilde{\Sigma}\} \gtrsim 1$, the GC-LDA always fails to predict the capacitance and the BMCSL-LDA fails to describe EDLs with larger co-ions. The BMCSL-LDA only captures PM EDLs with $\sigma_{\mathrm{c}}/\sigma_{\mathrm{co}} \geq 1$ across all bulk volume fractions and applied surface charge densities. This suggests BMCSL-LDA predictions of the simulated electrostatic

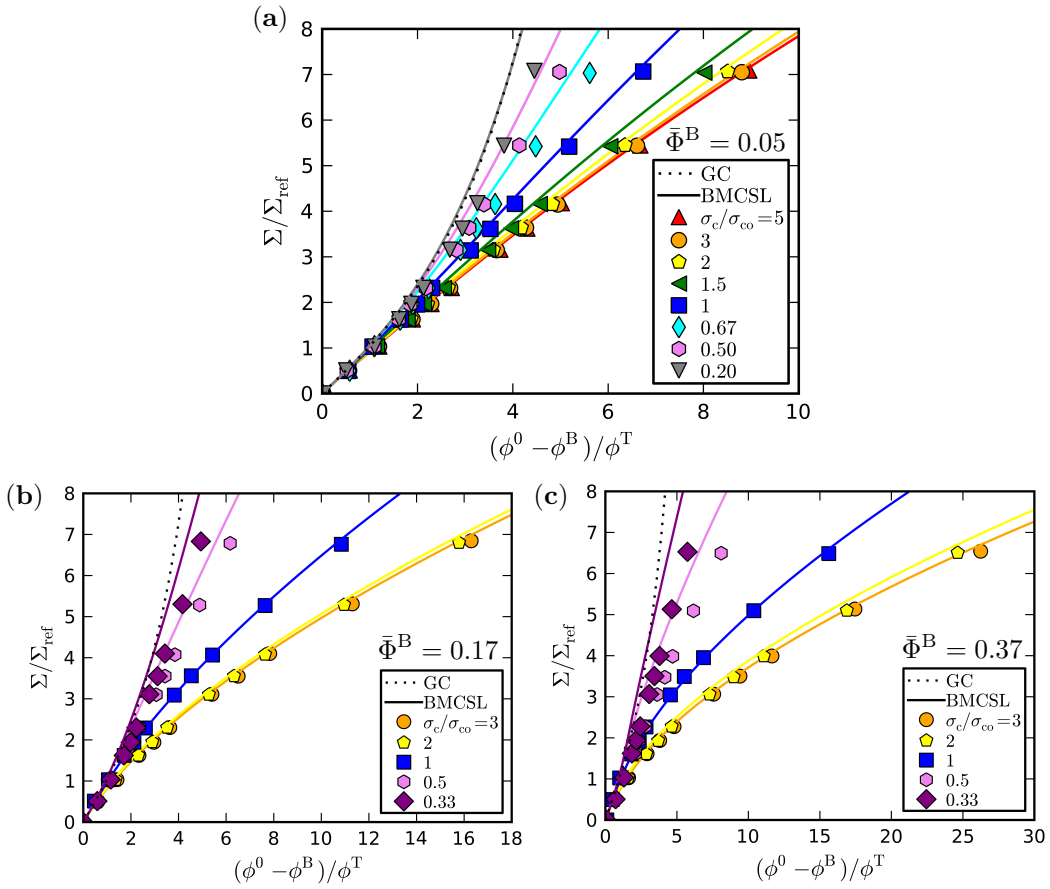

Figure IV.1: Surface charge density versus potential drop of Primitive Model and BMCSL local-density approximations of electrolytes with differently-sized ions and bulk volume fractions $\bar{\Phi}^{\mathrm{B}} = 0.05$ (a), $\bar{\Phi}^{\mathrm{B}} = 0.17$ (b), and $\bar{\Phi}^{\mathrm{B}} = 0.37$ (c). All simulations collapse onto LDA predictions in the linear capacitance regime $\{\tilde{\Sigma}, \tilde{\phi}_0\} \ll 1$. Beyond $\tilde{\phi}_0 \gtrsim 1$, the Gouy-Chapman and BMCSL-LDA overestimate the capacitance $(\tilde{\Sigma}/\tilde{\phi}_0)$ of PM EDLs comprised of co-ions that are larger than counter-ions $\sigma_{\mathrm{c}}/\sigma_{\mathrm{co}} < 1$. Furthermore, the BMCSL-LDA predictions worsen as $\sigma_{\mathrm{c}}/\sigma_{\mathrm{co}} \to 0$. The BMCSL-LDA captures the PM EDLs across a wide range of surface potentials, charge densities, and volume fractions for large ion size ratios $\sigma_{\mathrm{c}}/\sigma_{\mathrm{co}} \geq 1$.

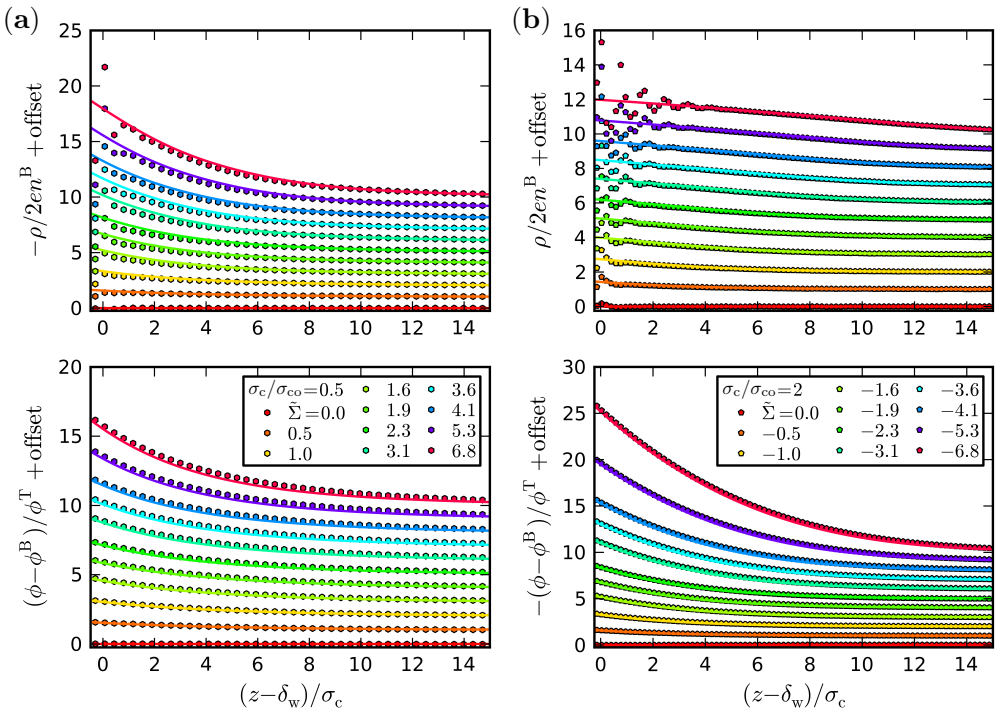

Figure IV.2: BMCSL-LDA and Primitive Model-derived free charge density [top] and electrostatic potential [bottom] profiles for an electrolyte comprised of anions half as large as cations with $\bar{\Phi}^{\mathrm{B}} = 0.17$. At the cathode (a), counter-ions are smaller than co-ions and the BMCSL-LDA overestimates the free charge density and underestimates the voltage. At the anode (b), counter-ions, which are larger than co-ions, layer at the anode under large applied fields $\tilde{\Sigma} \lesssim -1$. The BMCSL-LDA capture the free charge density outside the oscillatory region and the voltage over the entire domain.

potential will be lower for a given surface charge density and the BMCSL free charge density will be larger than PM values when co-ions are larger than counter-ions.

The BMCSL-LDA captures the total capacitance for PM EDL systems over a wide range of electrode surface charge densities and bulk volume fractions [Fig. IV.1] in cases with co-ions that are smaller than counter-ions, but not for $\sigma_{\mathrm{c}}/\sigma_{\mathrm{co}} < 1$. Considering this, how well does it describe spatial profiles for each of the free charge density, voltage, and chemical potential components? Figure IV.2 compares BMCSL-LDA profiles from the cathode and anode for a single PM EDL simulation with a moderate bulk volume fraction

[shown in Fig. IV.1(b)]. At the cathode, co-ions are twice as large as counter-ions, where the BMCSL-LDA gives inaccurate predictions of the PM values. We truncate the profiles at fifteen ion diameters from the wall, beyond which the simulated and BMCSL-LDA and PM profiles converge to their bulk values. In accordance with Figure IV.1, BMCSL-LDA predictions best-describe PM EDLs with large σ_c/σ_{co} ratios and in regions far from weakly-charged electrodes where profiles are observed to be monotonic.

In Figure IV.2(a) for EDLs with $\sigma_c/\sigma_{co} = 0.5$, the BMCSL-LDA gives slightly larger values for the PM free charge density for nonzero cathode charge densities. Also, the PM electrostatic potential profiles are slightly larger than BMCSL-LDA predictions for surface charge densities $\tilde{\Sigma} \gtrsim 1.9$. At the cathode, larger counter-ions layer at the electrode where the free charge density profiles exhibit overcharging as far out as $\sim 5\sigma_c$ at the most strongly applied charge densities. Beyond this layering, the BMCSL-LDA accurately captures the data. The electrostatic potential profiles agree over the entire anodic region. Comparing Figs. IV.2(a) and (b), the BMCSL-LDA performs better large ions outnumber small ions in highly concentrated regions. Therefore, BMCSL more accurately describes EDLs where counter-ions are larger than co-ions.

Figure IV.3 details the ideal and exclude volume chemical potential profiles for the PM EDL shown in Fig. IV.2 with $\bar{\Phi}^B = 0.17$. Fig. IV.3(a) shows the cathodic profiles ($\sigma_{co} = 2\sigma_c$) are poorly described by the BMCSL-LDA. The BMCSL-LDA only captures the co- and counter-ion ideal chemical potentials in the bulk region beyond $\sim 10\sigma_c$. The ideal chemical potential of PM co-ions is grossly underestimated, e.g. at $\tilde{\Sigma} = 3.6$, the predicted ideal co-ion chemical potential at the surface is ~ 150 times smaller than the simulated values and the disagreement is worse at larger $\tilde{\Sigma}$. The PM counter-ion

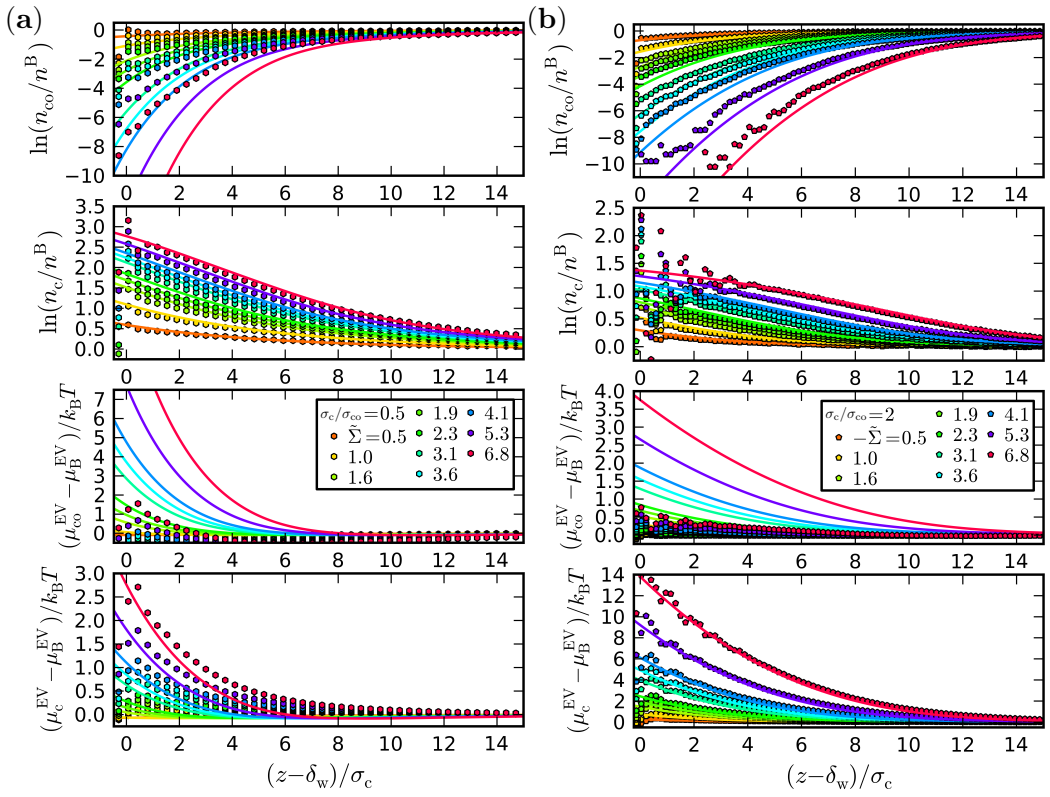

Figure IV.3: Chemical potential profiles from the BMCSL-LDA and Primitive Model of EDLs with large co-ions (a) and large counter-ions (b) [same simulations as in Fig. IV.2 with $\bar{\Phi}^B = 0.17$]. The BMCSL-LDA only describes the ideal chemical potential [first row] of co-ions that are smaller than counter-ions. The ideal chemical potential of counter-ions [second row] is captured by the BMCSL-LDA, except where ions layering occurs near highly-charged electrodes $|\tilde{\Sigma}| \gtrsim 1$. EDLs with larger counter-ions exhibit more pronounced oscillations in both the ideal counter-ion and excluded volume chemical potential of co-ions [$\tilde{\mu}_{co}^{EV}$, third row]. The BMCSL-LDA grossly overestimates $\tilde{\mu}_{co}^{EV}$ in each simulation. The excluded volume chemical potential of counter-ions [$\tilde{\mu}_c^{EV}$, fourth row] collapses onto BMCSL-LDA predictions only for EDLs with larger counter-ions. The BMCSL-LDA overestimates $\tilde{\mu}_c^{EV}$ for EDLs smaller co-ions and also predicts a shallow minimum between 8 and $12\sigma_c$ that is not present in the PM profiles.

ideal chemical potential exhibits oscillations within $\sim 1\sigma_c$ at cathodic charge densities $\tilde{\Sigma} \gtrsim 3.1$, which the BMCSL-LDA cannot describe. Outside of the non-monotonic regime, the BMCSL-LDA qualitatively matches the simulated profiles, but gives slightly higher values for all $\tilde{\Sigma}$ within $\sim 10\sigma_c$. BMCSL-LDA overestimates the counter-ion profiles and underestimates the co-ion densities, which suggests why the BMCSL-LDA over predicts the free charge density in Figure (IV.2).

The BMCSL-LDA does not describe the co- and counter-ion excluded volume chemical potential profiles within $\lesssim 13\sigma_c$ from the cathode where counter-ions are smaller. The BMCSL-LDA completely misses the non-monotonicity exhibited by the simulated excess chemical potential of profiles co-ions. The excess chemical potential of PM co-ions is at least an order of magnitude lower than BMCSL-LDA predictions. BMCSL-LDA also does not qualitatively describe the counter-ion excess chemical potential, especially at the largest surface charge density, where it instead predicts slight non-monotonic behavior between 8 and $12\sigma_c$. In the PM simulations, smaller counter-ions concentrate $\sim \exp(2)/\exp(-5) \approx 1000$ times more at the electrode than do larger co-ions. In regimes where the large species is dilute and the small species is concentrated, the BMCSL-LDA , which assumes a homogenous mixture, misses the excluded volume chemical potential of *both* species and overestimates $\tilde{\mu}_{co}^{EV} (= \tilde{\mu}_{big}^{EV})$ and underestimates $\tilde{\mu}_{c}^{EV}$.

Fig. IV.3(b) shows the anodic chemical profiles where co-ions are smaller than counter-ions ($\sigma_c = 2\sigma_{co}$). Although the BMCSL-LDA underestimates the ideal co-ion chemical potential at $-\tilde{\Sigma} \gtrsim 1$, it qualitatively matches the behavior of PM simulations. The BMCSL-LDA captures the PM ideal counter-ion chemical potential beyond $\gtrsim 5\sigma_c$, where the simulations exhibit oscillations. The counter-ion ideal chemical potentials of the PM

and BMCSL-LDA agree beyond the oscillatory region. Beyond the linear limit $\tilde{\Sigma} \gtrsim 1$, the co-ion density is exponentially small and thus the free charge density is dominated by counter-ions. Thus, although the BMCSL-LDA underestimates the ideal co-ion chemical potential, the BMCSL-LDA still is able to predict the free charge density of EDLs with larger counter-ions in Figure (IV.2). The excess chemical potential of co-ions is poorly described for non-bulk regions and the BMCSL-LDA grossly overestimates the measured values. Although the excluded volume chemical potentials predictions of co-ions are off by as much as four times at the highest charged anode, the counter-ion profiles are well described by the BMCSL-LDA. In regimes where the large species is concentrated and the small species is dilute, the BMCSL-LDA accurately describes the excluded volume chemical potential of the small species and overestimates that of the big species.

Figures (IV.2) and (IV.3) show the BMCSL model to completely miss regimes where small ions outnumber large ones and only capture the excluded volume chemical potential of concentrated regions populated mainly by large particles. In Figure IV.4, we observe the discrepancy between BMCSL predictions of the excluded volume chemical potential for big and small particles in systems with fixed bulk volume fraction as a function of particle size ratio and relative concentration of big particles. To do this, we employ the Widom insertion method to measure $\tilde{\mu}^{\mathrm{EV}}_{\mathrm{big}}$ and $\tilde{\mu}^{\mathrm{EV}}_{\mathrm{small}}$ from a series of fully periodic MD simulations of uncharged WCA particles where electrostatic correlations and wall-ordering effects are explicitly omitted. An additional benefit is that these simulations require $\lesssim 10\%$ the computational expense of the PM EDL simulations that require Ewald summations to account for Coulombic ion-ion interactions.

Fig. IV.4 shows the BMCSL to give accurate predictions in limit of indistinguishable

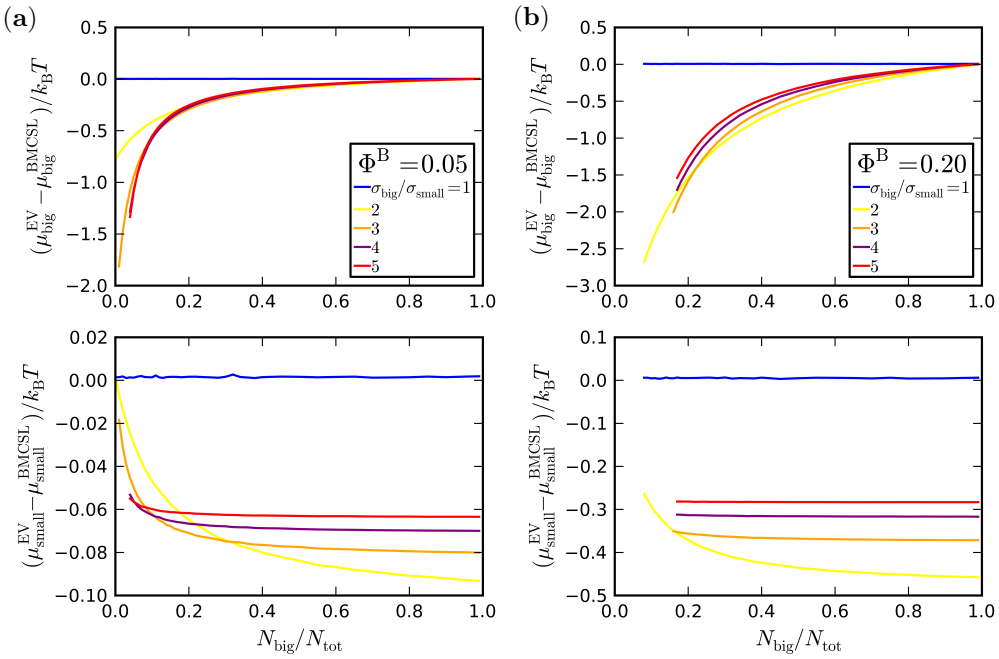

Figure IV.4: Deviations of BMCSL equation of state predictions of the chemical potential of fully periodic systems of uncharged asymmetrically-sized WCA particles at fixed bulk volume fraction $\Phi^{\mathrm{B}} = 0.05$ (a) and $\Phi^{\mathrm{B}} = 0.20$ (b). BMCSL fails to capture the chemical potential of both big [top] or small [bottom] particles outside of the single-component regime, $\sigma_{\mathrm{big}}/\sigma_{\mathrm{small}} = 1$, that is well captured by the Carnahan-Starling equation of state. The BMCSL model captures the excess chemical potential in the limit of nearly pure systems: $N_{\mathrm{big}}/N_{\mathrm{tot}} \to 1$ for big ions or $N_{\mathrm{big}}/N_{\mathrm{tot}} \to 0$ for small ions. The disagreement is worse at small concentrations of big particles and at larger bulk volume fractions.

particles ($\sigma_{\text{big}} \rightarrow \sigma_{\text{small}}$) where it recoups the CS model as described in Eq. IV.2.14. In the limit of a nearly pure system for systems with unequal particles sizes described by Eq.(IV.2.13), the BMCSL model only captures the excess chemical potential of the dominant component. In this nearly pure limit, however, the discrepancy is the worst for the minority component. The BMCSL predictions are slightly better for smaller particles and at lower volume fractions for the entire range of relative concentration of large particles. Overall, the BMCSL excess chemical potential is only accurate for the majority component in nearly pure systems or in the limit of indistinguishable particles where it predicts the CS form for both species.

In Figures IV.2-IV.4, we find the BMCSL-LDA does not describe the total capacitance nor spatial profiles of the chemical potential components in regions where large ions are outnumbered by small ions. The BMCSL-LDA appears to fail to predict electric double layer behavior for electrolytes with co-ions that are smaller than counter-ions. Can we develop a more suitable model within the LDA framework that improves upon the BMCSL excess chemical potential?

To determine if the LDA approach can possibly describe EDLs with smaller co-ions, we can apply the model-free test for LDA EDL behavior discussed in Chapter II.2. In order for the general LDA approach to hold, EDL profiles from a given electrolyte must collapse when plotted along a similarity coordinate

$$S = \tilde{\Sigma} \exp\left(-\tilde{z} - \int_0^{\tilde{\Sigma}} \left[\frac{1}{\tilde{\rho}(0, \hat{\Sigma}; ...)} + \frac{1}{\hat{\Sigma}} \right] \mathrm{d}\hat{\Sigma} \right). \tag{IV.4.1}$$

Equation (IV.4.1) requires an expression for the contact value $\tilde{\rho}(0, \hat{\Sigma}; ...)$ that captures all the data. One can investigate whether a $\tilde{\rho}(0, \hat{\Sigma}; ...)$ will collapse measured EDL profiles

by parametrically plotting free charge density along the effective charge density

$$\tilde{\Sigma}(\tilde{z}) \equiv \frac{\Sigma(z/\lambda_{\mathrm{D}})}{\Sigma_{\mathrm{ref}}} = \int_0^{\tilde{z}} \tilde{\rho} \mathrm{d}\hat{z}. \tag{IV.4.2}$$

In Figure IV.5, we investigate PM EDL profiles with $\sigma_{\mathrm{co}} = 2\sigma_{\mathrm{c}}$ and $\bar{\Phi}^{\mathrm{B}} = 0.17$, parametrically plot $\tilde{\rho}(\tilde{z})$ versus $\tilde{\Sigma}(\tilde{z})$, and find no suitable $\tilde{\rho}(0, \hat{\Sigma}; ...)$ exists. Excluded volume effect cause oscillations in the free charge density that prevent the overall collapse of the data. We include BMCSL-LDA predictions to show that it also does not describe all the PM EDLs. Since there is not a form for $\tilde{\rho}(0, \hat{\Sigma}; ...)$ that captures all of the simulations, we must investigate alternative non-LDA approaches in an attempt to describe EDLs with co-ions are larger than counter-ions.

IV.5 Alternative Non-LDA Electric Double Layer Models

There are a variety of compressibility expressions for hard-sphere systems [Mulero et al., 1999] that can be tried in attempt to improve upon the BMCSL approach; however, they must be benchmarked against experimental data or simulation to be certain of their accuracy [Henderson and Boda, 2009]. The BMCSL EOS has been compared to CS predictions of vapor-liquid equilibria [Dimitrelis and Prausnitz, 1986] for a variety of mixtures of non polar spherical molecules that differ in molecular size, e.g. neon/argon, argon/neopentane, methane/n-decance, etc. Although BMCSL outperforms the CS model for $\sigma_{\mathrm{big}} \gtrsim 2\sigma_{\mathrm{small}}$, the BMCSL EOS overestimates the pressure at a given composition for all of the experimental systems at every temperature and especially at higher

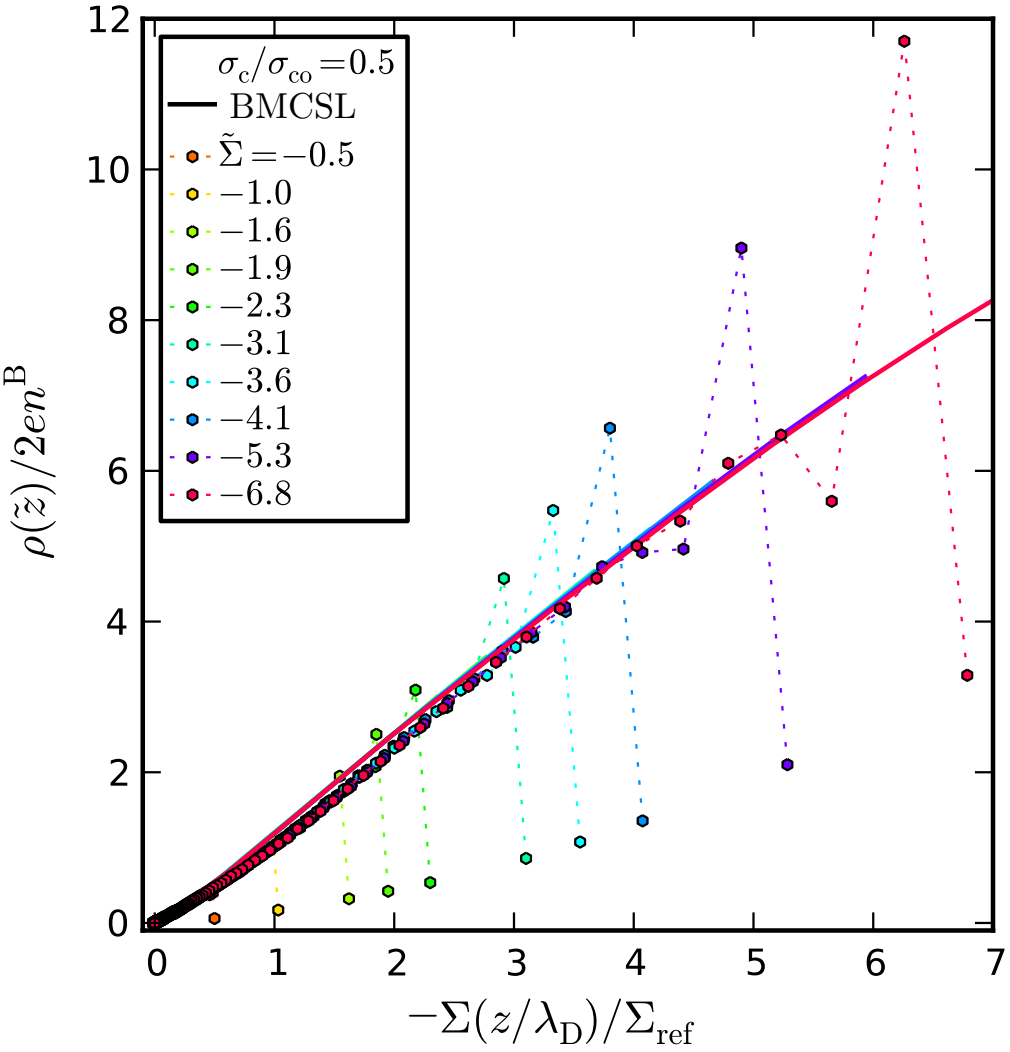

Figure IV.5: Contact value expressions $\tilde{\rho}(0,\tilde{\Sigma})$ for Primitive Model and BMCSL electric double layers with $\bar{\Phi}^B = 0.17$. PM EDLs collapse onto BMCSL contact value expressions only in the low charge limit $\tilde{\Sigma} \to 0$ and/or in the bulk $\tilde{\rho} \to 0$. The general LDA approach is not suitable wherever the PM EDL profiles do not collapse.

concentrations. MC simulations of hard spheres show the performance of BMCSL contact value predictions to drop significantly for dilute solutions of large particles, also for cases where $\sigma_{\text{big}} \gtrsim 2\sigma_{\text{small}}$ [Feng and Chapman, 2011]. BMCSL estimates of the pressure of MC simulations of three component hard-sphere mixtures were five times lower than numerical error [Hansen-Goos and Roth, 2006]. Considering the deficiencies of the BMCSL model reported in the literature and apparent inability of LDAs to describe EDLs with smaller co-ions [Fig. IV.5], we briefly discuss alternative non-LDA EDL models that do not rely solely on the BMCSL EOS.

Density Functional Theory (DFT) is a computational integral equation technique that has been extensively tested against bulk and inhomogenous hard sphere systems [Roth, 2010]. The essential task of DFT is to determine a functional for the Helmholtz free energy, Ω, that can be expressed as a functional of the density distribution, $\Omega = \Omega[\rho(\mathbf{r})]$, of particles that comprise that system. Furthermore, the equilibrium density profile, $\rho_0(\mathbf{r})$, is determined as that which minimizes the functional: $\Omega[\rho(\mathbf{r}) \neq \rho_0(\mathbf{r})] > \Omega[\rho_0(\mathbf{r})]$. Therefore, by fully minimizing the free energy functional one obtains the thermodynamic properties of the system via Ω and the structure of the system in the form of $\rho_0(\mathbf{r})$ [Roland, 2006].

A popular extension of DFT is called Fundamental Measure Theory that can accurately describe mixtures of hard-sphere systems. Fundamental Measure Theory is a non-local approach that uses weighted densities to account for behavior within inhomogeneous systems [Bazant et al., 2009]. These "weighted density approximations" (WDA) are then used within chemical potential expressions to more accurately account for packing effects between differently-sized particles [Roth, 2010]. WDAs have been used to

develop electric double layer models that require solutions to non-linear integral equations to obtain ion distributions and voltage profiles. LDAs have been shown to fail where WDAs succeed in describing planar EDL systems comprised of equal [Patra and Ghosh, 2002, Wang et al., 2011] and asymmetric [Gillespie et al., 2005] ions, and in colloidal systems [Antypov et al., 2005] that exhibit overcharging. These approaches, which go beyond the LDA assumptions, may be required to properly describe the detailed structure of concentrated EDLs with excluded volume effects.

IV.6 Conclusion

We find the BMCSL-LDA accurately predicts the integrated capacitance across a wide range of applied surface charge densities, electrostatic surface potentials, and bulk volume fractions *only* when the counter-ion size is greater or equal to the co-ion. The BMCSL-LDA slightly underestimates the free charge density and voltage profiles when $\sigma_c/\sigma_{co} < 1$, but captures these quantities outside of regions where larger counter-ions layer at highly charged electrodes. Overall, the BMCSL-LDA is a poor descriptor of ideal and excluded volume chemical potential component profiles for EDLs with co-ions larger than counter-ions. BMCSL predictions of excluded volume chemical potential measurements of bulk systems of differently sized WCA particles reveal the BMCSL model to only describe nearly pure systems characterized by infinitesimal concentrations of one species or indistinguishable particles in the limit where BMCSL recovers the Carnahan-Starling EOS. We probe PM EDL profiles with $\sigma_{co} = 2\sigma_{co}$ and $\bar{\Phi}_B = 0.17$ and find that no contact value expression collapses the simulation data. By self-similarity scaling arguments, we

determine alternative non-LDA modeling techniques are required to accurately describe size asymmetric PM EDLs where co-ions are the smaller species.

Chapter V

Conclusions

V.1 Implications

In Chapter II, we developed a general and powerful formalism to identify and elucidate LDA behavior in EDLs that follows from a remarkably simple observation: in any LDA, an ion does not know where the interface is located. Without assumptions, our approach enables one to analyze planar EDLs and determine directly from contact value expressions whether any LDA can possibly succeed, without considering any specific LDA models. If a LDA will work, measured profiles of the free charge density for many different electrolyte systems will collapse onto a single, master curve as a function of an intrinsic, derivable similarity variable. Where measured EDL profiles do not collapse onto a similarity variable, the test reveals the boundaries of LDA feasibility space, beyond which more sophisticated treatments capable of addressing correlation effects are needed. Our model-free approach is broadly applicable, and will be valuable in assessing potential LDA behavior in more general electrolytes, *e.g.* where finite-sized effects (as

discussed in Chapters II and III), solvation effects, emergent electrostatic correlations, and/or discrete interfacial charges play an important role.

It is straightforward to apply this model-free approach to much more general electrolytes. The simplest extension would involve asymmetric electrolytes – with two or more ion species of different size (as discussed in Chapter IV) and/or valence. In that case, one can anticipate that some $\mu_{\pm}^{\mathrm{ex}}(\Phi_{\pm})$ [Biesheuvel and Soestbergen, 2007], analogous to $\mu_{\mathrm{CS}}^{\mathrm{ex}}$ for equi-sized ions, could be found to work in a trial LDA. No obvious $\mu_{\pm}^{\mathrm{ex}}$, however, exists for less straightforward electrolytes – *e.g.* measured or computed with explicit solvent and specific chemical force fields. Nonetheless, our model-free test will immediately reveal whether any LDA can be found that captures such EDL behavior.

Similarity variables from distinct LDAs have distinct functional forms. For example, S_{GC} (which collapses point-like EDL profiles) diverge, whereas S_{CS} (which collapses semi-dilute EDL profiles) do not. Any difference in S observed between anodic and cathodic EDLs immediately reveals anions and cations to have unequal size and/or valence. Indeed, these model-free similarity-variables may serve as "fingerprints" specific to that particular electrolyte. Our approach is broadly applicable to EDL profiles from simulations, x-ray reflectivity measurements, etc., and will be valuable in assessing potential LDA behavior in more general electrolytes, *e.g.* where solvation effects, discrete interfacial, and/or electrostatic and excluded volume correlations charges play a significant role.

In Chapter III, we explore the specific case of size-induced correlations in which nonlocal ion layering gives rise to oscillatory free charge densities. We also examine spatial free charge densities to determine the boundary between correlated and diffuse EDL

regimes, ℓ_{cor}. We illustrate a model-free technique in Fig. III.6 to extract the correlation length by identifying the boundary where oscillations the PM EDL charge density profiles are due to bulk fluctuations versus excluded volume effects. We apply this method to a series of PM EDL simulations and can map the thickness of the correlated region as a function of bulk volume fraction and electrode charge density [Fig. III.7]. In principle, a variant of this approach could be applied to characterize empirically derived ion density profiles. With this information, an empirical description of the correlation length as a function of electrode charge density and bulk volume fraction could help to interpret broad classes of electrolytes and/or ionic liquid systems. When electrostatic contributions also become relevant, we may be able to define a correlation length; however, we explore only systems where finite-sized effects contribute to correlations.

Models that predict the location where correlations begin may provide reasonable estimates for deciding what regimes to model using rapidly solvable LDAs versus where more detailed analysis is required. Extrapolating these results to experimental systems, chemically specific effects may be constrained to some region near the interface that is analogous to correlated regimes within highly-charged and/or concentrated PM EDLs. This could help to interpret x-ray reflectivity, neutron scattering, or other experimental probes of EDL systems. As photons or neutrons are reflected, they scatter in different directions with a probability proportional the squared amplitude. When the diffraction signals are counted, information about the relative phases is lost. The well-known "phase problem" does not allow a unique determination of ion density profiles. Thus, a common practice is to construct a model for $n^{\pm}(z)$ from physical and chemical considerations, calculate a structure factor from this guess, and make iterative adjustments until the

model reproduces reflectivity data [Sloutskin et al., 2005]. In the case of molecular dynamics [Luo et al., 2006] and Monte Carlo simulations that are used to compute guesses for $n^{\pm}(z)$, considerable computational expense could be saved by combining the diffuse and correlated descriptions.

In Chapter IV, we explore LDA and PM simulations of EDL for electrolytes comprised of differently-sized ions. Specifically, we investigate the Boublík, Mansoori, Carnahan, Starling, and Leland-LDA (BMCSL-LDA) [Boublík, 1970, Mansoori et al., 1971] that is derived from an extension of the Carnahan-Starling equation of state. We use the BMCSL-LDA to analyze a variety of EDL systems with moderate volume fractions of asymmetrically sized ions that are weakly and oppositely charged. We find the BMCSL-LDA predicts PM EDL behavior when the counter-ions are larger than co-ions. We briefly discuss a variety of non-local approaches that go beyond the LDA assumptions in order to obtain detailed descriptions of asymmetric EDL systems.

V.2 Future Directions: Primitive Models and Local-Density Approximations of Solvent Effects

The mean-field local density approximations and Primitive Models of the electric double layer that we have discussed assume implicit solvent electrolytes comprised of ions in a continuum. In real EDL systems, solvent has structure and its ability to solvate ionic species and participate in neutralizing electrode surface charge drastically influences ion concentration profiles [Israelachvili, 1992]. There are a variety of promising modeling

approaches to treat solvent interactions within electrolytic systems; however, no model is universally accepted [Maginn and Elliott, 2010]. The choice of a suitable method involves a trade off between computational expense and accuracy amongst the myriad of available theoretical and computational techniques.

Explicit solvent models of aqueous electrolytes often treat ions as charge-centered particles and solvent as neutral particles, possibly with attractive ion-ion, ion-solvent, and solvent-solvent interactions. The simplest approach that captures non-trivial ion-solvent interactions is a variant of the Primitive Model. The Solvent PM includes additional uncharged particles that represent solvent and charged-centered particles that represent ions. Adaptations to the Solvent PM may replace hard- or WCA-spheres with Lennard-Jones particles to treat van der Walls-like effects. The Solvent PM is a relatively less computationally less expensive compared to other models that use force fields characteristics specific to a particular electrolyte system. A prominent molecular solvent model treats water as a rigid triangle with simple point-charges (SPC) that is parameterized using empirical data [Burt et al., 2014, Berendsen et al., 1987]. Molecular Dynamics simulations of aqueous EDLs that use a SPC solvent show solvated ions to layer at the both charged and uncharged electrodes causing density oscillations [Crozier et al., 2000, Spohr, 1998, Spohr, 2002]. In addition, explicit water simulations with asymmetrically-sized ions demonstrate that smaller ions tend to acquire rigid solvation shells, which prevents surface adsorption and results in different density profiles at the anode and cathode [Spohr, 1998, Spohr, 2002].

A natural extension of this work involves understanding the key solvation features of a model electrolyte without the complexities (and computational difficulties) of treating

water itself. For example, it is straightforward to modify the PM molecular simulation input files used in this thesis [Appendix B] by adding uncharged particles into the simulation. However, these Solvent PM simulations require at least ten times the particles of implicit solvent models to explore electrolytes with reasonable bulk volume fractions, $\Phi_{\mathrm{B}} \gtrsim 0.65$. Since the computational expense scales as $\mathcal{O}(N^2)$, we are motivated to find a simpler model system that contains sufficient, nontrivial, and relevant physics to explore an extensive range of EDL behavior.

We now present novel three component LDA models that seek to address a variety of non-ideal solvent interactions within the EDL. To do this, we assume chemical potential models for finite-sized anions, cations, and neutral solvent species

$$\begin{aligned} \tilde{\mu}^{-} &= \frac{\mu^{-} - \mu_{\mathrm{B}}^{-}}{k_{\mathrm{B}}T} = \ln \tilde{n}^{+} + q\tilde{\phi} + \tilde{\mu}_{\mathrm{ex}}^{-}(\tilde{n}^{+}, \tilde{n}^{-}, \tilde{n}^{\mathrm{S}}) \equiv 0\,, \\ \tilde{\mu}^{+} &= \frac{\mu^{+} - \mu_{\mathrm{B}}^{+}}{k_{\mathrm{B}}T} = \ln \tilde{n}^{-} - q\tilde{\phi} + \tilde{\mu}_{\mathrm{ex}}^{+}(\tilde{n}^{+}, \tilde{n}^{-}, \tilde{n}^{\mathrm{S}}) \equiv 0\,, \\ \tilde{\mu}^{\mathrm{S}} &= \frac{\mu^{\mathrm{S}} - \mu_{\mathrm{B}}^{\mathrm{S}}}{k_{\mathrm{B}}T} = \ln \tilde{n}^{\mathrm{S}} + \tilde{\mu}_{\mathrm{ex}}^{\mathrm{S}}(\tilde{n}^{+}, \tilde{n}^{-}, \tilde{n}^{\mathrm{S}}) \equiv 0. \end{aligned} \tag{V.2.1}$$

In the limit of point-sized solvent particles $\tilde{\mu}_{\mathrm{ex}}^{\mathrm{S}} \to 0$, the solvent does not interact with ions and behaves like a ideal gas

$$\tilde{\mu}^{\mathrm{S}} = \ln \tilde{n}^{\mathrm{S}} \equiv 0\,, \tag{V.2.2}$$

with uniform concentration $\tilde{n}^{\mathrm{S}} = 1$. If we then assume equi-sized ions to obey the Carnahan-Starling equation of state, Equation (V.2.1) returns the CS-LDA that describes the electrolyte as a homogeneous mixture of charged hard spheres in a vacuum. In the limit of point-sized ions $\tilde{\mu}_{\mathrm{ex}}^{\pm} \to 0$ in a finite-sized solvent, the total ion chemical potential is given by the BMCSL-LDA for vanishing small to large particle size ratios given by

Eq. (IV.2.12). In the ideal limit where all species are point-sized, Eqs. (V.2.1) returns GC-LDA described by Eq. (I.3.14).

One might model the Solvent PM by assuming the CS excess chemical potential for all species $\tilde{\mu}^i_{\rm ex} = \mu_{\rm CS,ex}[\Phi]$ in Eq. (V.2.1). In this regime, the Solvent-LDA describes a homogeneous system of equal-sized charged and uncharged hard-spheres. Following the general procedure outlined in Chapter I.3.1 to solve a LDA model, we determine the free charge density of ions in a LDA solvent:

$$\tilde{\rho}_{\rm CS-Solvent} \equiv \frac{\rho_{\rm CS-Solvent}}{2eI} = \frac{1}{2I}\sum_i^{\pm} n^i q^i \exp\left(-q^i\tilde{\phi} - \tilde{\mu}_{\rm CS,ex}[\Phi]\right) , \tag{V.2.3}$$

which depends on the local volume fraction of all three species

$$\Phi(\mathbf{r}) = \frac{\pi}{6}\sum_i^{+,-,\rm S} \sigma^i n^i(\mathbf{r}) \equiv \Phi^+ + \Phi^- + \Phi^{\rm S}. \tag{V.2.4}$$

We insert Eq. (V.2.3) into Eqs. (I.3.6) and (I.3.11) to compute the surface charge density versus potential curves and density profiles.

Figure V.1 shows the integrated capacitance and density profiles for Solvent-LDA EDLs in three distinct regimes: equal and finite-sized species (CS-Solvent), point-sized solvent with finite-sized ions (CS-LDA), and point-sized ions and solvent (GC-LDA). Preliminary results from these predictions suggest the total capacitance to increase with the volume fraction of hard-sphere solvent. This agrees with Solvent Primitive Model systems that demonstrate an increased capacitance as the concentration of solvent particles increases [Boda et al., 1998, Boda et al., 2000, Boda and Henderson, 2000]. Comparing the CS-LDA and CS-Solvent LDAs, the counter- and co-ion concentrations are larger when the excluded volume of the solvent is treated. Excluded volume interactions within highly concentrated regions cause the solvent density to deplete near the electrode.

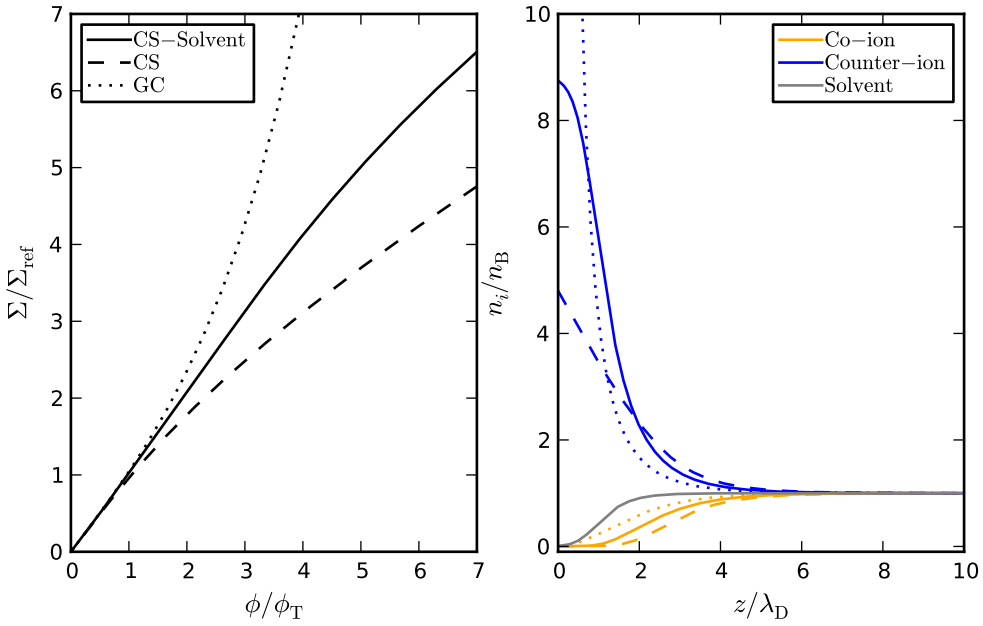

Figure V.1: Solvent-LDA predictions of surface charge density versus electrostatic potential drop [left] and ion and solvent density profiles [right]. In the the linear capacitance regime $\{\tilde{\Sigma}, \tilde{\phi}\} \to 0$, all LDAs converge onto the GC-LDA (dotted) that describes point-sized ions $\Phi_{\rm B}^{\pm} \to 0$ and solvent $\Phi_{\rm B}^{\rm S} \to 0$. Beyond the low charge limit $\{\tilde{\Sigma}, \tilde{\phi}\} > 1$, the GC-LDA diverges whereas LDAs that describe equi-sized ions with $\Phi_{\rm B}^{+} + \Phi_{\rm B}^{-} = 0.15$ predict larger capacitances for finite-sized solvent with $\Phi_{\rm B}^{\rm S} = 0.50$ (solid, Solvent-LDA) compared to assuming the solvent to be point-sized (dashed, CS-LDA). At a fixed surface voltage $\tilde{\phi}_0 = 7$, counter-ion densities are largest in the GC-LDA model and smallest in the CS-LDA. Co-ion densities are lowest in the CS-LDA and largest in the GC-LDA. Near the electrode, the Solvent-LDA predicts a depleted region of solvent density that converges to the bulk value within $\sim 4\lambda_{\rm D}$.

Solvent and ion species interact through both excluded volume and van der Waals forces within real electric double layer systems. To account for solvation interactions within our LDA model, we might express the excess Helmholtz free energy due to solvation interactions $A_{\rm ex}^{\rm S}$ per volume V as

$$A_{\rm ex}^{\rm S} \equiv \sum_{i}^{+,-,{\rm S}} N^i w^i \frac{N^{\rm S}}{V} = N^+ w^+ \frac{N^{\rm S}}{V} + N^- w^- \frac{N^{\rm S}}{V}\,, \tag{V.2.5}$$

where the number of ions N^i of type i interact with $N^{\rm S}$ solvent molecules with solvation interaction energy w^i. The solvation energy could be parameterized from the Born ion solvation energy or the characteristic energy scale of Solvent PM electrolytes that include attractive interactions. Negative values correspond to attractive interactions and $w^i = 0$ represents a hard-sphere system. One might assume the solvent equally solvates the ions $w^i = w^{\pm}$.

The excess chemical potential due to solvation is determined from Eq. (V.2.5)

$$\mu_{\rm ex}^{{\rm S}-i} = \frac{\partial A_{\rm ex}^{\rm S}}{\partial N^i}. \tag{V.2.6}$$

to obtain the reduced solvent-ion interactions

$$\tilde{\mu}_{\rm ex}^{{\rm S}-\pm} \equiv \frac{\mu_{\rm ex}^{{\rm S}-\pm} - \mu_{\rm ex,B}^{{\rm S}-\pm}}{k_{\rm B}T} = \frac{w^{\pm}}{k_{\rm B}T}(n^{\rm S} - n_{\rm B}^{\rm S}) = \tilde{w}^{\pm}\left(\tilde{n}^{\rm S} - 1\right) \tag{V.2.7}$$

and solvent-solvent interactions

$$\tilde{\mu}_{\rm ex}^{{\rm S}-{\rm S}} \equiv \frac{\mu_{\rm ex}^{{\rm S}-{\rm S}} - \mu_{\rm ex,B}^{{\rm S}-{\rm S}}}{k_{\rm B}T} = \tilde{w}^{\pm}\left(\tilde{n}^{+} + \tilde{n}^{-} - 2\right). \tag{V.2.8}$$

Eqs. (V.2.7) and (V.2.8) and the CS excess chemical potential can then incorporated into Eq. (V.2.1) to account for electrolytes comprised of charge-centered hard cores that are solvated by uncharged hard spheres.

Another important interaction to account for when modeling electrolytes is the dielectric response of a polarizable solvent [Bazant et al., 2009]. To address dielectric saturation, a theory based on the Poisson-Boltzmann equation was posed that introduced a field-dependent permittivity [Grahame, 1950]. Another approach involves the Dipolar Poisson-Boltzmann equation (DPBE), which has been developed to explicitly capture features of a dipolar solvent within the mean-field LDA framework [Abrashkin et al., 2007]. The DPBE is derived by assuming that each molecular dipole has a fixed magnitude p_0 and that ions can be either point-sized or behave as a Bikerman lattice gas. Solutions to the DPBE predict an increase in the permittivity in EDL regions near the electrode, which disagrees with empirical findings [Bazant et al., 2009]. It also permits unphysical large concentrations near the electrode [Abrashkin et al., 2007].

One might attempt to account for size-effects by assuming an electrolyte comprised of monovalent hard-sphere ions within a dipolar solvent confined between two oppositely charged plates separated by distance L. If one assumes the excluded volume effects are described by the Carnahan-Starling equation of state, the modified form of the DPBE is given by

$$-\frac{\mathrm{d}^2\tilde{\phi}}{\mathrm{d}\tilde{z}^2} = -\tilde{\rho}_{\mathrm{CS-Solvent}} + \tilde{\Sigma}(0) - \tilde{\Sigma}(L/\lambda_{\mathrm{D}}) + \left(\frac{n_{\mathrm{B}}^{\mathrm{S}}}{n_{\mathrm{B}}^{\pm}}\right)\frac{p_0}{e\lambda_{\mathrm{D}}}\frac{\mathrm{d}}{\mathrm{d}\tilde{z}}\mathcal{G}\left[\frac{p_0}{e\lambda_{\mathrm{D}}}\frac{\mathrm{d}\tilde{\phi}}{\mathrm{d}\tilde{z}}\right], \qquad \text{(V.2.9)}$$

where the function $\mathcal{G}(u) = \cosh u/u - \sinh u/u^2$ is related to the Langevin function $\mathcal{L}(u) = \coth u - 1/u$ by $\mathcal{G} = (\sinh u/u)\mathcal{L}$. The boundary condition at the $\tilde{z} = 0$ charge plane is

$$-\frac{\mathrm{d}\tilde{\phi}(0)}{\mathrm{d}\tilde{z}} = \frac{p_0}{e\lambda_{\mathrm{D}}}\left(\frac{n_{\mathrm{B}}^{\mathrm{S}}}{n_{\mathrm{B}}^{\pm}}\right)\mathcal{G}\left[\frac{p_0}{e\lambda_{\mathrm{D}}}\frac{\mathrm{d}\tilde{\phi}(0)}{\mathrm{d}\tilde{z}}\right] + \tilde{\Sigma}\,, \qquad \text{(V.2.10)}$$

and at $\tilde{z} = L/\lambda_{\mathrm{D}}$ is

$$-\frac{\mathrm{d}\tilde{\phi}(L/\lambda_{\mathrm{D}})}{\mathrm{d}\tilde{z}} = \frac{p_0}{e\lambda_{\mathrm{D}}}\left(\frac{n_{\mathrm{B}}^{\mathrm{S}}}{n_{\mathrm{B}}^{\pm}}\right)\mathcal{G}\left[\frac{p_0}{e\lambda_{\mathrm{D}}}\frac{\mathrm{d}\tilde{\phi}(L/\lambda_{\mathrm{D}})}{\mathrm{d}\tilde{z}}\right] - \tilde{\Sigma}. \tag{V.2.11}$$

Equations (V.2.9)-(V.2.11) account for hard-sphere interactions amongst charged ions and hard-sphere solvent dipoles. However, one may also account for van der Waals interactions by incorporating models for the excess chemical potential due to solvation as in Eqns. (V.2.7)-(V.2.8).

Using these simple, yet physically intuitive Solvent-LDAs alongside complementary Solvent Primitive Model simulations, we can begin to address the following questions:

• How does the capacitance and equilibrium density and chemical potential profiles respond as we vary the size and concentration of solvent?

• How do these model electrolytes respond when ions preferably solvate one ion versus the other, i.e. $w^+ < w^i$?

• How do these model electrolytes respond to a polarizable solvent?

• How do the Solvent-LDA and Solvent PM compare to each other? Can simple models capture the essential physics without the computational expense?

• Can we develop improved LDA models using simulation results from Solvent PM or more molecularly detailed solvent models?

• How well do LDA similarity coordinates collapse empirically derived EDL profiles?

• Can we rationalize specific ion-ion or ion-solvent systems in order to develop improved models that describe actual EDL systems?

In this dissertation, we have shown the venerable LDA modeling approach to provide simple, yet qualitatively accurate descriptions of electric double layers. We illustrate that

it is possible to reveal the feasibility space of LDA models and to develop more suitable LDA chemical potentials that are specific to experimentally-interesting regimes. In addition to what we have shown here, numerous scientific efforts have demonstrated LDA models to accurately describe and engineer a variety of electrochemical systems: ionic liquids, aqueous electrolytes, asymmetric electrolytes comprised of ions with different size and/or valence, electric double layer capacitors, and capacitance desalination devices.

Appendices

Appendix A

General Local-density Approximation Solver Source Code

Below we provide source code that can be used to solve general local-density approximation models using both numerical and analytical techniques. We provided detailed solutions of the Bikerman, Carnahan-Starling, and BMCSL asymmetrically-sized ion models. We also show how to numerically compute similarity variable from the CS model, i.e. S_{CS}. Although we chose to write this code using Mathematica, it is possible to use open-source languages such as python-based Sage.

```
ClearAll["Global*"];

(*Define constants*)
(*C for cations and A for anions*)
qC = 1;
qA = -qC;

ρAbulk = 0.00185418910071;
ρCbulk = ρAbulk;
```

```
(*Ionsizes = 0.90 * σWCA*)
σC = 2.47227980171;
σA = 4.94455055541;

ζ = 5.27;  (*zeta-potential*)

zB = 10.; (* In units of λ_D*)

step = 0.001;

(*Carnahan − Starling chemical potential*)
μCS[Φ_]:=Φ(8−9*Φ+3*Φ^2)/(1−Φ)^3

(* Two Component BMCSL chemical potential*)
ξ[n_, A_, C_]:=(π/6) * (ρAbulk * A * σA^n + ρCbulk * C * σC^n)
Φion = ξ[3, 1, 1]

μBMCSL[A_, C_, σ_]:=
−(1 + 2*σ^3*ξ[2,A,C]^3/ξ[3,A,C]^3 − 3*σ^2*ξ[2,A,C]^2/ξ[3,A,C]^2) * Log[1 − ξ[3, A, C]]
+3*σ*ξ[2,A,C]+3*σ^2*ξ[1,A,C]+σ^3*ξ[0,A,C]/1−ξ[3,A,C] +
3*σ^2*ξ[2,A,C]/(1−ξ[3,A,C])^2 (ξ[2,A,C]/ξ[3,A,C] + σ * ξ[1, A, C])
−σ^3 * ξ[2, A, C]^3 * (ξ[3,A,C]^2−5*ξ[3,A,C]+2/ξ[3,A,C]^2*(1−ξ[3,A,C])^3)

(*This solves MPB − Bik to determine z − dependence*)
NDSolve [{ψ'[z] == −Sqrt [2Log[1+2*Φion*Sinh[ψ[z]/2]^2]/Φion], ψ[0] == ζ},
ψ, {z, 0, zB}, AccuracyGoal → 12]

ψBik[z_] = ψ[z]/.%[[1]];

CBik[ψBik_]:=1/2*Exp[ψBik]+Φion(1−2*Exp[ψBik]+Exp[2*ψBik])

ABik[ψBik_]:=Exp[2*ψBik]/2*Exp[ψBik]+Φion(1−2*Exp[ψBik]+Exp[2*ψBik])

(*CS LDA Solver*)
(*ui = 1 − ni*)
uA0[ψ_, ΦB_]:=
Min [Exp[ψ] − 1, If [ΦB > 0, 0.99 (2/ΦB(Exp[−2ψ]+1) − 1), Exp[ψ] − 1]]

uA1[ψ_, ΦB_]:=v/.
FindRoot[Exp[ψ − μCS[ΦB(v + 1)(Exp[−2ψ] + 1)/2] + μCS[ΦB]] − 1 == v,
{v, uA0[ψ, ΦB]}]
```

```
uA[ψ_, ΦB_]:=If[ψ ≥ 0, uA1[ψ, ΦB], (uA1[−ψ, ΦB] + 1)Exp[2ψ] − 1]

ACSguess0 = Interpolation[Table[{ψ, 1 + uA[ψ, Φion]}, {ψ, −0.5, ζ * 2, step}]];

CCSguess0 = Interpolation[Table[{ψ, Exp[−2 * ψ] * (1 + uA[ψ, Φion])},
{ψ, −0.5, ζ * 2, step}]];

uAinterp0 = Interpolation[Table[{ψ, uA[ψ, Φion]}, {ψ, −0.5, ζ * 2, step}]];

ifreeCS = Interpolation[Table[{ψ, CCSguess0 − ACSguess0},
{ψ, −0.5, 30, step}]];

(*Charge − voltage can be determined without solving Poisson's equation*)
ChargeVoltageCS[ψ_]:=√(2 * Abs[NIntegrate[ifreeCS[volt], {volt, ψ, 0}]]);

(* Modified PBE for CS − LDA to determine z − dependence*)
NDSolve [{ψ"[z] + ((uAinterp0[ψ[z]]+1)(Exp[−2ψ[z]]−1))/2 == 0,
ψ[0] == ζ, ψ[zB]==0}, ψ, {z, 0, zB},
Method → {"Shooting", "MaxIterations" → 10000}, AccuracyGoal → 12];

ψCS[z_] = ψ[z]/.%[[1]];

uAsoln[z_]:=uAinterp0[ψCS[z]]

uCsoln[z_]:=(uAsoln[z] + 1)Exp[−2ψCS[z]] − 1

FreeCS[z_]:=0.5 * (uCsoln[z] − uAsoln[z])

CCS[z_]:=1 + uCsoln[z]

ACS[z_]:=1 + uAsoln[z]

(*Computing similarity variable from CS − LDA, SCS.
Similarity variables from other LDAs can be computed similarly*)
contactGC[Σ_]:= − Σ√(1 + (Σ/2)^2);

SGC[z_, Σapp_]:= (2 / (1 + √((Σapp/2)^2 + 1))) * Σapp * Exp[−z];

ΣCS = −Table[NIntegrate[ifreeCS[x], {x, z, zB}], {z, 0, zB, step}];

rhoCS = Table[ifreeCS[z], {z, 0, zB, step}];
```

```
contactCS = {}; Do[AppendTo[contactCS, List[ΣCS[[i]], rhoCS[[i]]]],
{i, 1, Length[ΣCS]}]; contactCS = Interpolation[contactCS];

dlnhCS[Σ_]:=1/contactGC[Σ] - 1/contactCS[Σ]

(*find where dlnh goes to zero*)
ΣvalCS = Σ/.FindRoot[dlnhCS[Σ] == 0., {Σ, .5}];

(*artificially modify dlnh so that it goes to zero and stays there*)
dlnh2CS[Σ_]:=If[Σ > ΣvalCS, dlnhCS[Σ], 0.]

lnhCS[Σapp_]:=NIntegrate[dlnh2CS[Σ], {Σ, 0., Σapp}]

SCS[z_, Σapp_]:=SGC[z, Σapp]Exp[lnhCS[Σapp]]

(*BMCSL LDA Solver*)
ABMCSLhighvolt[ψ_]:=A/.
FindRoot[Log[A] == -qA * ψ - μBMCSL[A, 0, σA] + μBMCSL[1, 1, σA],
{A, 0.55 * ACSguess0[ψ]}, MaxIterations → 10000];

ABMCSL0 = Interpolation[Table[{ψ, ABMCSLhighvolt[ψ]},
{ψ, -0.5, ζ * 2, step}]];
ABMCSL[ψ_]:=Re[A]/.FindRoot[{
Log[C] == -qC * ψ - μBMCSL[A, C, σC] + μBMCSL[1, 1, σC],
Log[A] == -qA * ψ - μBMCSL[A, C, σA] + μBMCSL[1, 1, σA]},
{{A, 0.5 * ABMCSL0[ψ]}, {C, CCSguess0[ψ]}},
MaxIterations → 10000];

CBMCSL[ψ_]:=Re[C]/.FindRoot[{
Log[C] == -qC * ψ - μBMCSL[A, C, σC] + μBMCSL[1, 1, σC],
Log[A] == -qA * ψ - μBMCSL[A, C, σA] + μBMCSL[1, 1, σA]},
{{A, 0.5 * ABMCSL0[ψ]}, {C, CCSguess0[ψ]}},
MaxIterations → 10000];

FBMCSL[ψ_]:=((qC * Re[C] + qA * Re[A])/2)/.FindRoot[{
Log[C] == -qC * ψ - μBMCSL[A, C, σC] + μBMCSL[1, 1, σC],
Log[A] == -qA * ψ - μBMCSL[A, C, σA] + μBMCSL[1, 1, σA]},
{{A, 0.5 * ABMCSL0[ψ]}, {C, CCSguess0[ψ]}},
MaxIterations → 10000];

iABMCSL = Interpolation[Table[{ψ, ABMCSL[ψ]},
{ψ, -0.5, ζ * 1.5, step}]];

iCBMCSL = Interpolation[Table[{ψ, CBMCSL[ψ]},
{ψ, -0.5, ζ * 1.5, step}]];
```

```
iFreeBMCSL = Interpolation[Table[{ψ, FBMCSL[ψ]},
{ψ, −0.5, ζ * 1.5, step}]];

ChargeVoltageBMCSL[ψ_]:=
√(2 * Abs[NIntegrate[iFreeBMCSL[volt], {volt, ψ, 0}]]);

(* Modified PBE for BMCSL − LDA to determine z − dependence*)
NDSolve[{ψ"[z] + iFreeBMCSL[ψ[z]] == 0, ψ[0] == ζ,
ψ[zB]==0}, ψ, {z, 0, zB},
Method → {"Shooting", "MaxIterations" → 10000}, AccuracyGoal → 12];

ψBMCSL[z_] = ψ[z]/.%[[1]];

ABMCSL[z_]:=iABMCSL[ψBMCSL[z]];

CBMCSL[z_]:=iCBMCSL[ψBMCSL[z]];

FreeBMCSL[z_]:=iFreeBMCSL[ψBMCSL[z]];
```

Appendix B

LAMMPS Source Code

Here we provide example Molecular Dynamics code for differently-sized WCA ions in a Langevin solvent. The time evolution of a MD system is deterministic and governed by Newton's equations of motion. The MD Primitive Model developed in this research uses the Verlet algorithm to propagate the particles by a time step, Δt. The algorithm is derived from a Taylor expansion of a particle's position vector, $\mathbf{r}^i$, in time, t, and is presented in simplified form below:

$$\mathbf{r}^i(t+\Delta t) = 2\mathbf{r}^i(t) - \mathbf{r}^i(t-\Delta t) + \frac{\mathbf{f}_i(t)}{m_i}\Delta t^2 + \mathcal{O}(\Delta t^4). \tag{B.0.12}$$

A particle's mass, m_i, current, $\mathbf{r}^i(t)$, and past, $\mathbf{r}_i(t-\Delta t)$, coordinates, as well as current total force, $\mathbf{f}_i(t)$, determine the future particle positions, $\mathbf{r}^i(t+\Delta t)$. The derivative of the potential, $U(\mathbf{r})$ described in Eq. (I.3.27) gives the force on a particle

$$\mathbf{f}^i = -\nabla U(\mathbf{r}). \tag{B.0.13}$$

Unlike the Monte Carlo method that can only be used to simulate systems at equilibrium, MD can be used to extract dynamical information on the properties of the system [Frenkel and Smit, 2001, Allen and Tildesley, 1987].

We use LAMMPS to compute our MD simulations and provide example code below. Detailed information about the LAMMPS can be found at lammps.sandia.gov.

```
1 # Initialize simulation box
2 dimension    3
3 boundary     p p f
4 units        lj
5 atom_style   charge
6 region    simbox block -12 12 -12 12 -251 251 units box
7 create_box   2 simbox
8
9 # Place 1162 ions in an equilibrium configuration according
    to GC theory with input parameters:
```

```
# (Debye Length,Bjerrum,zeta) = (~15,0.1,3.0)
create_atoms  1 single -10.88 -10.93 -248.50 units box
create_atoms  2 single -11.06 -11.28 248.50 units box
#     Omitting 1158 insertions for brevity
create_atoms  1 single -3.93 -3.35 -0.50 units box
create_atoms  2 single -3.83 -3.55 0.50 units box

# Create groups
group   A type 1
group   C type 2
group   ions type 1 2

# Set masses and charges
mass    1 1.0
mass    2 1.0
set     group A charge -1
set     group C charge 1

# Set Bjerrum length, which equals 1/dielectric for these
    ion valences and pairwise potentials
dielectric  10.0

# Set time step
timestep      0.001

# Setup output format of thermodynamic information
thermo_style  custom step temp etotal pe ecoul evdwl cpu
thermo        1000

# Parameterize Langevin thermostat with implicit solvent
    interactions
velocity  all create 1.0 3
fix   thermostat all langevin 1.0 1.0 25 3
fix   timeintegration all nve

# Set potentials:
# Bound particles within repulsive 9/3 walls
fix anode all wall/lj93 zlo -251 1 1.165 1 units box
fix cathode all wall/lj93 zhi 251 1 1.165 1 units box

# This pushes potentially overlapping particles apart
pair_style   soft 3.0
pair_coeff   * * 60.0 3.0
run          35000

```

```
53 # Add single-body interaction with uniformly charged
     electrode with surface charge density ~ Force*dielectric
54 fix    A_field A addforce 0.0 0.0 0.28390
55 fix    C_field C addforce 0.0 0.0 -0.28390
56
57 # Parameterize charge-centered WCA spheres with size ratio
     of 3
58 pair_style  lj/cut/coul/long 5.61513 15.0
59 pair_coeff  1 * 1. 1.61887 1.81712
60 pair_coeff  2 * 1. 5.00251 5.61513
61
62 # Parameterize slab PPPM Ewald summations
63 kspace_style    pppm 1E-4
64 kspace_modify   slab 3.0
65 pair_modify     shift yes
66
67 # Equilibration run
68 run      5000000
69
70 # Production run
71 dump     dump1 all custom 1000 OutputFilename.gz id type x y
     z xu yu zu vx vy vz fx fy fz
72 run      50000000
73 undump   dump1
74
75 # Generate short trajectory for movie-making purposes
76 dump     Movie_dump all atom 1000 MovieOutput.all
77 run      500000
```

Appendix C

Copyright License

Bibliography

[Abrashkin et al., 2007] Abrashkin, A., Andelman, D., and Orland, H. (2007). Dipolar Poisson-Boltzmann Equation: Ions and Dipoles Close to Charge Interfaces. *Phys. Rev. Lett.*, 99:077801.

[Allen and Tildesley, 1987] Allen, M. P. and Tildesley, D. J. (1987). *Computer Simulation of Liquids*, Oxford University Press, New York, New York.

[Andelman, 1995] Andelman, D. (1995). Chapter 12 Electrostatic Properties of Membranes: The Poisson-Boltzmann Theory. In Lipowsky, R. and Sackmann, E., editors, *Structure and Dynamics of Membranes*, volume 1 of *Handbook of Biological Physics*, pages 603 – 642. North-Holland.

[Antypov et al., 2005] Antypov, D., Barbosa, M. C., and Holm, C. (2005). Incorporation of Excluded-Volume Correlations into Poisson-Boltzmann Theory. *Physical Review E*, 71(6):061106.

[Attard, 1993] Attard, P. (1993). Simulation of the Chemical Potential and the Cavity Free Energy of Dense Hard-Sphere Fluids. *The Journal of Chemical Physics*, 98(3):2225.

[Attard, 1996] Attard, P. (1996). Electrolytes and the Electric Double Layer. *Advances in Chemical Physics*, 92:1–160.

[Balducci et al., 2007] Balducci, A., Dugas, R., Taberna, P., Simon, P., Plee, D., Mastragostino, M., and Passerini, S. (2007). High Temperature Carbon-Carbon Supercapacitor Using Ionic Liquid as Electrolyte. *J Power Sources*, 165(2):922–927.

[Barker and Henderson, 1976] Barker, J. and Henderson, D. (1976). What Is "Liquid?" Understanding the States of Matter. *Rev Mod Phys*, 48(4):587–671.

[Bazant et al., 2009] Bazant, M. Z., Kilic, M. S., Storey, B. D., and Ajdari, A. (2009). Towards an Understanding of Induced-Charge Electrokinetics at Large Applied Voltages in Concentrated Solutions. *Adv. Colloid Interface Sci.*, 152:48 – 88.

[Bazant et al., 2011] Bazant, M. Z., Storey, B. D., and Kornyshev, A. A. (2011). Double Layer in Ionic Liquids: Overscreening Versus Crowding. *Phys. Rev. Lett.*, 106:046102.

[Berendsen et al., 1987] Berendsen, H. J. C., Grigera, J. R., and Straatsma, T. P. (1987). The Missing Term in Effective Pair Potentials. *The Journal of Physical Chemistry*, 91(24):6269–6271.

[Berryman, 1983] Berryman, J. (1983). Random Close Packing of Hard Spheres and Disks. *Physical Review A*, 27(2):1053.

[Bhuiyan and Henderson, 2011] Bhuiyan, L. B. and Henderson, D. (2011). A Local, Semi-Empirical Contact Condition for the Charge Profile in an Electric Double Layer with Size-Asymmetric Ions at Low Electrode Charge: Comparison with Simulations. *Mol. Simulat.*, 37(4):269–276.

[Biesheuvel and Soestbergen, 2007] Biesheuvel, P. and Soestbergen, M. V. (2007). Counterion Volume Effects in Mixed Electrical Double Layers. *J. Colloid Interface Sci.*, 316(2):490 – 499.

[Biesheuvel and Bazant, 2010] Biesheuvel, P. M. and Bazant, M. Z. (2010). Nonlinear Dynamics of Capacitive Charging and Desalination by Porous Electrodes. *Phys. Rev. E*, 81:031502.

[Bikerman, 1942] Bikerman, J. (1942). XXXIX. Structure and Capacity of Electrical Double Layer. *Philo. Mag. Series 7*, 33(220):384–397.

[Boda et al., 1998] Boda, D., Chan, K., and Henderson, D. (1998). Monte Carlo Simulation of an Ion-Dipole Mixture as a Model of an Electrical Double Layer. *The Journal of Chemical Physics*, 109:7362.

[Boda and Henderson, 2000] Boda, D. and Henderson, D. (2000). The Capacitance of the Solvent Primitive Model Double Layer at Low Effective Temperatures. *The Journal of Chemical Physics*, 112:8934.

[Boda et al., 2000] Boda, D., Henderson, D., Patrykiejew, A., and Sokołowski, S. (2000). Simulation and Density Functional Study of a Simple Membrane. II. Solvent Effects Using the Solvent Primitive Model. *The Journal of Chemical Physics*, 113:802.

[Bonthuis et al., 2011] Bonthuis, D. J., Gekle, S., and Netz, R. R. (2011). Dielectric Profile of Interfacial Water and Its Effect on Double-Layer Capacitance. *Phys. Rev. Lett.*, 107:166102.

[Boublík, 1970] Boublík, T. (1970). Hard-Sphere Equation of State. *The Journal of Chemical Physics*, 53(1):471.

[Burt et al., 2014] Burt, R., Birkett, G., and Zhao, X. S. (2014). A Review of Molecular Modeling of Electric Double Layer Capacitors. *Physical Chemistry Chemical Physics*, pages 1–20.

[Caprio et al., 2004] Caprio, D. D., Borkowska, Z., and Stafiej, J. (2004). Specific Ionic Interactions within a Simple Extension of the Gouy-Chapman Theory Including Hard Sphere Effects. *J. Electroanal. Chem.*, 572(1):51 – 59.

[Carnahan and Starling, 1969] Carnahan, N. F. and Starling, K. E. (1969). Equation of State for Nonattracting Rigid Spheres. *J. Chem. Phys.*, 51(2):635–636.

[Chapman, 1913] Chapman, D. L. (1913). A Contribution to the Theory of Electrocapillarity. *Philos. Mag. Series 6*, 25(148):475–481.

[Chmiola et al., 2006] Chmiola, J., Yushin, G., Gogotsi, Y., Portet, C., Simon, P., and Taberna, P.-L. (2006). Anomalous Increase in Carbon Capacitance at Pore Sizes Less Than 1 Nanometer. *Science*, 313(5794):1760–1763.

[Conway, 1999] Conway, B. E. (1999). *Electrochemical Supercapacitors: Scientific Fundamentals and Technological Applications*. Plenum Publishers, New York, New York.

[Crozier et al., 2000] Crozier, P. S., Rowley, R. L., and Henderson, D. (2000). Molecular Dynamics Calculations of the Electrochemical Properties of Electrolyte Systems between Charged Electrodes. *The Journal of Chemical Physics*, 113(20):9202–9207.

[Deryagin and Dukhin, 1969] Deryagin, B. and Dukhin, S. (1969). Theory of Surface Conductance. *Colloid Journal-Ussr*, 31(3):277.

[Dimitrelis and Prausnitz, 1986] Dimitrelis, D. and Prausnitz, J. (1986). Comparison of Two Hard-Sphere Reference Systems for Perturbation Theories for Mixtures. *Fluid Phase Equilibria*, 31(1):1–21.

[DOE, 2007] DOE, U. (2007). Basic Research Needs for Electrical Energy Storage: Report of the Basic Energy Sciences Workshop on Electrical Energy Storage. pages 1–186.

[Ed-China, 2010] Ed-China (1 July 2010). Ultracapacitor. *Web*, www.Ed-China.com.

[Fedorov et al., 2010] Fedorov, M., Georgi, N., and Kornyshev, A. (2010). Double Layer in Ionic Liquids: The Nature of the Camel Shape of Capacitance. *Electrochem. Commun.*, 12(2):296 – 299.

[Fedorov and Kornyshev, 2008] Fedorov, M. V. and Kornyshev, A. A. (2008). Ionic Liquid Near a Charged Wall: Structure and Capacitance of Electrical Double Layer. *J. Phys. Chem. B*, 112(38):11868–11872.

[Fedorov and Kornyshev, 2014] Fedorov, M. V. and Kornyshev, A. A. (2014). Ionic Liquids at Electrified Interfaces. *Chemical Reviews*, 114(5):2978–3036.

[Feng and Chapman, 2011] Feng, Z. and Chapman, W. (2011). Contact Values of Highly Asymmetric Hard Sphere Mixtures from Fundamental Measure Density Functional Theory. *Molecular Physics*, 109(13):1717–1726.

[French et al., 2010] French, R. H., Parsegian, V. A., Podgornik, R., Rajter, R. F., Jagota, A., Luo, J., Asthagiri, D., Chaudhury, M. K., Chiang, Y.-M., Granick, S., Kalinin, S., Kardar, M., Kjellander, R., Langreth, D. C., Lewis, J., Lustig, S., Wesolowski, D., Wettlaufer, J. S., Ching, W.-Y., Finnis, M., Houlihan, F., Von Lilienfeld, O. A., Van Oss, C. J., and Zemb, T. (2010). Long Range Interactions in Nanoscale Science. *Rev. Mod. Phys.*, 82:1887–1944.

[Frenkel and Smit, 2001] Frenkel, D. and Smit, B. (2001). *Understanding Molecular Simulation, Second Edition: From Algorithms to Applications*, Academic Press, London, UK.

[Giera et al., 2013] Giera, B., Henson, N., Kober, E., Squires, T., and Shell, M. (2013). Model-Free Test of Local-Density Mean-Field Behavior in Electric Double Layers. *Physical Review E*, 88(1):011301.

[Gillespie et al., 2011] Gillespie, D., Khair, A. S., Bardhan, J. P., and Pennathur, S. (2011). Efficiently Accounting for Ion Correlations in Electrokinetic Nanofluidic Devices Using Density Functional Theory. *J. Colloid Interface Sci.*, 359(2):520 – 529.

[Gillespie et al., 2005] Gillespie, D., Valisk, M., and Boda, D. (2005). Density Functional Theory of the Electrical Double Layer: The RFD Functional. *Journal of Physics: Condensed Matter*, 17(42):6609.

[González-Tovar et al., 2004] González-Tovar, E., Jiménez-Ángeles, F., Messina, R., and Lozada-Cassou, M. (2004). A New Correlation Effect in the Helmholtz and Surface Potentials of the Electrical Double Layer. *The Journal of Chemical Physics*, 120:9782.

[Gouy, 1910] Gouy, M. (1910). Sur la Constitution de la Charge Electronique a la Surface D'un Electrolyte. *J. Phys. Theor. Appl.*, 9(457).

[Grahame, 1950] Grahame, D. C. (1950). Effects of Dielectric Saturation upon the Diffuse Double Layer and the Free Energy of Hydration of Ions. *The Journal of Chemical Physics*, 18(7).

[Greberg and Kjellander, 1998] Greberg, H. and Kjellander, R. (1998). Charge Inversion in Electric Double Layers and Effects of Different Sizes for Counterions and Coions. *The Journal of Chemical Physics*, 108:2940.

[Grochowski and Trylska, 2007] Grochowski, P. and Trylska, J. (2007). Continuum Molecular Electrostatics, Salt Effects, and Counterion Binding: A Review of the Poisson–Boltzmann Theory and Its Modifications. *Biopolymers*, 89(2):93.

[Grosberg et al., 2002] Grosberg, A., Nguyen, T., and Shklovskii, B. (2002). Colloquium: The Physics of Charge Inversion in Chemical and Biological Systems. *Rev. Mod. Phys.*, 74(2):329–345.

[Guerrero-García et al., 2010] Guerrero-García, G. I., Gonzalez-Tovar, E., and Olvera De La Cruz, M. (2010). Effects of the Ionic Size-Asymmetry around a Charged Nanoparticle: Unequal Charge Neutralization and Electrostatic Screening. *Soft Matter*, 6:2056–2065.

[Guldbrand et al., 1984] Guldbrand, L., Jönsson, B., Wennerström, H., and Linse, P. (1984). Electrical Double Layer Forces. A Monte Carlo Study. *The Journal of Chemical Physics*, 80:2221.

[Hansen and McDonald, 1986] Hansen, J. and McDonald, I. (1986). *Theory of Simple Liquids*. Academic Press, San Diego.

[Hansen and Lowen, 2000] Hansen, J.-P. and Lowen, H. (2000). Effective Interactions between Electric Double Layers. *Annu. Rev. Phys. Chem.*, 51:209–242.

[Hansen-Goos and Roth, 2006] Hansen-Goos, H. and Roth, R. (2006). A New Generalization of the Carnahan-Starling Equation of State to Additive Mixtures of Hard Spheres. *The Journal of Chemical Physics*, 124(15):154506.

[Hapiot and Lagrost, 2008] Hapiot, P. and Lagrost, C. (2008). Electrochemical Reactivity in Room-Temperature Ionic Liquids. *Chem. Rev*, 108(7):2238–2264.

[Henderson, 1983] Henderson, D. (1983). Recent Progress in the Theory of the Electric Double Layer. *Prog. Surf. Sci.*, 13(3):197 – 224.

[Henderson and Boda, 2009] Henderson, D. and Boda, D. (2009). Insights from Theory and Simulation on the Electrical Double Layer. *Phys. Chem. Chem. Phys.*, 11:3822–3830.

[Henderson et al., 1983] Henderson, D., LozadaCassou, M., and Blum, L. (1983). The Application of the HNC/MSA Approximation to Bulk Electrolytes. *The Journal of Chemical Physics*, 79:3055.

[Hill, 1960] Hill, T. L. (1960). *An Introduction to Statistical Thermodynamics*, Courier Dover Publications, New York, New York.

[Hockney and Eastwood, 1989] Hockney and Eastwood (1989). *Computer Simulation Using Particles*, Taylor & Francis, New York, NY.

[Israelachvili, 1992] Israelachvili, J. N. (1992). *Intermolecular and Surface Forces*. Academic Press, London.

[Jimenez-Angeles et al., 2003] Jimenez-Angeles, F., Messina, R., Holm, C., and Lozada-Cassou, M. (2003). Ion Pairing in Model Electrolytes: A Study Via Three-Particle Correlation Functions. *The Journal of Chemical Physics*, 119:4842.

[Joly et al., 2004] Joly, L., Ybert, C., Trizac, E., and Bocquet, L. (2004). Hydrodynamics within the Electric Double Layer on Slipping Surfaces. *Phys. Rev. Lett.*, 93:257805.

[Jonsson et al., 1980] Jonsson, B., Wennerstrom, H., and Halle, B. (1980). Ion Distributions in Lamellar Liquid-Crystals: A Comparison between Results from Monte-Carlo Simulations and Solutions of the Poisson-Boltzmann Equation. *The Journal of Physical Chemistry*, 84(17):2179–2185.

[Kalcher et al., 2010] Kalcher, I., Schulz, J. C. F., and Dzubiella, J. (2010). Ion-Specific Excluded-Volume Correlations and Solvation Forces. *Phys. Rev. Lett.*, 104:097802.

[Kilic et al., 2007a] Kilic, M., Bazant, M., and Ajdari, A. (2007a). Steric Effects in the Dynamics of Electrolytes at Large Applied Voltages. II. Modified Poisson-Nernst-Planck Equations. *Physical Review E*, 75(2):21503.

[Kilic et al., 2007b] Kilic, M. S., Bazant, M. Z., and Ajdari, A. (2007b). Steric Effects in the Dynamics of Electrolytes at Large Applied Voltages. I. Double-Layer Charging. *Phys. Rev. E*, 75:021502.

[Kornyshev, 2007] Kornyshev, A. A. (2007). Double-Layer in Ionic Liquids: A Paradigm Change? *J. Phys. Chem. B*, 111(20):5545–5557.

[Lamperski and Henderson, 2011] Lamperski, S. and Henderson, D. (2011). Simulation Study of Capacitance of the Electrical Double Layer of an Electrolyte Near a Highly Charged Electrode. *Mol. Simulat.*, 37(4):264–268.

[Lamperski et al., 2014] Lamperski, S., Sosnowska, J., Bhuiyan, L. B., and Henderson, D. (2014). Size Asymmetric Hard Spheres as a Convenient Model for the Capacitance of the Electrical Double Layer of an Ionic Liquid. *The Journal of Chemical Physics*, 140(1):014704.

[Largeot et al., 2008a] Largeot, C., Portet, C., Chmiola, J., Taberna, P.-L., Gogotsi, Y., and Simon, P. (2008a). Relation between the Ion Size and Pore Size for an Electric Double-Layer Capacitor. *J. Am. Chem. Soc.*, 130(9):2730–2731.

[Largeot et al., 2008b] Largeot, C., Portet, C., Chmiola, J., Taberna, P.-L., Gogotsi, Y., and Simon, P. (2008b). Relation between the Ion Size And Pore Size for an Electric Double-Layer Capacitor. *Journal of the American Chemical Society*, 130(9):2730–2731.

[Lauw et al., 2009] Lauw, Y., Horne, M. D., Rodopoulos, T., and Leermakers, F. A. M. (2009). Room-Temperature Ionic Liquids: Excluded Volume and Ion Polarizability Effects in the Electrical Double-Layer Structure and Capacitance. *Phys. Rev. Lett.*, 103:117801.

[Lebowitz and Rowlinson, 1964] Lebowitz, J. and Rowlinson, J. (1964). Thermodynamic Properties of Mixtures of Hard Spheres. *The Journal of Chemical Physics*, 41:133.

[Levin, 2002] Levin, Y. (2002). Electrostatic Correlations: From Plasma to Biology. *Rep. Prog. Phys.*, 65(11):1577.

[Lewandowski and Galiski, 2004] Lewandowski, A. and Galiski, M. (2004). Carbon-Ionic Liquid Double-Layer Capacitors. *Journal of Physics And Chemistry of Solids*, 65(2-3):281–286.

[Lin et al., 2009] Lin, R., Taberna, P., Chmiola, J., Guay, D., Gogotsi, Y., and Simon, P. (2009). Microelectrode Study of Pore Size, Ion Size, and Solvent Effects on the Charge/Discharge Behavior of Microporous Carbons for Electrical Double-Layer Capacitors. *J Electrochem Soc*, 156:A7.

[López-García et al., 2011] López-García, J. J., Horno, J., and Grosse, C. (2011). PoissonBoltzmann Description of the Electrical Double Layer Including Ion Size Effects. *Langmuir*, 27(23):13970–13974.

[Lue et al., 1999] Lue, L., Zoeller, N., and Blankschtein, D. (1999). Incorporation of Nonelectrostatic Interactions in the Poisson Boltzmann Equation. *Langmuir*, 15(11):3726–3730.

[Luo et al., 2006] Luo, G., Malkova, S., Yoon, J., Schultz, D., Lin, B., Meron, M., Benjamin, I., Vanýsek, P., and Schlossman, M. (2006). Ion Distributions Near a Liquid-Liquid Interface. *Science*, 311(5758):216.

[MacDonald and Jr, 1962] MacDonald, J. and Jr, C. B. (1962). Theory of DoubleLayer Differential Capacitance in Electrolytes. *The Journal of Chemical Physics*, 36:3062.

[Maginn and Elliott, 2010] Maginn, E. and Elliott, J. (2010). Historical Perspective and Current Outlook for Molecular Dynamics as a Chemical Engineering Tool. *Ind. Eng. Chem. Res*, 49(7):3059–3078.

[Mansoori et al., 1971] Mansoori, G., Carnahan, N., Starling, K., and Jr, T. L. (1971). Equilibrium Thermodynamic Properties of the Mixture of Hard Spheres. *The Journal of Chemical Physics*, 54:1523.

[Martin-Molina et al., 2006] Martin-Molina, A., Quesada-Perez, M., and Hidalgo-Alvarez, R. (2006). Electric Double Layers with Electrolyte Mixtures: Integral Equations Theories and Simulations. *J. Phys. Chem. B*, 110(3):1326–1331.

[McQuarrie, 1976] McQuarrie, D. A. (1976). *Statistical Mechanics*. University Science Books, Sausalito.

[Messinger and Squires, 2010] Messinger, R. J. and Squires, T. M. (2010). Suppression of Electro-Osmotic Flow by Surface Roughness. *Phys. Rev. Lett.*, 105:144503.

[Moreira and Netz, 2002] Moreira, A. and Netz, R. (2002). Simulations of Counterions at Charged Plates. *The European Physical Journal E: Soft Matter And Biological Physics*, 8(1):33–58.

[Moreira and Netz, 2004] Moreira, A. and Netz, R. (2004). Computer Simulations of the Electric Double Layer. In Karttunen, M., Lukkarinen, A., and Vattulainen, I., editors, *Novel Methods in Soft Matter Simulations*, volume 640 of *Lecture Notes in Physics*, pages 2256–2256. Springer Berlin / Heidelberg.

[Mulero et al., 1999] Mulero, A., Faúndez, C., and Cuadros, F. (1999). Chemical Potential for Simple Fluids from Equations of State. *Molecular Physics*, 97(3):453–462.

[Naji et al., 2005] Naji, A., Jungblut, S., Moreira, A. G., and Netz, R. R. (2005). Electrostatic Interactions in Strongly Coupled Soft Matter. *Physica A*, 352(1):131 – 170.

[Netz, 2001] Netz, R. (2001). Electrostatistics of Counter-Ions at and between Planar Charged Walls: From Poisson-Boltzmann to the Strong-Coupling Theory. *The European Physical Journal E: Soft Matter And Biological Physics*, 5(5):557–574.

[Netz, 2003] Netz, R. R. (2003). Electrofriction and Dynamic Stern Layers at Planar Charged Surfaces. *Phys. Rev. Lett.*, 91:138101.

[Paasch and Übensee, 1982] Paasch, G. and Übensee, H. (1982). A Modified Local Density Approximation. Electron Density in Inversion Layers. *Physica Status Solidi (B)*, 113(1):165–178.

[Pandolfo and Hollenkamp, 2006] Pandolfo, A. G. and Hollenkamp, A. F. (2006). Carbon Properties and Their Role in Supercapacitors. *J Power Sources*, 157(1):11–27.

[Pascall and Squires, 2010] Pascall, A. J. and Squires, T. M. (2010). Induced Charge Electro-Osmosis over Controllably Contaminated Electrodes. *Phys. Rev. Lett.*, 104:088301.

[Patra and Ghosh, 2002] Patra, C. N. and Ghosh, S. K. (2002). Structure of Electric Double Layers: A Self-Consistent Weighted-Density-Functional Approach. *The Journal of Chemical Physics*, 117(19):8938–8943.

[Plimpton, 1995] Plimpton, S. (1995). Fast Parallel Algorithms for Short-Range Molecular Dynamics. *J. Comput. Phys.*, 117(1):1–19.

[Qiao and Aluru, 2003] Qiao, R. and Aluru, N. R. (2003). Ion Concentrations and Velocity Profiles in Nanochannel Electroosmotic Flows. *J. Chem. Phys.*, 118(10):4692–4701.

[Qiao and Aluru, 2004a] Qiao, R. and Aluru, N. R. (2004a). Charge Inversion and Flow Reversal in a Nanochannel Electro-Osmotic Flow. *Phys. Rev. Lett.*, 92:198301.

[Qiao and Aluru, 2004b] Qiao, R. and Aluru, N. R. (2004b). Multiscale Simulation of Electroosmotic Transport Using Embedding Techniques. *Int. J. Mult. Comp. Eng.*, 2(2).

[Quesada-Pérez et al., 2003] Quesada-Pérez, M., González-Tovar, E., Martín-Molina, A., Lozada-Cassou, M., and Hidalgo-Álvarez, R. (2003). Overcharging in Colloids: Beyond the Poisson-Boltzmann Approach. *Chemphyschem*, 4(3):234–248.

[Quesada-Perez et al., 2004] Quesada-Perez, M., Martin-Molina, A., and Hidalgo-Alvarez, R. (2004). Simulation of Electric Double Layers with Multivalent Counterions: Ion Size Effect. *The Journal of Chemical Physics*, 121:8618.

[Rica et al., 2012] Rica, R. A., Ziano, R., Salerno, D., Mantegazza, F., and Brogioli, D. (2012). Thermodynamic Relation between Voltage-Concentration Dependence and Salt Adsorption in Electrochemical Cells. *Phys. Rev. Lett.*, 109:156103.

[Rogde and Hafskjold, 1983] Rogde, S. and Hafskjold, B. (1983). Equilibrium Properties of a 2:2 Electrolyte Model. *Molecular Physics*, 48(6):1241–1253.

[Roland, 2006] Roland, R. (2006). Introduction to Density Functional Theory of Classical Systems: Theory and Applications. Front Researcher Development Program. Kyushu University, Fukuoka, Japan. Nov. 2006. Lecture.:1–49.

[Roth, 2010] Roth, R. (2010). Fundamental Measure Theory for Hard-Sphere Mixtures: A Review. *Journal of Physics: Condensed Matter*, 22(6):063102.

[Russel et al., 1989] Russel, W. B., Saville, D. A., and Schowalter, W. R. (1989). *Colloidal Dispersions*. Cambridge University Press, Cambridge.

[Sato et al., 2004] Sato, T., Masuda, G., and Takagi, K. (2004). Electrochemical Properties of Novel Ionic Liquids for Electric Double Layer Capacitor Applications. *Electrochimica Acta*, 49(21):3603–3611.

[Schneider and Stoll, 1978] Schneider, T. and Stoll, E. (1978). Molecular-Dynamics Study of a Three-Dimensional One-Component Model for Distortive Phase Transitions. *Phys. Rev. B*, 17:1302–1322.

[Schoch et al., 2008] Schoch, R. B., Han, J., and Renaud, P. (2008). Transport Phenomena in Nanofluidics. *Rev. Mod. Phys.*, 80:839–883.

[Shapovalov et al., 2007] Shapovalov, V., Ryskin, M., Konovalov, O., Hermelink, A., and Brezesinski, G. (2007). Elemental Analysis within the Electrical Double Layer Using Total Reflection X-Ray Fluorescence Technique. *The Journal of Physical Chemistry B*, 111(15):3927–3934.

[Shapovalov and Brezesinski, 2006] Shapovalov, V. L. and Brezesinski, G. (2006). Breakdown of the Gouy-Chapman Model for Highly Charged Langmuir Monolayers: Counterion Size Effect. *J. Phys. Chem. B*, 110(20):10032–10040.

[Shim and Kim, 2010] Shim, Y. and Kim, H. J. (2010). Nanoporous Carbon Supercapacitors in an Ionic Liquid: A Computer Simulation Study. *ACS Nano*, 4(4):2345–2355.

[Simon and Gogotsi, 2008] Simon, P. and Gogotsi, Y. (2008). Materials for Electrochemical Capacitors. *Nat. Mater.*, 7(11):845–854.

[Simon and Gogotsi, 2010] Simon, P. and Gogotsi, Y. (2010). Charge Storage Mechanism in Nanoporous Carbons and Its Consequence for Electrical Double Layer Capacitors. *Phil. Trans. R. Soc. A*, 368(1923):3457–3467.

[Sloutskin et al., 2005] Sloutskin, E., Ocko, B., Tamam, L., Kuzmenko, I., Gog, T., and Deutsch, M. (2005). Surface Layering in Ionic Liquids: An X-Ray Reflectivity Study. *Journal of the American Chemical Society*, 127(21):7796–7804.

[Song et al., 1989] Song, Y., Mason, E., and Stratt, R. (1989). Why Does the Carnahan-Starling Equation Work So Well? *The Journal of Physical Chemistry*, 93(19):6916–6919.

[Spohr, 1998] Spohr, E. (1998). Computer Simulation of the Structure of the Electrochemical Double Layer. *J Electroanal Chem*, 450(2):327–334.

[Spohr, 2002] Spohr, E. (2002). Molecular Dynamics Simulations of Water and Ion Dynamics in the Electrochemical Double Layer. *Solid State Ionics*, 150(1-2):1–12.

[Squires and Bazant, 2004] Squires, T. and Bazant, M. (2004). Induced-Charge Electro-Osmosis. *J. Fluid Mech.*, 509(1):217–252.

[Svensson et al., 1991] Svensson, B., Åkesson, T., and Woodward, C. E. (1991). On the Simulation of Thermodynamic and Structural Properties of Simple Liquids. *The Journal of Chemical Physics*, 95(4):2717.

[Torrie and Valleau, 1980] Torrie, G. and Valleau, J. (1980). Electrical Double Layers. I. Monte Carlo Study of a Uniformly Charged Surface. *The Journal of Chemical Physics*, 73:5807.

[Tsuda and Hussey, 2007] Tsuda, T. and Hussey, C. (2007). Electrochemical Applications of Room-Temperature Ionic Liquids. *Electrochemical Society Interface*, page 43.

[Ultracapacitor, 2010] Ultracapacitor, L. (1 July 2010). Introduction to Ultracapacitor. *Web*, www.Ultracapacitor.co.kr/Ultracapacitor.

[Van Der Heyden et al., 2006] Van Der Heyden, F. H. J., Stein, D., Besteman, K., Lemay, S. G., and Dekker, C. (2006). Charge Inversion at High Ionic Strength Studied By Streaming Currents. *Phys. Rev. Lett.*, 96:224502.

[Van Der Heyden et al., 2005] Van Der Heyden, F. H. J., Stein, D., and Dekker, C. (2005). Streaming Currents in a Single Nanofluidic Channel. *Phys. Rev. Lett.*, 95:116104.

[Vangaveti and Travesset, 2012] Vangaveti, S. and Travesset, A. (2012). General Solution to the Electric Double Layer with Discrete Interfacial Charges. *J. Chem. Phys.*, 137(6):064708.

[Vlachy, 1999] Vlachy, V. (1999). Ionic Effects Beyond Poisson-Boltzmann Theory. *Annu. Rev. Phys. Chem.*, 50(1):145–165.

[Wang and Wang, 2011] Wang, R. and Wang, Z.-G. (2011). Effects of Ion Solvation on Phase Equilibrium and Interfacial Tension of Liquid Mixtures. *J. Chem. Phys.*, 135:014707.

[Wang et al., 2011] Wang, Z., Liu, L., and Neretnieks, I. (2011). The Weighted Correlation Approach for Density Functional Theory: A Study on the Structure of the Electric Double Layer. *Journal of Physics: Condensed Matter*, 23(17):175002.

[Weeks et al., 1971] Weeks, J. D., Chandler, D., and Andersen, H. C. (1971). Role of Repulsive Forces in Determining the Equilibrium Structure of Simple Liquids. *J. Chem. Phys.*, 54(12):5237–5247.

[Welton, 1999] Welton, T. (1999). Room-Temperature Ionic Liquids. Solvents for Synthesis and Catalysis. *Chem. Rev*, 99(8):2071–2084.

[Widom, 1978] Widom, B. (1978). Structure of Interfaces from Uniformity of the Chemical Potential. *Journal of Statistical Physics*, 19(6):563–574.

[Williams et al., 1998] Williams, G., Soper, A., Skipper, N., and Smalley, M. (1998). High-Resolution Structural Study of an Electrical Double Layer by Neutron Diffraction. *The Journal of Physical Chemistry B*, 102(45):8945–8949.

[Zhao et al., 2012] Zhao, R., Soestbergen, M. V., Rijnaarts, H., Wal, A. V. D., Bazant, M., and Biesheuvel, P. (2012). Time-Dependent Ion Selectivity in Capacitive Charging of Porous Electrodes. *J. Colloid Interface Sci.*, 384(1):38 – 44.